DCT 171

MMFX Rebar Evaluation for I-95 Service Road Bridge 1-712-B

by

Michael J. Chajes
Matthew McNally
Daniel R. Richardson
Gary C. Wenzcel
Wei Liu
Department of Civil and Environmental Engineering
University of Delaware

March 2005

Delaware Center for Transportation
University of Delaware
355 DuPont Hall
Newark, Delaware 19716
(302) 831-1446

MMFX Rebar Evaluation for I-95 Service Road Bridge 1-712-B

by

MICHAEL J. CHAJES
MATTHEW MCNALLY
DANIEL R. RICHARDSON
GARY C. WENCZEL
WEI LIU
Department of Civil and Environmental Engineering
University of Delaware
Newark, Delaware 19716

DELAWARE CENTER FOR TRANSPORTATION
University of Delaware
Newark, Delaware 19716

This work was sponsored by the Delaware Center for Transportation and was prepared in cooperation with the Delaware Department of Transportation. The contents of this report reflect the views of the authors who are responsible for the facts and accuracy of the data presented herein. The contents do not necessarily reflect the official views of the Delaware Center for Transportation or the Delaware Department of Transportation at the time of publication. This report does not constitute a standard, specification, or regulation.

The Delaware Center for Transportation is a university-wide multi-disciplinary research unit reporting to the Chair of the Department of Civil and Environmental Engineering, and is co-sponsored by the University of Delaware and the Delaware Department of Transportation.

DCT Staff

Ardeshir Faghri
Director

Jerome Lewis
Associate Director

Wanda L. Taylor
Assistant to the Director

Lawrence H. Klepner
T^2 Program Coordinator

Sandi Wolfe
Secretary

DCT Policy Council

Robert Taylor, Co-Chair
Chief Engineer, Delaware Department of Transportation

Eric Kaler, Co-Chair
Dean, College of Engineering

The Honorable Tony DeLuca
Chair, Delaware Senate Transportation Committee

The Honorable Richard Cathcart
Chair, Delaware House of Representatives Transportation Committee

Timothy K. Barnekov
Dean, College of Human Resources, Education and Public Policy

Michael J. Chajes
Chair, Civil and Environmental Engineering

Ralph A. Reeb
Director of Planning, Delaware Department of Transportation

Stephen Kingsberry
Director, Delaware Transit Corporation

Shannon Marchman
Representative of the Director of the Delaware Development Office

Roger Roy
Representative, Transportation Management Association

Jim Johnson
Executive Director, Delaware River & Bay Authority

Delaware Center for Transportation
University of Delaware
Newark, DE 19716
(302) 831-1446

MMFX Rebar Evaluation for I-95 Service Road Bridge 1-712-B

by Michael J. Chajes, Matthew McNally, Daniel R. Richardson, Gary C. Wenczel, and Wei Liu

DEPARTMENT OF
CIVIL & ENVIRONMENTAL ENGINEERING
UNIVERSITY OF DELAWARE

The Center For
INNOVATIVE
BRIDGE ENGINEERING

March 2005

Executive Summary

The goal of this research was to study an innovative application of new materials in the reconstruction of Bridge 1-712B, Ramp J located in the I-95 service area in Newark, Delaware. Originally constructed in 1963, Bridge 1-712B is a single-span concrete structure. The bridge is approximately 30 feet long and 28 feet wide. Biannual inspections of the original bridge showed that it was deficient due to insufficient moment capacity of the beams. DelDOT decided to upgrade the bridge by replacing the beams and deck using an innovative design with non-corrosive reinforcement. The original design called for using carbon fiber-reinforced polymer (CFRP) rebar and epoxy-coated rebar, but DelDOT changed the plan after the introduction of MMFX steel, a new type of steel designed to be highly resistant to corrosion. The CFRP design was retained as an alternative to the MMFX. Since both designs used new forms of non-corrosive rebar, a testing program was established by the University of Delaware to validate the use of MMFX and CFRP in the new design, and a field testing program on the completed bridge was also developed.

MMFX Microcomposite steel was designed to be both strong and non-corrosive at a cost that is competitive with conventional steel. The difference between MMFX steel and conventional steel is in the atomic configuration and make up. MMFX's atomic composition separates the micro galvanic cells, using nano sheets of austenite, where the electro-chemical reaction that produces rust occurs. The process of producing this material also leads to a higher strength than conventional steel. These properties make MMFX desirable for use in decks.

Fiber-reinforced polymers (FRPs) consist of glass, carbon, or aramid fibers embedded in a polymeric resin matrix. FRPs are anisotropic in nature and have high tensile strength in the fiber direction. Developed and used primarily by the aerospace industry due to their high strength and light weight, the use of FRPs in civil and structural applications is relatively recent. Unlike steel, FRPs are elastic until fracture and do not yield. They also have very high tensile strengths but low shear strengths. The main property that separates FRPs from steel is that FRPs are non-corrosive making them ideal for use in concrete.

Both MMFX and FRP rebar have been used in structural applications. MMFX has been use primarily in bridge decks, while prior bridge applications of FRP include prestressing tendons and CFRP rebar as a replacement for steel in concrete deck slabs. So far there have been no reported problems with either MMFX or CFRP rebar in field applications.

The design procedures and requirements used for designing the concrete bridge beams for bridge 1-712B using either MMFX or FRP rebar came from the AASHTO "LRFD Bridge Design Specifications" (AASHTO, 1998) and the ACI 440.1 R-01 "Guide for the Design and Construction of Concrete Reinforced with FRP Bars"(ACI Committee 440, 2001). The design procedures and requirements for using MMFX or FRP rebar in concrete bridge beams are very similar but have one unique difference: the failure state of the beams.

To validate the design methods and the performance of MMFX and CFRP rebar, both laboratory and field studies were conducted. Through observations in the laboratory and field, the following conclusion were drawn:

- Since MMFX has a yield strength close to twice that of regular steel, designers must be careful not to design beams that are over-reinforced when using MMFX as a direct replacement for standard steel reinforcement.

- Designers must also be aware that MMFX does not exhibit a clear yield point and its ductility is clearly less than that of regular steel rebar.

- MMFX reinforced beams may exhibit larger cracks than standard reinforced beams, especially if fewer higher strength bars are used for the tensile reinforcement.

- When designing with CFRP, it was found that deflection controlled the design. As such, CFRP beams will have somewhat excessive strength.

Based on the work done in this project, the following are needed areas of future study:

- Since tensile testing of the CFRP rebar to failure was difficult due to slipping of the rebar prior to failure, better ways of gripping the CFRP rebar are needed.

- Since MMFX has a distinctly different stress-strain behavior from normal rebar (no distinct yield point), analytical methods are needed to allow better prediction of MMFX reinforced beam load-deformation behavior up to failure.

- Current AASHTO and ACI Codes limit the use of high strength steel for conventional reinforced concrete beams. Additional testing should be conducted to evaluate the given limits

Details of this project are contained in the attached report, "Behavior of Reinforced Concrete Beams Designed with MMFX and CFRP Rebar." The report comprises the following components:

- Chapter 1: Introduction

- Chapter 2: Research Background For MMFX and FRP Rebar

- Chapter 3: Design of Bridge 1-712B Beams and Laboratory Test Beams

- Chapter 4: Laboratory Testing and Results

- Chapter 5: Diagnostic Load test of Bridge 1-712B
- Chapter 6: Conclusions

Continued monitoring of the MMFX corrosion resistance properties is needed. As part of a corollary study, researchers at the University of Delaware conducted a comparative study of MMFX, stainless clad, epoxy-coated, and normal steel rebar on Bridge1-712B. Six-inch sections of different types of bars were tied to the MMFX grid in the deck and monitored with V2000 sensors. Although no conclusive results have been obtained to date, the following facts were observed:

- MMFX and normal steel rebar behave similarly.
- Stainless clad bars yielded unstable corrosion readings which are strongly dependent upon ambient temperature.
- Epoxy-coated bars have relatively high voltage readings but very low current readings through the entire monitoring process.
- For epoxy-coated bar, the integrity of the coating is very important—the rebar is vulnerable to corrosion when the coating is damaged but not if the coating is intact. Some specimens were purposely damaged in the study.

Details of this comparative corrosion study are documented in a separate report following Chapter 6 of the main report.

BEHAVIOR OF REINFORCED CONCRETE BEAMS DESIGNED WITH MMFX AND CFRP REBAR

by

Matthew M. McNally

A thesis submitted to the Faculty of the University of Delaware in partial fulfillment of the requirements for the degree of Master of Civil Engineering

Spring 2003

BEHAVIOR OF REINFORCED CONCRETE BEAMS

DESIGNED WITH MMFX AND CFRP REBAR

by

Matthew M. McNally

Approved: _____
Michael J. Chajes, Ph.D.
Professor in charge of thesis on behalf of the Advisory Committee

Approved: _____
Michael J. Chajes, Ph.D.
Chair of the Department of Civil and Environmental Engineering

Approved: _____
Eric W. Kaler, Ph.D.
Dean of the College of Engineering

Approved: _____
Conrado M. Gempesaw II, Ph.D.
Vice Provost for Academic and International Programs

ACKNOWLEDGMENTS

I would like to thank Dr. Chajes for all of his instruction, guidance and support in completing this project and graduate degree over the past two years. I would also like to thank Dr. Mertz who clarified all of my questions regarding the AASHTO bridge code.

I would like to thank Gary Wenczel and Danny Richardson for all of their work and help in the laboratory and in the field. All of the members, faculty and staff, of the structures department have been of great help and importance to me over my past years here at the University of Delaware. Even though I am leaving the University of Delaware, I know I can always count on their knowledge and understanding as a source of help in the future.

I would like to thank the Delaware Department of Transportation who funded this research. I would, in particular, like to thank Jason Hastings for his help and patience in answering all of my questions.

Most importantly, I would like to thank my parents, John and Kathleen, who have always supported me in everything that I have done. Their love, support and guidance has made me a better person and I hope they understand that without them none of this would have been possible.

TABLE OF CONTENTS

LIST OF TABLES

LIST OF FIGURES

ABSTRACT

Corrosion of reinforcing steel is a major problem for our concrete bridge inventory. In reconstructing bridge 1-712B, Ramp J located in the I-95 service area in Newark, Delaware, an innovative design utilizing non corrosive reinforcement was selected. MMFX steel was used as the non corrosive reinforcement in the design while CFRP reinforcement was chosen as an alternative design.

Since both designs used new and innovative types of non corrosive rebar, a testing program was set up by the University of Delaware to validate their use. The testing program included four 20 foot long concrete test beams that were reinforced with MMFX, CFRP and standard grade 60 rebar. The cross sections of the test beams were 16 inches wide by 20 inches deep. Each beam was tested to failure in four point bending. The testing program was used to validate the use of both CFRP and MMFX in the design of bridge 1-712B and to validate the design process of each. The beams with MMFX reinforcing were able to utilize the higher strength of the rebar, but exhibited less ductility than beams reinforced with standard rebar. The CFRP reinforced beam failed as designed with the concrete crushing before the CFRP bars fractured. It was found that MMFX steel does have much higher yield strength than standard steel but does not have a clear yield point. The CFRP reinforced beam was found to have performed well when compared to the design prediction.

Field testing of the completed bridge was used to validate the final design. Bridge 1-712B was subjected to a diagnostic load test shortly after the bridge was built. The load test was used to calculate a distribution factor for the bridge and to compare it to the calculated distribution factor used in the design. The load test results were also used to evaluate the support conditions of the bridge. The results of the load test were compared to the results of the laboratory tests to compare the flexural behavior.

MMFX and CFRP rebar were used in the design and alternative design of bridge 1-712B due to their non corrosive properties. The testing program set up by the University of Delaware focused on the flexural behavior of both MMFX and CFRP reinforced concrete beams. A separate research program is investigating the corrosion resistance of the MMFX rebar. From the standpoint of strength, designs of both MMFX and CFRP reinforced beams were found to perform well. The constructed bridge was found to be adequately designed and load tests have verified that the bridge is performing well.

Chapter 1

INTRODUCTION

1.1 Bridge 1-712B

The motivation for this thesis was to study an innovative application of new materials in the reconstruction of bridge 1-712B, Ramp J located in the I-95 service area in Newark, Delaware. Bridge 1-712B was originally constructed in 1963. The bridge is a single span concrete structure. The dimensions of the bridge are approximately 30 feet long and 28 feet wide. Through inspections of the original bridge, done every two years, the bridge was found to be deficient. Insufficient moment capacity of the beams caused the bridge to be rated as deficient. With a deficiency rating of 40 out of 100 and ranking 23rd on the Delaware Department of Transportation's (DelDOT) bridge deficiency list, DelDOT decided to upgrade bridge 1-712B by removing the beams and deck and replacing them with new ones. It was decided that the new beams and deck for bridge 1-712B would utilize an innovative design using non corrosive reinforcement. Corrosion of reinforcing steel is a major problem in our current bridge inventory. New forms of rebar that are supposed to be highly corrosion resistant are entering the marketplace. DelDOT bridge engineers designed a replacement bridge as part of the Federal Highway Administration's Innovative Bridge Research and Construction (IBRC)

Program. In the first design, carbon fiber- reinforced polymer (CFRP) rebar was going to be used as the flexural reinforcement for the bridge beams. DelDOT came up with a preliminary design for bridge 1-712B using CFRP and epoxy coated rebar, but soon changed after the introduction of MMFX steel. MMFX steel is a new type of steel that is supposed to be very corrosion resistant. It was decided that the new design of bridge 1-712B would use MMFX not only in the flexural reinforcement, but throughout the entire bridge. The MMFX design replaced the CFRP design for several reasons. One of the reasons was that MMFX rebar made the design more economical since MMFX is less expensive than CFRP rebar. The designers also felt more comfortable designing a concrete bridge reinforced with steel rather than CFRP since the use of CFRP as a structural component in beams is not common. The CFRP design was retained as an alternative to the MMFX. Since both designs used new forms of non corrosive rebar, a testing program was established by the University of Delaware to validate the use of MMFX and CFRP in the new design was developed. A field testing program on the completed bridge was also developed.

1.2 Thesis Outline

Chapter 2 discusses background in terms of the use of CFRP and MMFX in concrete bridge beams. It examines the ACI 440.1 R-01 "Guide for the Design and Construction of Concrete Reinforced with FRP Bars" (ACI Committee 440, 2001) that was recently developed by ACI Committee 440. Chapter 2 also comments on the prior testing and results

of CFRP and MMFX. Chapter 3 examines the design process for beams reinforced with MMFX and CFRP rebar, presents the final bridge 1-712B design, and finally presents the design of beams fabricated for laboratory testing. Chapter 4 presents the results from the laboratory tests and discusses how they compare to the predicted design behavior found in Chapter 3. Chapter 5 presents the data from the diagnostic load test of bridge 1-712B and compares the behavior to the design in Chapter 3. Chapter 6 presents concluding remarks and comments on suggested future testing of MMFX and CFRP reinforced concrete beam applications.

Chapter 2

RESEARCH BACKGROUND FOR MMFX AND FRP REBAR

2.1 Introduction

This chapter explores the history, material differences, common uses, and prior testing of both MMFX and FRP rebar. Unlike standard rebar, both MMFX and FRP are intended to be able to reduce or eliminate rebar corrosion. "Corrosion costs in all industrialized nations amount to 3% of the GNP of each country." (H.H. Uhlig, M.I.T. – T.P. Hoar, University of Cambridge UK). Corrosion of steel reinforcing in concrete beams or decks reduces the design life of most structures. That is why new materials such as FRP and MMFX rebar are being developed. If successful, these new materials may one day replace conventional steel rebar. Several types of non-corrosive rebar are currently available for use such as epoxy coated and stainless clad rebar. This chapter will explore only MMFX and FRP rebar.

2.2 MMFX Rebar

MMFX Microcomposite steel is produced by the MMFX Steel Corporation of America, a subsidiary of MMFX Technologies Corporation, which was formed on June 28, 1998. The inventor of MMFX steel is Professor Gareth Thomas who is also the Vice President of Research and Development at MMFX Steel Corporation of America. The MMFX Steel

Corporation's objective for MMFX steel was to produce a new type of steel that was both strong and non-corrosive at a cost that was competitive with conventional steel.

The difference between MMFX steel and conventional steel is in the atomic configuration and make up. MMFX's atomic composition separates the micro galvanic cells, using nano sheets of austenite, where the electro-chemical reaction that produces rust occurs (MMFX Steel Corporation of America). This separation of the cells where the electro-chemical reaction of producing rust occurs makes MMFX virtually non-corrosive. The process of producing MMFX steel also leads to a higher strength than conventional steel. Conventional grade 60 steel has a yield strength of approximately 60 ksi, where MMFX has a yield strength of approximately 120 ksi and has the same modulus of elasticity, 29,000 ksi, as conventional steel.

Currently there is no special design manual for the use of MMFX in concrete bridge decks or beams, however, an MMFX Design and Construction Practices Manual is currently being produced (www.mmfxsteel.com). Designing concrete decks and beams with MMFX steel uses conventional methods of design such as those given in the "Notes on ACI 318-99 Building Code Requirements for Structural Concrete" (Portland Cement Association, 1999) and the AASHTO "LRFD Bridge Design Specifications" (AASHTO, 1998). However, both the Notes on ACI 318-99 code and the AASHTO LRFD Bridge code put restrictions on the yield strength that may be used for design. The AASHTO LRFD Bridge code

states that "Yield strengths in excess of 75 ksi shall not be used for design purposes" (AASHTO, Section 5.4.3.1). The Notes on ACI 318-99 Building Code states that "An upper limit of 80,000 psi is placed on the yield strength of reinforcing steels other than prestressing tendons" (Portland Cement Association, Page 5-11). The reason for these limits on yield strength, given by the Notes on ACI 318-99 Building Code, is that "...the yield strain of 80,000 psi steel is about equal to the maximum usable strain of concrete in compression" (Portland Cement Association, Page 5-11). Because of these restrictions MMFX steel rebar appears to be prohibited for use in the design of concrete beams according to both the AASHTO LRFD Bridge code and the Notes on ACI 318-99 Building Code. The above mentioned codes, however, do not provide any restrictions on the yield strength of steel that may be used in concrete decks. This makes MMFX desirable for use in decks due to its non-corrosive properties.

2.3 FRP Rebar

Fiber-reinforced polymer (FRP) technology has been around since the end of World War II (ACI Committee 440, 2001). FRPs consist of fibers either glass, carbon or aramid that are embedded in a polymeric resin matrix. The FRPs are anisotropic in nature and have high tensile strength in the direction of the fibers. Fiber-reinforced polymers were developed and used primarily by the aerospace industry due to characteristics of having high strengths and being lightweight. The use of FRP's in civil and structural applications did not come about until the 1980s, and were primarily used in seawall construction, airport runways

and electronic laboratories (Brown and Bartholomew, 1996). FRPs became useful in structural projects in the 1990s as an alternative replacement for deteriorating steel reinforcing in bridge decks and other structures (Benmokrane, Chaallal and Masmoudi, 1996).

Unlike steel, FRPs are elastic until fracture and do not yield. They also
have very high tensile strengths. GFRPs, glass fiber-reinforced polymers, CFRPs, carbon fiber-reinforced polymers, and AFRPs, aramid fiber-reinforced polymers, have tensile strengths that range between 70 to 230 ksi, 87 to 535 ksi, and 250 to 368 ksi respectively (ACI Committee 440, Table 3.3). The modulus of elasticity of the GFRPs, CFRPs and AFRPs range between 5100 to 7400 ksi, 15,900 to 84,000 ksi, and 6,000 to 18,200 ksi respectively unlike steel who's modulus is a constant 29,000 ksi (ACI Committee 440, Table 3.3). Unlike steel rebar FRPs can not be bent once they have been manufactured unless a thermoplastic resin, which can be heated, is used. As a result, FRPs have to be fabricated with bends. Also, FRPs do not have high shear strengths. The resin governs the shear strength unless the fibers are orientated on an offset; standard test methods have not been established to characterize FRP's shear behavior. The main property that separates FRPs from steel is that FRPs are non-corrosive making them ideal for use in concrete.

Due to the many different material properties and behaviors of FRPs, a special design guide for using FRPs was developed. ACI Committee 440 published the ACI 440.1 R-01 "Guide for the Design and

Construction of Concrete Reinforced with FRP Bars" in 2001. This was not the only guide to be published on designing concrete with FRP. Japan, Canada and some European countries have also developed guides and recommendations for the use of FRPs.

2.4 ACI 440.1 R-01 Guide

As mentioned above, the ACI 440.1 R-01 "Guide for the Design and Construction of Concrete Reinforced with FRP Bars" was published by ACI Committee 440 in 2001. This publication serves as a guide to designing concrete with FRP rebar.

There are differences in the design of concrete reinforced with FRP rather than steel. One important reason for this is the fact that FRP rebar does not yield prior to failure. The main focus of this section is to present the differences in the flexural design of concrete beams designed with FRP as opposed to standard rebar. ACI 440 R-01 states the design of flexural members with FRP reinforcing is only valid for rectangular sections since experiments on the behavior of non rectangular sections have not yet been confirmed (ACI Committee 440, Section 8.1). When designing with steel reinforcing an under reinforced beam is required. Under reinforced beams guarantee that the steel yields prior to failure before the compression concrete crushes. Since FRP rebar does not have a yield point, FRP reinforced beams can fail due to either FRP rupture or concrete crushing. The ACI 440 R-01 guide allows for designing an FRP beam to fail when the compression concrete crushes as well as fracturing of the FRP rebar. The failure mode of the FRP bars fracturing first leads to a

catastrophic failure where as the concrete crushing exhibits some plastic behavior before failure (ACI Committee 440, Section 8.1.1). ACI 440 R-01 does allow for both types of failure modes in design. However, the flexural strength reduction factor of 0.9 used for steel is lowered to a range of 0.5 for fracture of the FRP bars to 0.7 for the concrete crushing. The calculation for the reduction factor can be found in section 3.4. The ACI 440 R-01 guide also describes how to calculate the nominal moment capacity for a concrete beam in a slightly different manner. ACI 440 R-01 lists four different methods for calculating the nominal moment. The moment calculations are very similar to the moment calculations used for steel reinforcing. One major difference in the design of a flexural member reinforced with FRP is that moment redistribution should not be considered due to FRPs linear-elastic behavior up to failure. Section 3.4 presents further analysis of the moment equations.

"FRP reinforced members have a relatively small stiffness after cracking" (ACI Committee 440, Section 8.3). Due to the lower stiffness, deflection criteria usually control the design of flexural members. The process for calculating deflections for FRP reinforced beams is very similar to the process for steel reinforced beams. The ACI 440 R-01 guide modifies the traditional Branson equation for calculating the effective moment of inertia by introducing a bond-dependent coefficient. The effective moment of inertia equation is presented in section 3.4. This coefficient takes into account the lower modulus of FRP and the different bond behavior of FRP.

"The substitution of FRP for steel on an equal area basis, for example, would typically result in wider crack widths" (ACI Committee 440, Section 8.3.1). However, since FRP rebar is non-corrosive, crack width limits have been relaxed when designing for corrosion protection. The ACI 440 R-01 guide's calculation for crack width is very similar to traditional calculations. The guide modifies the traditional Gergely-Lutz equation by adding a coefficient that takes into account the bond strength of the FRP bars. This equation is generic and is dependent on the type of FRP that is being used. Equations 2.1 and 2.2 present the traditional Gergely-Lutz and the ACI 440 guide's equation for calculating crack widths in concrete beams reinforced with either steel or FRP rebar.

$$w = 0.076\beta(E_s\varepsilon_s)\sqrt[3]{d_c A} \qquad (2.1)$$

(Gergely-Lutz)

$$w = \frac{2200}{E_f}\beta k_b f_f \sqrt[3]{d_c A} \qquad (2.2)$$

(ACI 440 R-01)

Where: $\beta =$ ratio of the distance from the neutral axis to extreme tension fiber to the distance from the neutral axis to the center of the tensile reinforcement, $E_s =$ modulus of elasticity of steel, $\varepsilon_s =$ strain in steel reinforcement, $d_c =$ thickness of the concrete cover measured from extreme tension fiber to center of bar or wire location closest thereto, $A =$ the effective tension area of concrete, the area of concrete having the same centroid as that of tensile reinforcement, divided by the number of

bars, E_f = modulus of elasticity of FRP, k_b = bond-dependent coefficient, and f_f = stress in FRP reinforcement at compression failure.

Shear strength in a FRP reinforced concrete member is lower than that of an equivalent steel member due to the lower axial stiffness of FRP (ACI Committee 440, Section 9.2). The ACI 440 R-01 guide takes into account the lower stiffness and adds a coefficient that affects the traditional shear strength of the concrete. This coefficient is a ratio of FRP to equivalent steel. The calculation for FRP shear strength is very similar to that of steel. The difference is in the design tensile strength of the FRP rebar. The design tensile strength can not be greater than the strength of the bend in the stirrup which is typically 40 to 50% less than that of a straight bar (Nanni, A.; Rizkalla, S.; Bakis, C.E.; Conrad, J.O.; and Abdelrahman, A.A., 1998).

Overall the ACI 440 R-01 "Guide for the Design and Construction of Concrete Reinforced with FRP Bars" (ACI Committee 440, 2001) uses modified equations from steel reinforced concrete members that take into account the differences in properties between FRP and steel rebar.

2.5 Prior Testing of MMFX Rebar

The purpose for the testing of concrete beams reinforced with FRP and MMFX rebar in flexure presented in this thesis was due to the Delaware Department of Transportation's need for a full scale laboratory test on how the beams behaved to verify designs for bridge 1-712B. This section will introduce some of the prior testing of both MMFX and FRP

rebar. Though there have been numerous studies and tests performed on MMFX and FRP rebar this section will only focus on the prior testing of concrete beams reinforced with either MMFX or FRP rebar in flexure.

The University of North Florida, West Virginia University, and the Florida Department of Transportation all have done testing of the behavior of MMFX rebar in concrete beams in flexure.

In 2002 Faris A. Malhas, Ph.D. from the University of North Florida tested 22 – 13 foot long beams with a 1 foot by 1.5 foot cross section. Two concrete strengths and three reinforcement ratios were used. The beams were tested to failure in four point bending. The results of the tests showed that all the beams failed in a ductile manner. One common result was that the MMFX beams were more flexible under service loads but did not exhibit excessive deflections.

In 2002 Vijay P.V., Ph.D., Hota V.S. GangaRao, Ph.D. and Woraphot Prachasaree from West Virginia University tested 4 – 13 foot long beams with a 1 foot by 1.5 foot cross section. Each beam had different reinforcement ratios and used different size rebar. The beams were tested to failure in four point bending. The results of the tests showed that the beams yielded and had significant elongation before the compression concrete crushed. Strains were found to be higher in the MMFX bars when compared to the theoretical values for regular steel at levels of 40, 60, 75, and 90 ksi. Crack widths and a deflection criteria of L/360 were both met at a level of stress around 40 ksi. At stress levels over 40 ksi both deflection and crack width criteria may not both be

satisfied. Deflections were closely approximated up to a stress level of 75 ksi. Overall, the results showed that the stress-strain behavior of MMFX rebar in concrete beams can be accurately modeled.

In 2002 Marcus H. Ansley from the Florida Department of Transportation tested 8 beams, 4 reinforced with MMFX rebar and 4 reinforced with standard grade 60 rebar. Three of the beams were tested in flexure by four point bending, two using lap splices at the midspan. The first three beams were 18 feet long and had a 1 foot by 1.5 foot cross section. The fourth beam was tested in shear and was 12 feet long and had a 1 foot by 1.5 foot cross section. The results of the testing showed that MMFX rebar compared favorably to the standard grade 60 rebar, however, ductility became an issue when a lap splice of 30.5 inches was used. Also, it was found that special consideration should be given when designing a concrete beam reinforced with MMFX rebar due to its lack of a distinct yield point.

2.6 Prior Testing of FRP Rebar

As mentioned in section 2.3 in this chapter, FRP technology has been around since the end of World War II and the use of FRPs in civil and structural applications have been around since the 1980s. Numerous studies and tests on FRP for use in structural applications have been performed, enough so that the ACI 440 R-01 guide was developed and published. Extensive research and testing of the flexural behavior of concrete beams reinforced with FRP rebar has been conducted by many including Hota V. GangaRao and Salem S. Faza. Both have tested and

studied the behavior of concrete beams reinforced with FRP rebar, and their test results contributed to the ACI 440 R-01 guide.

The following information regarding the prior testing of GFRP rebar was found in a literature review that was part of the research report "GFRP Reinforced Concrete Bridge Decks" by David Deitz from the Kentucky Transportation Center (Deitz, Harik, and Gesund, 2000).

In 1991 Faza and GangaRao tested and compared the bond behavior of smooth, sand coated and deformed GFRP reinforcement to conventional steel reinforcement in concrete beams. The beams were 2750 mm long and had a 305 mm by 150 mm cross section and each beam had a different reinforcement ratio. The four point bending test results indicated that there was no bond failures with the deformed GFRP rebar but there were bond failures with the smooth bars. Flexural cracks in the GFRP reinforced beams were found to be larger than in the corresponding steel reinforced beams and seemed to initiate suddenly. The conclusion reached by this study was that smooth GFRP bars should not be used as reinforcement in concrete beams.

In 1996 Brown and Bartholomew tested and compared the deflections of GFRP reinforced beams to conventional steel reinforced beams. The test beams were 1830 mm long and had a 150 mm by 100 mm cross section. The GFRP and steel reinforced beams had identical reinforcement ratios. The four point bending test results showed that the deflections under service loads in the GFRP beam were 3.76 times higher than those observed in the steel beam. The conclusion formed from these

tests was that modified techniques should be used to calculate long-term deflections in GFRP reinforced beams. This conclusion helped in the development of the modified effective moment of inertia equation used in the ACI 440 R-01 guide.

In 1996 Benmokrane, Chaallal and Masmoudi tested beams reinforced with GFRP and steel rebar. The beams were 3300 mm long and had varying cross sections with 200 mm widths and depths of 300 mm and 550 mm. Reinforcement ratios of 1.102% and 0.562% were used. The results of the four point bending tests showed that all the over-reinforced beams failed by having the compression concrete crush before the GFRP rebar fractured and that the load-displacement behavior of the GFRP reinforced beams was linear up to failure. The under reinforced beams failed by rupture of the GFRP bars before the concrete crushed and the load-displacement behavior was also linear up to failure.

2.7 Prior Field Applications of MMFX and FRP Rebar

Both MMFX and FRP rebar have been used in several structural applications. MMFX has been use primarily in bridge decks. Both the Iowa and Kentucky Department of Transportation have used MMFX rebar as reinforcement in bridge decks. The Oklahoma Department of Transportation used MMFX rebar as stirrups in one of their bridge projects. However, California and some other states have banned the use of MMFX rebar in structural applications. The ban is due to MMFX's high yield strength which leads to crack width size issues. Limitations in the size of rebar used in detailing and spacing limitations necessary to limit crack

widths make it difficult to design flexural members using MMFX's high yield strength which reduces the amount of reinforcement needed in a beam thus making these limitations hard to satisfy. If MMFX is used as a replacement for regular steel, designers must be careful that the beam does not become over-reinforced. Due to MMFX's low ductility it is very hard to use the inelastic region in the design of redundant members. Also, since MMFX has a very high yield stress, it can not currently be used in design under the AASHTO and ACI 318 bridge and building codes.

Prior bridge applications of FRP rebar have used FRP tendons for prestressing. The use of FRP rebar has not been used as a substitute for steel as the primary flexural reinforcing in concrete beams without being prestressed. Most commonly, FRP rebar has been used in concrete decks. The Joffre Bridge in Quebec used CFRP rebar as a replacement for steel in a portion of one of its concrete deck slabs.

So far there have been no reported problems with either MMFX or CFRP rebar in the above mentioned field applications.

Chapter 3

DESIGN OF BRIDGE 1-712B BEAMS AND LABORATORY TEST BEAMS

3.1 Overview of Design Requirements for use of MMFX and CFRP Rebar

All the design procedures and requirements used for designing the concrete bridge beams for bridge 1-712B using either MMFX or FRP rebar came from the AASHTO "LRFD Bridge Design Specifications" (AASHTO, 1998) and the ACI 440.1 R-01 "Guide for the Design and Construction of Concrete Reinforced with FRP Bars"(ACI Committee 440, 2001). The procedure used to design the test beams came from notes from CIEG 467 Structural Design: Concrete taken in spring 2000 (Chajes and Mertz, 2000), "Notes on ACI 318-99 Building Code Requirements for Structural Concrete" (Portland Cement Association, 1999), and the ACI 440 guide (ACI Committee 440, 2001).

The design procedures and requirements for using MMFX or FRP rebar in concrete bridge beams are very similar but have one unique difference. The difference in the design for MMFX and FRP rebar is the failure state of the beams. The design requirement when using MMFX steel, or any steel, for flexural reinforcement is that failure of the beam subjected to bending occurs when the tensile steel, or flexural reinforcement, yields before the compression concrete crushes. Placing a percentage of flexural reinforcement less than the balanced percentage

causes the steel rebar to reach its yielding strain before the compression concrete reaches its ultimate strain, commonly referred to as under-reinforcing the beam. After the tensile steel yields it can still carry load and will elongate for a period of time before fracture. When yielding occurs a beam with a sustained load will experience large deformations (noticeable by the human eye) and have significant cracking before the beam fails completely. The design requirement using FRP rebar for flexural reinforcement utilized in the design of the test beams and the alternative design of the bridge 1-712B beams is that the failure of the beam, subjected to bending, occurs when the compression concrete crushes. By placing more flexural reinforcement in the beam than it needs for strength the compression concrete reaches its ultimate strain before the flexural reinforcement reaches its rupture strain, commonly referred to as over-reinforcing the beam. Since FRP rebar under tensile loads does not exhibit yielding before it fractures, the only indication of failure is when the compression concrete starts to crack or crush. This is a more brittle mode of failure, yet it can occur at a rather large deformation state.

Sections 3.2 and 3.3 will describe bridge 1-712B and the procedure used to design bridge 1-712B. Section 3.4 will examine the procedure for the alternative CFRP design. Section 3.5 will examine the design of several test beams used to evaluate the behavior of the bridge beams at failure. Finally, section 3.6 presents a summary of the design strengths for the laboratory test beams.

3.2 Bridge 1-712B Description and Construction

As mentioned in section 1.1, bridge 1-712B is located in the I-95 Service area in Newark, Delaware. The bridge carries one way traffic from the west side of the service area to the east side and crosses a delivery road used for the service building and restaurant. The bridge primarily carries car traffic. Trash trucks for the service area also use the bridge frequently. Figure 3.1 shows the bridge and how it is situated.

Figure 3.1 Bridge 1-712B Looking North East

The bridge is a single span adjacent concrete beam structure. The beams designed for this bridge used simple supports for the end conditions. The bridge is slightly skewed and is approximately 30 feet long and 28 feet wide. Replacing the old bridge beams are 7 – 30 feet 7 inch long 4 feet

wide concrete beams reinforced with MMFX rebar. The depths of the beams were restricted due to the fact that large trucks use the delivery road beneath the bridge. From the bottom of the delivery road to the bottom the bridge beams is approximately 15 feet. Due to height restrictions, the beams designed had a depth of 15 inches with a 5 inch concrete deck poured on top. Section 3.3 presents the dimensions and design of the beams. The beams that made up the old bridge were saw cut and removed. Figure 3.2 shows the bridge with a few beams removed.

Figure 3.2 Bridge 1-712B with Old Beams Partially Removed

In order to stabilize the walls, once a few of the old beams were removed, new beams were installed. Figure 3.3 shows the new beams sitting next to the old beams.

Figure 3.3 New Beams Next to Old Beams

The beams span over the delivery road and each end rests on a bearing pad which sits on top of a retaining wall. MMFX dowel bars and rubberized joint filling material connected the beams, bearing pads and retaining wall. The MMFX bars and rubberized joint filler sat in three holes at each end of the beam, bearing pad and retaining wall. Figure 3.4 shows two beams, the bearing pads, and the retaining wall put together.

Figure 3.4 Beam, Bearing Pad, and Retaining Wall

Shear connecters, placed in the rebar cage of each beam before pouring, attached each beam to the adjacent beams. Metal plates welded to each of the shear connectors joined adjacent beams. A total of 15 shear connectors connected one beam to a neighboring beam. Grout at the top of the beams, also shown in Figure 3.4, and a tie rod placed through the middle of all the beams secured them together. MMFX stirrups protruding 2.5 inches out of the beams connect the 5 in concrete bridge deck to the beams. An MMFX rebar grid placed in the deck is used to control cracking. Concrete parapets poured on either side of the bridge finished the

structure. Figures 3.5 through 3.9 illustrate different phases of the construction for bridge 1-712B.

Figure 3.5 Saw Cutting and Removal of Old Beams

Figure 3.6 New Beams Placed on Bridge

Figure 3.7 All of New Beams Placed on Bridge

Figure 3.8 Concrete Deck Being Poured

Figure 3.9 Completed Bridge 1-712B

3.3 Design of Bridge 1-712B

As mentioned in section 1.1, the reconstruction of bridge 1-712B was necessary for the purpose of increasing bridge 1-712's load rating so that it could carry legal truck loads and also, because some of the concrete beams were deteriorating. Trucks that passed under the bridge had hit the outer beam causing some of the concrete to crack and chip off. Cores taken from the original bridge also indicated possible Alkai-Silica Reaction (ASR) had caused the concrete to deteriorate. DelDOT's bridge design group designed the new bridge 1-712B. This section will examine the procedure used for designing bridge 1-712B.

The first step of the design was to calculate the design loads for the bridge. Specifications for the design live loads for the bridge came from special design trucks in the AASHTO LRFD Bridge Design manual. Sections 3.6.1.2.2 to 3.6.1.2.4 in the AASHTO LRFD Bridge Design manual describe the design trucks. The truck that produced the greatest live load moment on bridge 1-712B was the design tandem placed at the center of the bridge. The design tandem is a truck with a pair of 25 kip axels located 4 feet apart from each other. The live load moment produced by this tandem load was approximately 317 ft-kip. Figure 3.10 shows the location and configuration of the design tandem used to calculate the design moment.

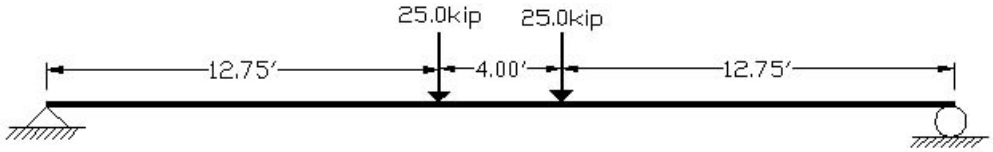

Figure 3.10 Design Tandem Load

The AASHTO LRFD Bridge Design manual states that a design lane load must be included in the calculation for live load moments. The design lane load is a 0.64 kip per linear foot load that spans the entire length of the bridge distributed over a 10 foot width. The live load moment produced on

the bridge by this design lane load was approximately 69 ft-kip. Figure 3.11 shows the design lane load on the bridge.

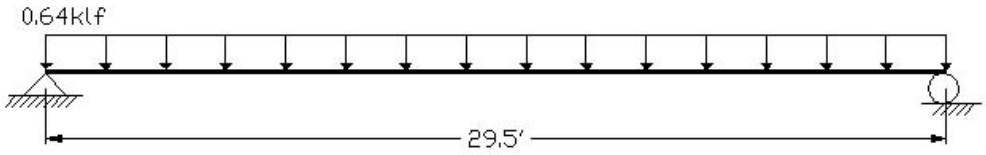

Figure 3.11 Design Lane Load

Calculation of a distribution factor for the bridge allows one to evenly distribute the live load moments to each of the beams. The distribution factor used in this design was for adjacent precast concrete box girders with concrete deck and one design lane loaded. The equation used to calculate the distribution factor for interior beams with one design lane comes from Table 4.6.2.2.2b-1 in the AASHTO LRFD Bridge Design manual and is given by

$$DF_{\text{int}1} = k\left(\frac{b}{33.3L}\right)^{0.5}\left(\frac{I}{J}\right)^{0.25} \qquad (3.1)$$

Where: $k = 2.5Nb^{-0.2}$, Nb = number of beams, b = beam width (inch), L = beam length (feet), I = moment of inertia (inch^4), $J = \frac{A^4}{40.0I_p}$, A =

area of beam cross section (inch^2), and I_p = polar moment of inertia (inch^4). Using Equation 3.1, the distribution factor calculated for moment was 0.283. By multiplying the design tandem and lane load by the distribution factor one can calculate how much of the live-load moment distributes to each beam. Normally distribution factors are calculated for both interior and exterior beams producing different moments on their beams. The distribution factor for exterior beams for this bridge calculated was lower than the distribution factor for interior beams so the interior beam distribution factor was used for the design of all the beams. For this bridge it was easier and more economical to design and produce identical interior and exterior beams. This also cuts down on potential errors during construction.

Load factors multiply the live load moment to reach the unfactored live load design moment. An impact factor of 1.33 increased the design tandem. The inclusion of the impact factor takes into account dynamic amplification of moving trucks. Multiplying the distributed design tandem by the impact factor and adding the distributed design lane load moments together yields the unfactored live load design moment for the bridge beams. The unfactored design live load moment including impact for each beam, M_u was approximately 140 ft-kip.

The next design load calculated was the dead load moment. The weight of each beam was approximately 15 tons. Also the dead load for the concrete parapets and hand rail are calculated. The total weight of the parapets and hand rail was approximately 13 tons. The dead load of

the parapets and hand rail was taken to distribute over the beams evenly producing approximately 1.86 tons on each beam. The design dead load moment calculated used the weight per foot of the beam, parapet and hand rail. The unfactored dead load moment M_{DL} on each beam was calculated to be approximately 122 ft-kip.

Load factors multiply both the live load and dead load moments to calculate the moment used in the design of the beams. The dead load and live load factors are 1.25 and 1.75 respectively. The increased live and dead load moments added together produces the design moment. Dividing the design moment by a resistance factor of 0.9 completes the calculation for the required nominal design moment. The factored design moment Mu/ϕ for each beam was approximately 435 ft-kip.

The calculation for design shear used the same process as the flexural calculations. Equation 4 shows the distribution factor for shear in interior beams with one lane loaded comes from Table 4.6.2.2.3a-1 in the AASHTO LRFD Bridge Design manual and is given by

$$DF_{\text{int}1} = \left(\frac{b}{130L}\right)^{0.15}\left(\frac{I}{J}\right)^{0.05} \qquad (3.2)$$

Where: b = beam width (inch), L = beam length (feet), I = moment of inertia (inch^4), $J = \frac{A^4}{40.0I_p}$, A = area of beam cross section (inch^2), and I_p = polar moment of inertia (inch^4). Using Equation 3.2, the distribution

factor calculated for shear was 0.49. The design truck for shear was the HS20. Figure 3.12 illustrates the HS20 design truck.

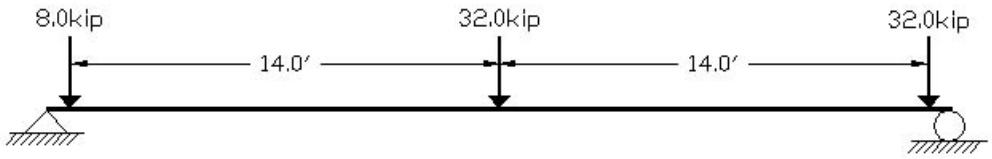

Figure 3.12 Design HS20 Truck

The design lane load and dead load of the beam also contribute to shear. Using the distribution factor for shear and the dead and live load factors the factored design shear load V_u for each beam was approximately 50 kips.

As mentioned in section 3.2, the dimensions of the seven bridge beams were 30 feet 7 inches long, 4 feet wide and 15 inches in depth with a 5 inch deck poured on top. A length of 29 feet 6 inches, approximately the center to center distance of the supports, was used in the design of the beams. Using the 435 ft-kip required nominal design moment M_u / ϕ each beam was designed with 11 - #6 MMFX rebar for flexural reinforcement located a distance "d" of 17.5 inches down from the top of the total depth of the beam, 20 inches. The bars are spaced at 4 inches on center. The shear reinforcement consists of 32 – #5 MMFX stirrups (each stirrup consists of 2 U-shaped stirrups, one of which is

inverted) spaced evenly throughout the beam at 12 inches on center. Figure 3.13 illustrates the U-shaped shear reinforcement. The strength of the concrete used in the design was 12 ksi for the beams and 6 ksi for the deck. The design moment capacity M_n for each beam was approximately 409 ft-kip (the required capacity was 435 ft-kip) and the design shear capacity ϕV_n was approximately 107 kips. Note that the required moment capacity for the beams is less than the moment used for design. This discrepancy was found after the beams had been fabricated however, since the yield stress of the MMFX bars, used as a direct substitution for standard rebar, suggested by the MMFX manufacture was 90 ksi the actual moment capacity of the beams was closer to 603 ft-kip, making the beams safe. Table 3.1 shows the design properties and design strengths of the beams and Figures 3.13 and 3.14 illustrate the beams cross section and elevation.

Table 3.1 Bridge 1-712B Beam Properties

Beam Dimensions			**MMFX and Concrete Properties**		
b =	48.0	inches	**Fy =**	60.00	ksi
h =	20.0	inches	**f'c (beam) =**	12.00	ksi
d =	17.5	inches	**f'c (slab) =**	6.00	ksi
L =	29.5	feet	**Es =**	29000.00	ksi
Design Strengths					
M n =	409.15	ft-kip			
V n =	58.7	kip			
Actual Strength					
M n =	665.9	ft-kip	(Assuming fy = 100 ksi)		

	6		
V n =	97.7	kip	

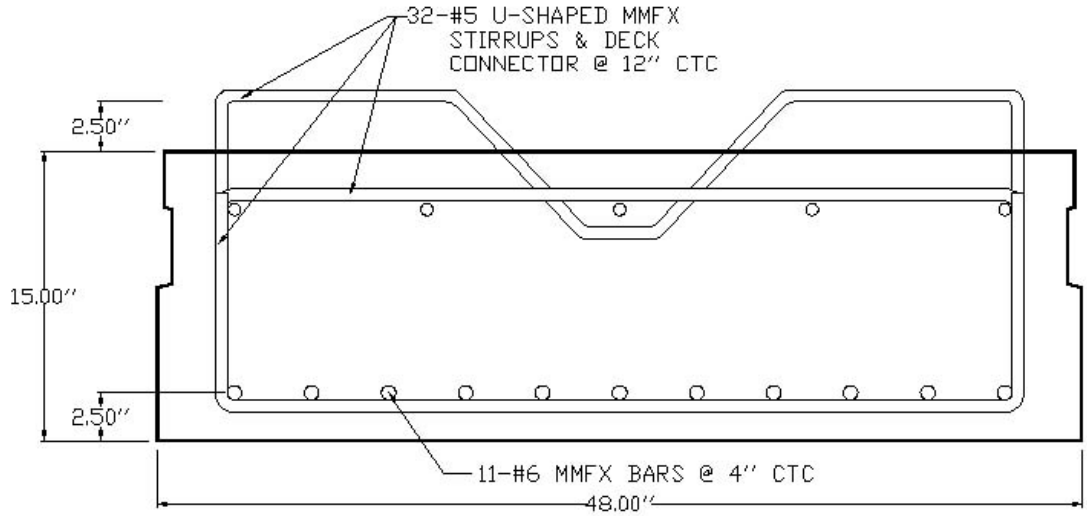

Figure 3.13 Cross Section of Bridge 1-712B MMFX Beam

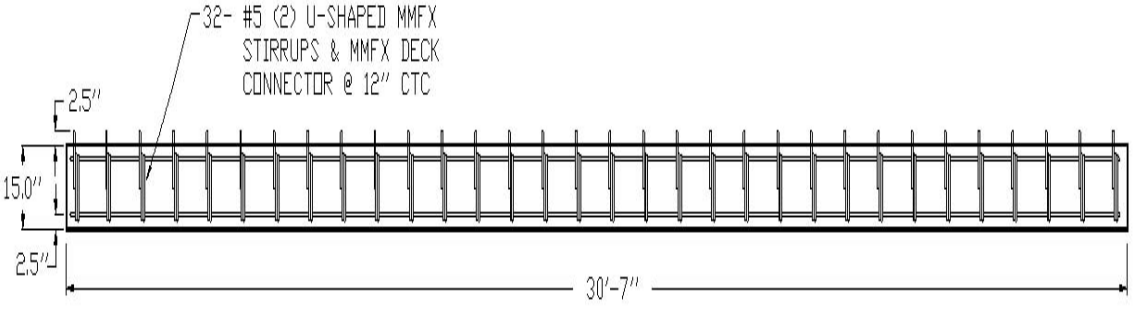

Figure 3.14 Elevation of Bridge 1-712B MMFX Beam

3.4 Design for the Alternative CFRP Beams

As mentioned in section 1.1, an alternative design for bridge 1-712B using CFRP rebar as the flexural reinforcement for the beams was developed. The design included seven voided beams reinforced with CFRP rebar. This section will examine the design procedure for the beams of bridge 1-712B using CFRP rebar.

As mentioned in section 3.1, the failure state of a beam reinforced with FRP rebar is when the compression concrete crushes or when the FRP bars fracture. This is due to FRP rebar not exhibiting any yielding properties. The failure design developed for the alternative design for bridge 1-712B was when the compression concrete crushed. To ensure that the concrete will crush before the FRP bars rupture the FRP reinforcement ratio ρ_f must be higher than the balanced condition ρ_{fb}. The calculation of the FRP reinforcement ratio ρ_f differs from the traditional reinforcement ratio ρ calculation by using FRP properties in the place of steel properties. The difference between the ACI 440 R-01 and ACI 318-99 in terms of calculating the balanced condition is that the properties of the FRP bars are used in place of the steel properties. Equations 3.3 and 3.4 present ACI 318-99 and ACI 440 R-01 calculations for the balanced condition of steel and FRP reinforced beams respectively.

$$\rho_b = \frac{0.85\beta_1 f'_c}{f_y}\frac{87{,}000}{87{,}000 + f_y} \qquad (3.3)$$

(ACI 318-99)

$$\rho_{fb} = 0.85\beta_1 \frac{f'_c}{f_{fu}} \frac{E_f \varepsilon_{cu}}{E_f \varepsilon_{cu} + f_{fu}} \qquad (3.4)$$

(ACI 440 R-01)

Where: $\beta_1 =$ factor based on concrete strength, $f'c =$ concrete strength, $f_y =$ steel yield strength, $E_f =$ FRP modulus of elasticity, $\varepsilon_{cu} =$ ultimate strain of concrete in compression (0.003) and $f_{fu} =$ design tensile strength of the FRP bar. Ensuring that $\rho_f > \rho_{fb}$ satisfies the failure state of the concrete crushing before the rupture of the FRP bars. In the same way, the ACI 440 R-01 moment capacity calculation for beams designed with FRP bars differs from the ACI318-99 guide. Again, FRP properties are used in place of steel properties. Equations 3.5 and 3.6 present the moment capacity equation for both the ACI 318-99 and the ACI 440 R-01 respectively.

$$Mn = A_s f_y \left(d - \frac{a}{2} \right) \qquad (3.5)$$

(ACI 318-99)

$$Mn = A_f f_f \left(d - \frac{a}{2} \right) \qquad (3.6)$$

(ACI 440 R-01)

Where: $A_s =$ area of steel reinforcement, $f_y =$ steel yield strength, $d =$ depth from extreme compression fiber to center of tensile reinforcement, $a =$ depth of rectangular compression block, $A_f =$ area of FRP reinforcement and $f_f =$ stress in FRP reinforcement at compression

failure. Equation 3.7 presents the ACI 440 guide's equation for calculating the stress in the FRP reinforcement equation at compression failure.

$$f_f = \sqrt{\frac{(E_f \varepsilon_{cu})^2}{4} + \frac{0.85\beta_1 f'_c}{\rho_f} E_f \varepsilon_{cu}} - 0.5 E_f \varepsilon_{cu} \le f_{fu} \qquad (3.7)$$

Where: $E_f =$ FRP modulus of elasticity, $\varepsilon_{cu} =$ ultimate strain of concrete in compression (0.003), $\beta_1 =$ factor based on concrete strength, $f'c =$ concrete strength, ρ_f = FRP reinforcement ratio, and $f_{fu} =$ design tensile strength of the FRP bar.

Since this calculation is theoretical and does not account for unforeseen strengths in the beam due to actual material properties used during fabrication the moment capacity is reduced using a reduction factor The reduction factor is based on the balanced condition and ranges from 0.50 when $\rho_f \le 1.4\rho_{fb}$ to 0.7 when $\rho_f \ge 1.4\rho_{fb}$. The equation $\rho_f / 2\rho_{fb}$ calculates the reduction factor when $\rho_{fb} < \rho_f < 1.4\rho_{fb}$. This reduction factor for the moment capacity differs from the factor used for steel reinforced beams. The reduction used in steel reinforced beams is 0.90. Strength of the beams calculated using the above procedure did not govern the design of the bridge 1-712B beams. The design was governed by deflection.

The ACI 440.1 R-01 Guide for the Design and Construction of Concrete Reinforced with FRP Bars uses a reduction coefficient β_d in the calculation of deflections. The β_d reduction factor reduces the gross moment of inertia I_g of the beam used in the calculation of the effective

moment of inertia I_e. Equation 3.8 presents the ACI 440 guide's equation for calculating the effective moment of inertia for a concrete beam reinforced with FRP.

$$I_e = \left(\frac{M_{cr}}{M_a}\right)^3 \beta_d I_g + \left[1 - \left(\frac{M_{cr}}{M_a}\right)^3\right] I_{cr} \le I_g \qquad (3.8)$$

Where: $M_{cr} = \frac{2 f_r I_g}{h}$ (cracking moment), $f_r = 7.5\sqrt{f_{cu}}$, $f_{cu} =$ ultimate stress of concrete, $h =$ depth of flexural member, $M_a =$ the maximum moment in a beam at a computed deflection, $\beta_d = \alpha\left(\frac{E_f}{E_s} + 1\right)$, $\alpha = 0.5$, $E_f =$ FRP modulus of elasticity, $E_s =$ modulus of elasticity of steel, $I_g =$ gross moment of inertia, $I_{cr} = \frac{bd^3}{3} k^3 + n_f A_f d^2 (1-k)^2$ (moment of inertia of cracked section), $b =$ width of member, $d =$ depth from extreme compression fiber to center of tensile reinforcement, $k = \sqrt{2\rho_f n_f + (\rho_f n_f)^2} - \rho_f n_f$, $\rho_f =$ FRP reinforcement ratio, $n_f = \frac{E_f}{E_c}$, and $E_c =$ modulus of elasticity of concrete. Also, the modulus of elasticity of the CFRP is approximately 57% less than that of steels. Due to the above, deflection controlled the design of the bridge 1-712B beams. To reduce the deflection of the beam due to live loads the design included voids in the beam to reduce the dead load. As specified by the section 2.5.2.6.2 in the AASHTO LRFD Bridge Design manual the deflection due to live load on a bridge can not exceed L/800, where L equals the span length of the

bridge. The deflection limit used in the design of the beams was for bridge 1-712B was 0.44 inches.

Using the design tandem, design lane load and dead load, the design moment for each beam was found to be approximately 663 ft-kip. Using the HS20, lane load and dead load the calculated design shear was approximately 62 kips. The higher design moment calculated is due to different properties of the beam such as moment of inertia resulting in a different distribution factor. The distribution factor used in the CFRP design was 0.361 for moment and 0.514 for shear.

The dimensions of the seven voided CFRP beams were very similar to the MMFX reinforced design. The beams were, on average, 31 feet 7 inches long, 4 feet wide and 20 inches in depth with 2- 8 inch high by 15 inch wide voids that ran through 24.5 feet of the beams. The flexural reinforcement in the beams consisted of 16 - #6 CFRP rebar located at a distance of 17.5 inches down from the top of the beam and 3 - #6 CFRP rebar located at a distance of 15 inches down from the top of the beam. The flexural reinforcement was spaced equally through the cross section. The design length of 29.5 feet used for the MMFX design was also used for the CFRP design. The strength of each bar was taken to be 225 ksi. Since the CFRP design was an alternative, the shear reinforcement was never calculated. One design for the shear reinforcement in the beams included 5 – #5 epoxy coated stirrups (each stirrup consists of 2 U-shaped stirrups, one of which is inverted) spaced at 6 inches center to center through the first 2 feet of either end of the beam and 26 – #5

epoxy coated U-shaped stirrups spaced at 12 inches center to center throughout the remaining section of the beam. The strength of the shear reinforcement was 60 ksi. The strength of the concrete used in the design was 6 ksi. The moment capacity of each beam was approximately 1201 ft-kip and the shear capacity, if calculated with the reinforcement given above, would have been approximately 140 kips. Because deflection governed the design, the moment capacity of the beams far exceeds what is necessary for strength. Table 3.2 shows the properties of the beam and Figures 3.15 and 3.16 illustrate the beams cross section and elevation.

Table 3.2 Alternative CFRP Beam Properties

Beam Dimensions			**CFRP and Concrete Properties**		
b =	48.0	inches	**ffu =**	225.00	ksi
h =	20.0	inches	**f'c =**	6.00	ksi
d =	17.1	inches	**Ef =**	16500.00	ksi
L =	29.5	feet			
2 Voids = 15.0" wide & 8.0" high					
Design Strengths					
M n =	1201.8	ft-kip	Moment Capacity		
V n =	140.0	kip	Shear Capacity		

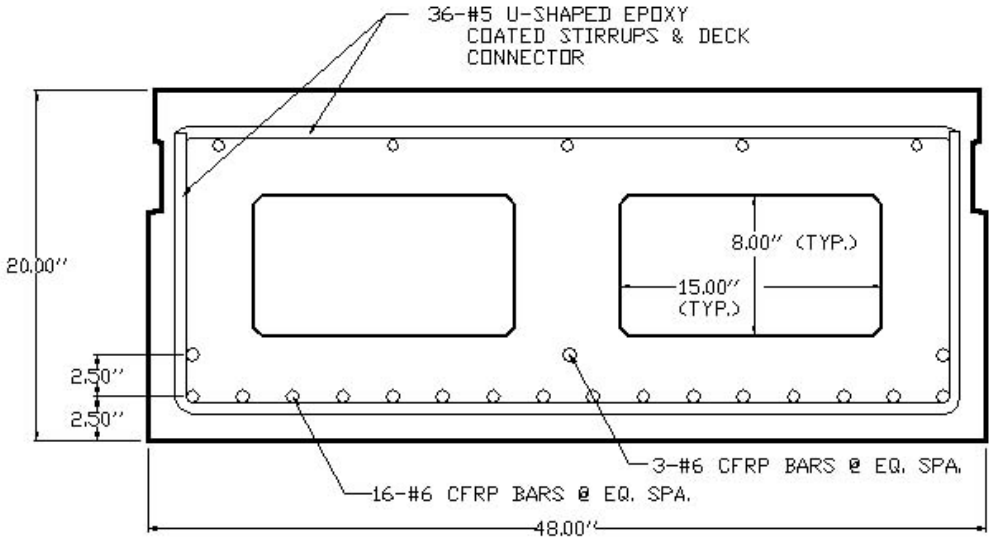

Figure 3.15 Cross Section of Alternative CFRP Beam

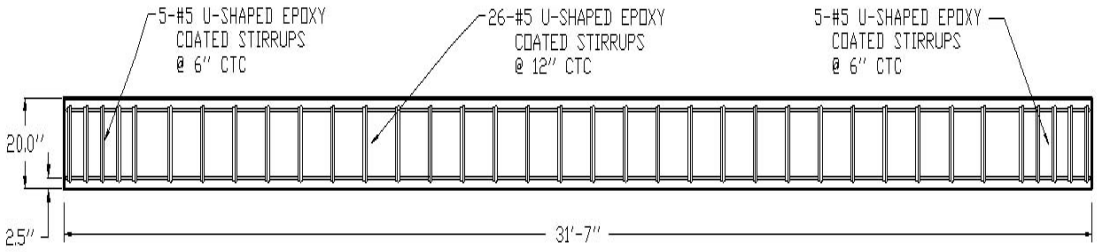

Figure 3.16 Elevation of Alternative CFRP Beam

3.5 Design of Laboratory Test Beams

Since MMFX and CFRP rebar are new to the State of Delaware, DelDOT felt that a laboratory testing program should be set up to evaluate the performance of the materials. In the past, due to their non-corrosive properties, bridge decks have used MMFX and CFRP rebar. It was necessary to test MMFX and CFRP rebar since they were being used for one of the first times as a structural component in the concrete bridge beams for bridge 1-712B. Another reason for laboratory testing was to validate the use of the higher yield strength of MMFX in design if the amount of steel in a beam is reduced. Since its introduction, MMFX has commonly been used in a direct one-to-one replacement of standard grade 60 rebar in bridge decks and other structures; not taking advantage of its higher yield strength. Testing was performed to make sure that the MMFX rebar in the bridge beams for bridge 1-712B would yield before the concrete crushed due to the fact that the design strength of the beams used was 60 ksi and not 100 ksi. The laboratory tests results could then be compared to the theoretical designs of the test beams which could then be used to predict the behavior of the beams designed for bridge 1-712B.

A full scale laboratory test of the MMFX and CFRP beams was not possible due to laboratory space and weight limits on the machinery in the laboratory. Because of this, it was necessary to scale down the dimensions of the test beams from the ones used on bridge 1-712B. As mentioned in section 3.2, the beams designed for bridge 1-712B were 30 feet 7 inches long and 4 feet wide. The scaled down test beams had a width of 16 inches, one-third that of the bridge beams. Each beam was 20

foot long with a rectangular cross section. The heights of the test beams were 20 inches, the same as the bridge 1-712B beams. Sections 3.5.1 through 3.5.4 will present in detail the dimensions of the laboratory test beams.

The first beam designed was with standard grade 60 rebar. This "Standard" beam acts as a reference for the other test beams. This beam had approximately one third of the moment capacity of the actual bridge 1-712B beams. The second beam designed was with MMFX rebar and had the same amount of MMFX flexural reinforcement as the standard grade 60 beam (direct substitution). This "MMFX4" beam is the same as was used for bridge 1-712B (but one-third the width) and does not make use of the MMFX's higher yield strength. The third beam designed was with MMFX rebar but had half the amount of bars as the standard Grade 60 and the other MMFX beam. The purpose of this "MMFX2" beam design was to examine beam performance for a design which made use of the higher yield strength of the MMFX rebar. The final beam designed was with CFRP rebar. The purpose of this "CFRP" beam design was to evaluate the performance of a beam with CFRP rebar. As mentioned previously, this was an alternative design for bridge 1-712B. The design procedures and requirements for the laboratory test beams came from the publications mentioned in section 3.1.

After designing the beams, Schuylkill Products, Inc. fabricated them. To measure the amount of strain in the beams during testing, strain gages were embedded in the beams during fabrication. The strain

gages, made by Measurements Group, Inc., had a resistance of $350 \pm 0.4\%$ ohms and a gage factor of $2.095 \pm 0.5\%$ at 24 degrees Celsius. The weldable strain gages were wired in a one quarter bridge and attached to a 16 inch sister bar. The sister bar consisted of a piece of #4 Grade 60 rebar. Each beam had two gages placed in them. The gages are located at the center of the beam at mid width, one next to the flexural reinforcement (approximately 2.5 inches up from the bottom of the beam) and the other placed at the same location but in the compression region of the concrete (approximately 2.625 inches down from the top of the beam). Zip ties attached the gages and lead wires to the rebar cage with the lead wires running out of the end of the beam. Figures 3.17 through Figure 3.19 show the strain gage attached to the sister bar and the strain gages attached to the rebar cage of the beams.

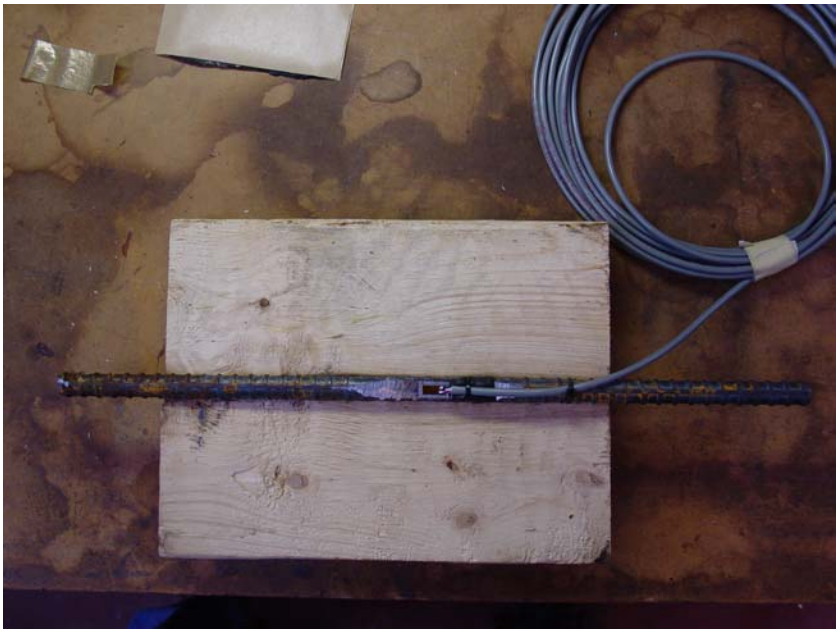

Figure 3.17 Typical Strain Gage and Sister Bar Set Up

Figure 3.18 Strain Gage Attached to Top of Beam

Figure 3.19 Strain Gage Attached to Bottom of Beam

3.5.1 Standard Beam Design

As mentioned previously the standard beam with grade 60 rebar was one third the width of the beams used for bridge 1-712B. The width of the beams designed for bridge 1-712B was 4 feet, meaning that the width of the standard beam was 16 inches. The length of the standard beam was 20 feet long. The depth of the beam was 20 inches. The flexural reinforcement in the beam consists of four - #6 grade 60 rebar that are located at a distance "d" of 17.5 inches down from the top of the beam and spaced at 3 inches on center. The strength of each bar was 60 ksi. The shear reinforcement in the beam consists of thirty - #4 grade 60 stirrups spaced evenly throughout the beam at 8 inches on center. The shear capacity of the standard test beam, as was the case for all of the test beams, was designed to eliminate shear as a failure mode (i.e. force a flexural failure). The shear design was not in any way associated with the bridge 1-712B beams. The strength of the concrete used in the design of the beam was 12 ksi. The design moment of the standard beam was 151 ft-kip, approximately one third of the beams used on bridge 1-712B, and the design shear strength was 77 kips. Table 3.3 and Figure 3.20 illustrate the design dimensions and the design strengths of the standard beam.

Table 3.3 Standard Beam Properties

Beam Dimensions			**Steel and Concrete Properties**		
b =	16.0	inches	**fy =**	60.00	ksi
h =	20.0	inches	**f'c =**	12.00	ksi
d =	17.5	inches	**Es =**	29000.00	ksi
L =	20.0	feet			
Design Strengths					
M n =	151.15	ft-kip	Moment Capacity		
V n =	77.0	kip	Shear Capacity		

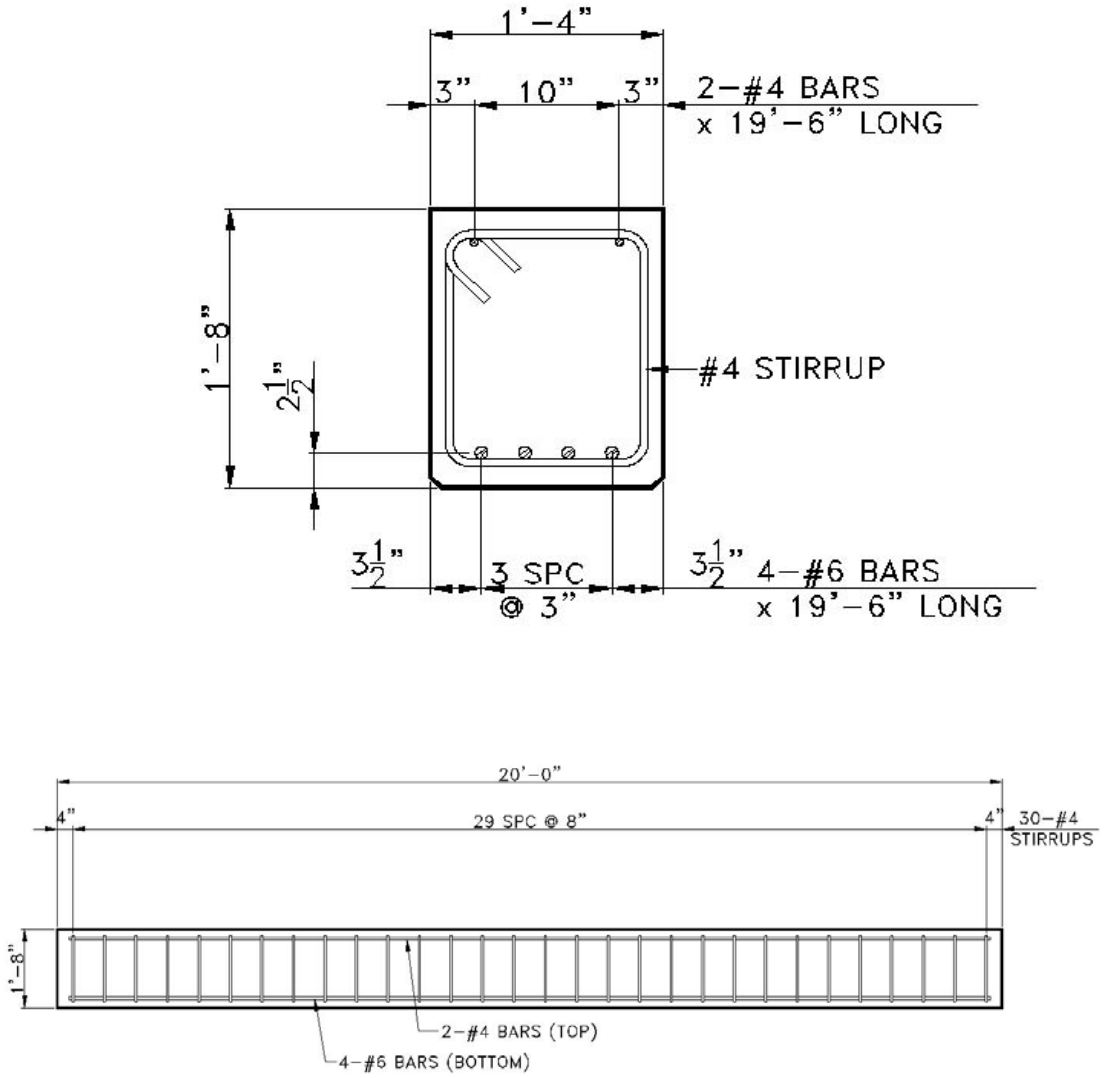

Figure 3.20 Cross Section and Elevation of Standard Beam (Schuylkill)

3.5.2 MMFX4 Beam Design

The design of the MMFX4 beam with four bars of flexural reinforcement was exactly the same as the standard beam. The width of the beam was 16 inches, the depth of the beam was 20 inches and the length of the beam was 20 feet. The flexural reinforcement in the beam consists of four - #6 MMFX rebar located at a distance "d" of 17.5 inches down from the top of the beam and spaced at 3 inches on center. The shear reinforcement consists of thirty - #4 grade 60 stirrups spaced evenly throughout the beam at 8 inches on center. As mentioned in section 3.5, this beam replicates the design of the beams in bridge 1-712B where the MMFX rebar design strength was 60 ksi. Since the MMFX rebar has higher yield strength than regular grade 60 rebar the actual moment capacity of the MMFX4 beam was not 151 ft-kip but was closer to 248.8 ft-kip (assuming a yield strength of 100 ksi). The design shear strength of the beam was 77 kips. The strength of the concrete used in the design of the beam was 12 ksi. Table 3.4 and Figure 3.21 illustrate the design dimensions and design strengths of the MMFX4 beam.

Table 3.4 MMFX4 Beam Properties

Beam Dimensions			**MMFX and Concrete Properties**		
b =	16.0	inches	**fy =**	60.00	ksi
h =	20.0	inches	**f'c =**	12.00	ksi
d =	17.5	inches	**Es =**	29000.00	ksi
L =	20.0	feet			
Design Strengths					
M n =	151.15	ft-kip	Moment Capacity		
V n =	77.0	Kip	Shear Capacity		
Actual Strength					
M n =	248.8	ft-kip	Moment Capacity (assuming fy = 100 ksi)		

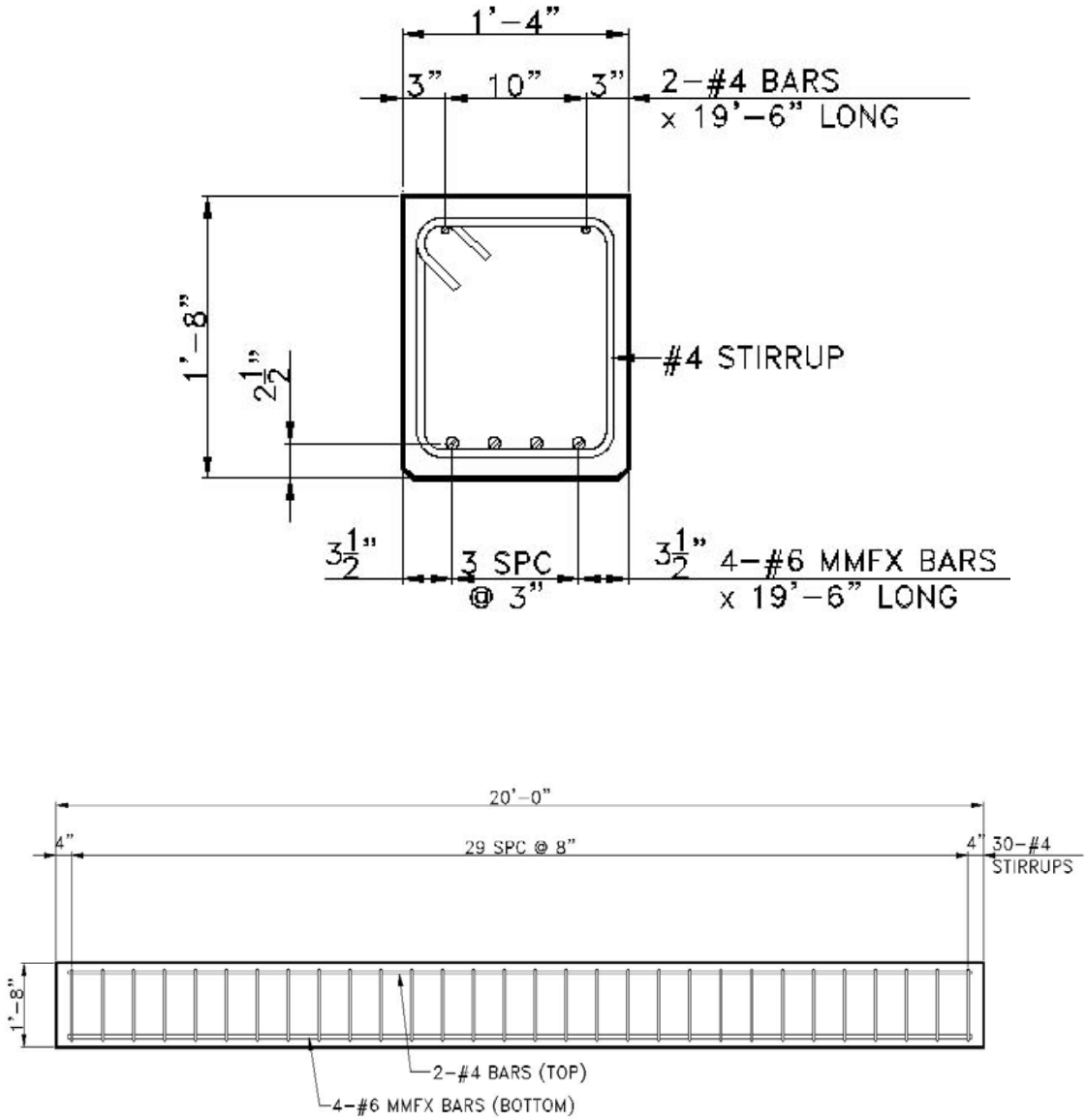

Figure 3.21 Cross Section and Elevation of MMFX4 Beam (Schuylkill)

3.5.3 MMFX2 Beam Design

The MMFX2 beam had the same dimensions as the MMFX4 beam. The width of the beam was 16 inches, the depth of the beam was 20 inches and the length of the beam was 20 feet. The flexural reinforcement in the beam consists of two - #6 MMFX rebar located at a distance "d" of 17.5 inches down from the top of the beam spaced at 8 inches on center. The shear reinforcement consists of thirty - #4 grade 60 stirrups spaced evenly throughout the beam at 8 inches on center. As mentioned in section 3.5, this design utilizes the higher yield strength of MMFX. The moment capacity of the beam was 126 ft-kip if one assumes a design yield strength of 100 ksi for the rebar. Because the size of the rebar used for the flexural reinforcement in the beam stayed the same as bridge 1-712B's reinforcement the moment capacity of the MMFX2 beam was slightly less than one third the capacity of the cross section of the bridge 1-712B beams. The strength of the concrete used in the design of the beam was 12 ksi. Table 3.5 and Figure 3.22 illustrate the design dimensions and design strengths of the MMFX2 beam.

Table 3.5 MMFX2 Beam Properties

Beam Dimensions			**MMFX and Concrete Properties**		
b =	16.0	inches	**fy =**	100.00	ksi
h =	20.0	inches	**f'c =**	12.00	ksi
d =	17.5	inches	**Es =**	29000.00	ksi
L =	20.0	feet			
Design Strengths					
M n =	126.36	ft-kip	Moment Capacity		
V n =	77.0	kip	Shear Capacity		

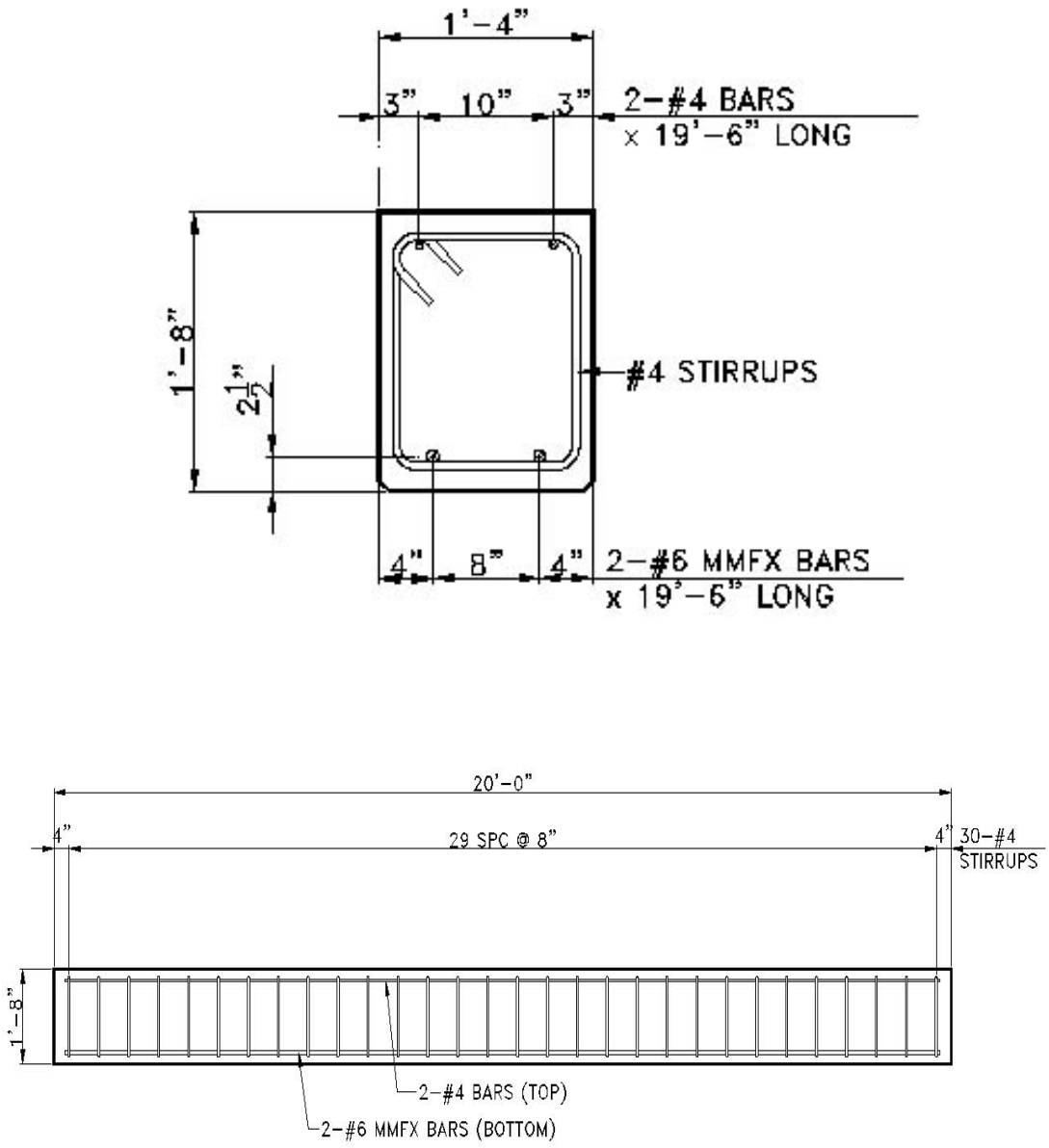

Figure 3.22 Cross Section and Elevation of MMFX2 Beam (Schuylkill)

3.5.4 CFRP Beam Design

The alternative design for bridge 1-712B was to utilize CFRP rebar as the flexural reinforcement. As such, a CFRP test beam was fabricated in case future designs utilize CFRP rebar. The design procedure for the CFRP beam came from the ACI 440.1 R-01 guide. The design of this beam wasn't strength controlled as was the case for the grade 60 and MMFX reinforced beams. The CFRP beam design was deflection controlled. As mentioned in section 3.4, the deflection due to the live load on a bridge can not exceed L/800, where L equals the span length of the bridge. Since the test beam was 20 feet long, L/800 equals 0.3 inches. Through the method of determining the distribution factor for live loads as mentioned in section 3.3, the distributed live load moment over 16 inches of a beam calculated was approximately 47 ft-kip. Using the amount of CFRP necessary for flexural strength the laboratory beams failed the deflection criteria. Increasing the area of flexural reinforcement in the beam caused the beam to meet the deflection criteria. By increasing the area of CFRP reinforcement the beam has more strength in flexure than it needs but has met the deflection criteria.

The CFRP reinforced beam had the same dimensions as the other three test beams. The width of the beam was 16 inches, the depth of the beam was 20 inches and the length of the beam was 20 feet. The flexural reinforcement in the beam consists of six - #6 CFRP rebar located at a distance "d" of 17.5 inches down from the top of the beam and spaced at 2 inches on center. The shear reinforcement in the beam consisted of fifty-nine - #4 grade 60 stirrups spaced evenly throughout the beam at 4

inches on center. The theoretical moment capacity of the beam was 582 ft-kip and used a design tensile strength of 225 ksi for each CFRP bar. Due to deflection governing the design, the moment capacity was approximately 4 times that of the standard test beam. The theoretical shear capacity of the beam was 72.5 kips. The strength of the concrete used in the design of the beam was 12 ksi. Table 3.6 and Figure 3.23 illustrate the design dimensions and design strengths of the CFRP beam.

Table 3.6 CFRP Beam Properties

Beam Dimensions			**CFRP and Concrete Properties**		
b =	16.0	inches	**f fu =**	225.00	ksi
h =	20.0	inches	**f'c =**	12.00	ksi
d =	17.5	inches	**Ef =**	16500.00	ksi
L =	20.0	feet			
Design Strengths					
M n =	581.75	ft-kip	Moment Capacity		
V n =	72.5	kip	Shear Capacity		

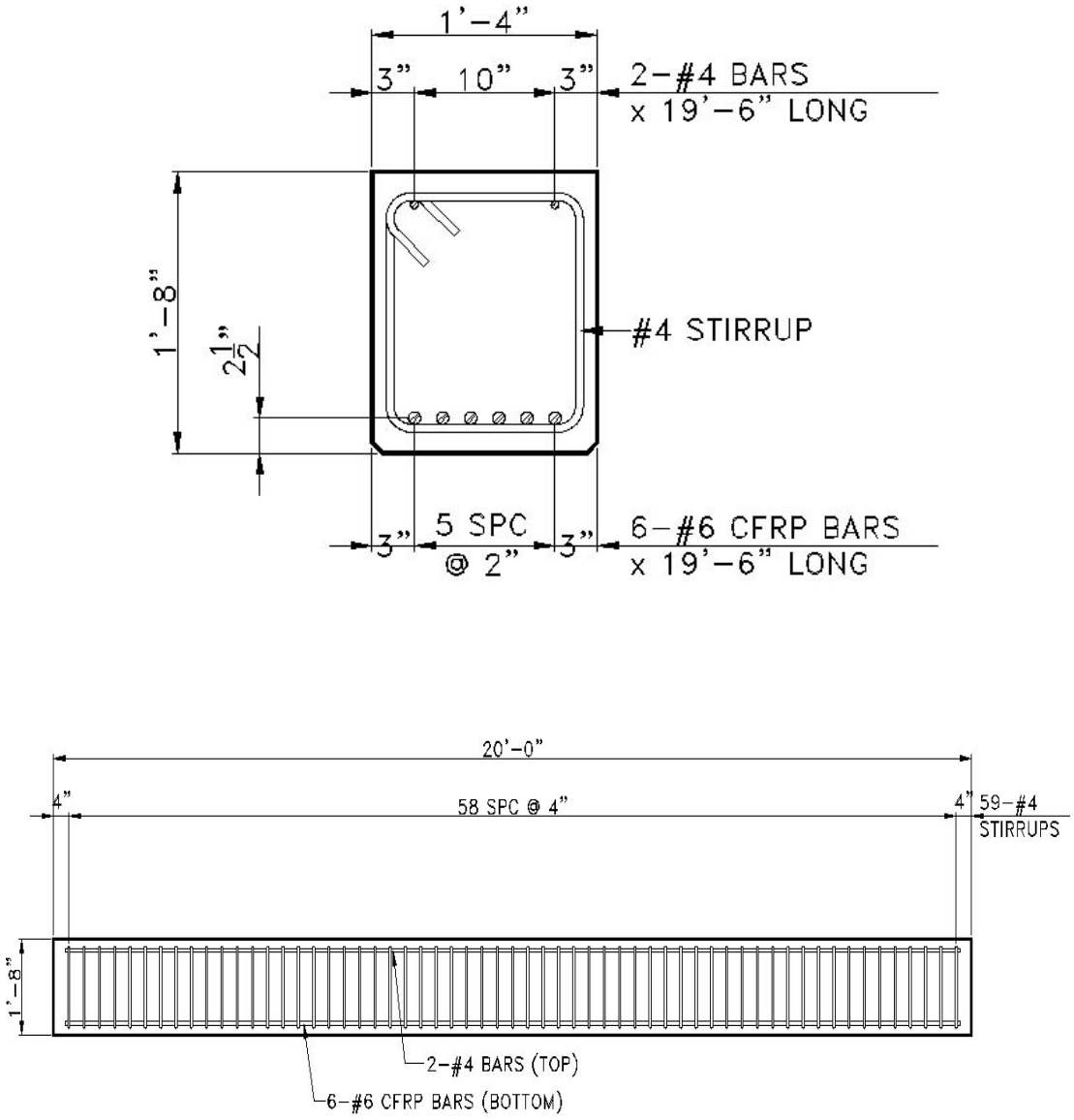

Figure 3.23 Cross Section and Elevation of CFRP Beam (Schuylkill)

3.6 Summary of Laboratory Design Strengths

Table 3.7 summarizes the design strengths of the standard, MMFX4, MMFX2, and CFRP beams.

Table 3.7 Summary of Laboratory Test Beams

Beam	Design Moment Capacity (ft-kip)	Design Shear Capacity (kip)
Standard	151.15	77.0
MMFX4	151.15 (248.8, fy=100 ksi)	77.0
MMFX2	126.36	77.0
CFRP	581.75	72.5

Chapter 4

LABORATORY TESTING AND RESULTS

4.1 Introduction

This chapter presents the testing of the laboratory beams described in chapter 3. Also presented is a comparison of design calculations from chapter 3 to the actual test results for each of the four beams. The primary purpose of the tests was to evaluate the effectiveness of the various types of reinforcement in the beams (MMFX, CFRP, and grade 60 rebar) and compare them to their design values. For each test, the procedure, important material properties, and results of the laboratory tests are given. The laboratory test data provides insight into how the beams in bridge 1-712B are performing.

4.2 Material Properties

Section 3.5 presented the design properties for each of the four test beams. This section presents the actual properties of the materials based on tests preformed in the laboratory. The concrete strength used in the design of the four beams was 12 ksi. Table 4.1 presents the strengths of the concrete found through cylinder tests.

Table 4.1 Concrete Strengths of Test Beams

MMFX Beam Cylinders		Standard Beam Cylinders		CFRP Beam Cylinders	
Test #	**Stress (psi)**	**Test #**	**Stress (psi)**	**Test #**	**Stress (psi)**
1	10740.0	1	8796.0	1	8024.0
2	9286.0	2	8965.0	2	9630.0
3	10280.0	3	9472.0	3	8640.0
Avg = 10.10 ksi		**Avg = 9.08 ksi**		**Avg = 8.76 ksi**	

The flexural reinforcement properties of the rebar were calculated from the results of laboratory tensile tests. Three tensile tests were performed on the MMFX, standard grade 60 and the CFRP rebar. Figure 4.1 and Table 4.2 illustrate the stress-strain curves and the properties of the materials (note that we were not able to test the CFRP rebar to failure).

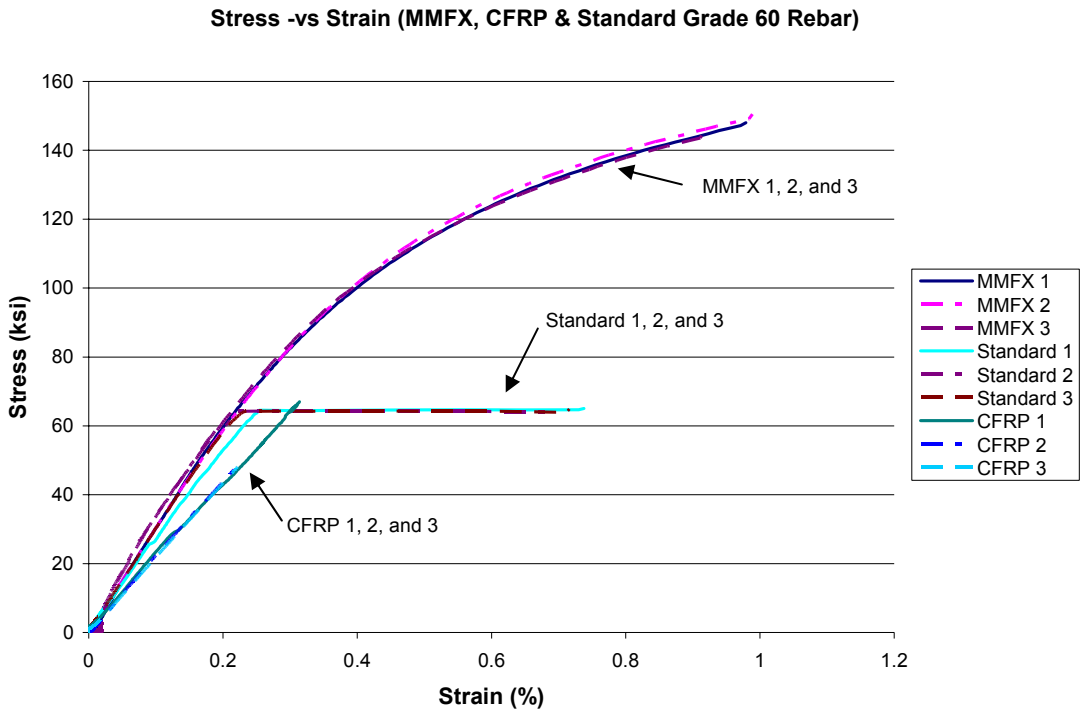

Figure 4.1 Tensile Test Results

Table 4.2 Flexural Reinforcement Properties

Material	Test #	Yield Point (ksi)	Ultimate (ksi)	Modulus (ksi)
MMFX #6 Bar	1	125.2	181.2	30,200
MMFX #6 Bar	2	127.3	181.0	30,300
MMFX #6 Bar	3	118.5	181.2	34,400
Average		**123.7**		**31,633**
Grade 60 #6 Bar	4	64.5	101.1	28,400
Grade 60 #6 Bar	5	64.1	101.2	35,400
Grade 60 #6 Bar	6	64.4	101.5	30,100
Average		**64.3**		**31,300**
CFRP #6 Bar	7	NA	-	24,100
CFRP #6 Bar	8	NA	-	23,400
CFRP #6 Bar	9	NA	-	22,200
Average		NA		**23,233**

All tests were conducted using a Tinius Olsen 200 kip Super "L" tensile testing machine. The yield stress of the MMFX #6 bars was calculated using a 0.2% offset. The MMFX #6 bars exhibited a linear behavior in the lower range of the elastic region but then exhibited a non-linear behavior prior to yielding. It is clear from Figure 4.1 and Table 4.2 that the MMFX rebar has a higher yield stress than the grade 60 rebar. The yield stress for the MMFX #6 rebar ranged from 118.5 to 127.3 ksi where the grade 60 yielding stress ranged from 64.1 to 64.5 ksi.

The CFRP bars were very difficult to test, the bars crushed in the tensile machine grips due to their low compressive strength. Several methods of testing the bars were developed but none of the methods enabled the bars to be tested to failure. The method that produced the best results was by placing an 18 inch steel tube over both ends of the bar. The tube was then filled with Sikadur 31, Hi-Mod Gel epoxy and left to cure. The total length of the test specimen was approximately 5 feet. Figure 4.2 illustrates the CFRP test specimens.

Figure 4.2 CFRP Test Specimens

When the CFRP specimens were tested, the bond failed before the bars developed their tensile capacity. The test did yield an average modulus of elasticity for the CFRP bars of 23,233 ksi which can be found in Table 4.2. The manufactures specified fracture stress of 225 ksi is used in all fracture calculations. Figure 4.3 illustrates the slipping and bond failure that occurred during testing.

Figure 4.3 Bond Failure of CFRP Rebar

4.3 Test Procedure

This section describes the test procedure and set up for the four test beams.

To test the moment capacity and flexural reinforcement of the beams a four point bending test was developed. By using a four point bending test a constant moment region was formed in the 20 foot long beams. Two MTS 150 kip actuators spaced at 4 feet apart at the center of each beam created the constant moment region. Loading plates and rollers were placed between the actuator and beam to distribute the load evenly to the beam and to prevent local crushing of concrete. Figures 4.4 and 4.5 illustrate the actuator locations for the tests.

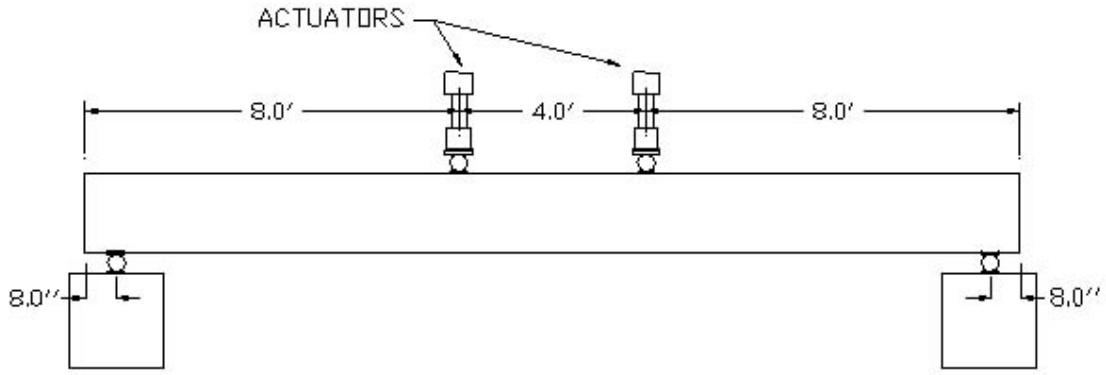

Figure 4.4 Actuators on Beams

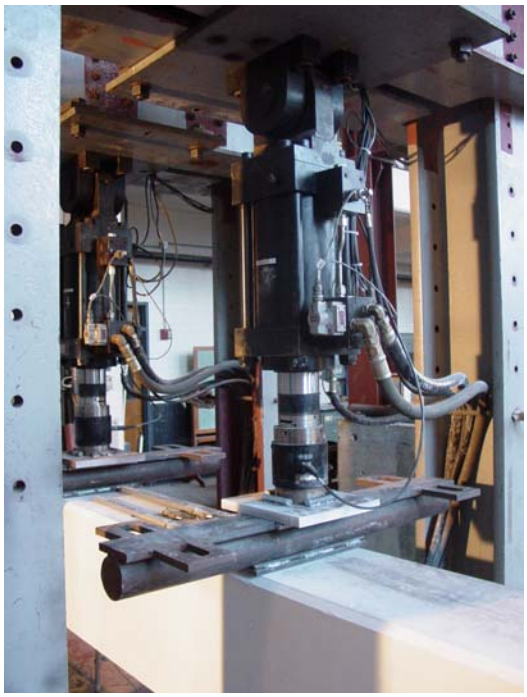

Figure 4.5 Actuator Set Up

The end supports for each beam consisted of rollers sandwiched between plates placed at 8 inches in from the ends of the beams. This created a simple support condition for the beams which is the support condition for bridge 1-712B.

As mentioned in section 3.5, foil strain gages placed on sister bars were used to measure the internal strain in both the tension and compression regions of each beam. The internal strain gages, located at the center of the beam 2.5 inches up from the bottom surface of the beam and 2.625 inches down from the top surface of the beam, were connected to a System 5000 data acquisition system. Strain transducers placed

along the top and bottom of the beam were also used to measured the strain on the external fibers of the beam. The strain transducers, manufactured by Bridge Diagnostics Incorporated (BDI), were used to verify that the internal strain gages were working properly. They were removed prior to the final loading cycle of the beams which involved loading the beams to failure. The BDI gages were also used for an ongoing research project of another graduate student working on damage detection. Figure 4.6 illustrates the locations of the sister bars and BDI gages.

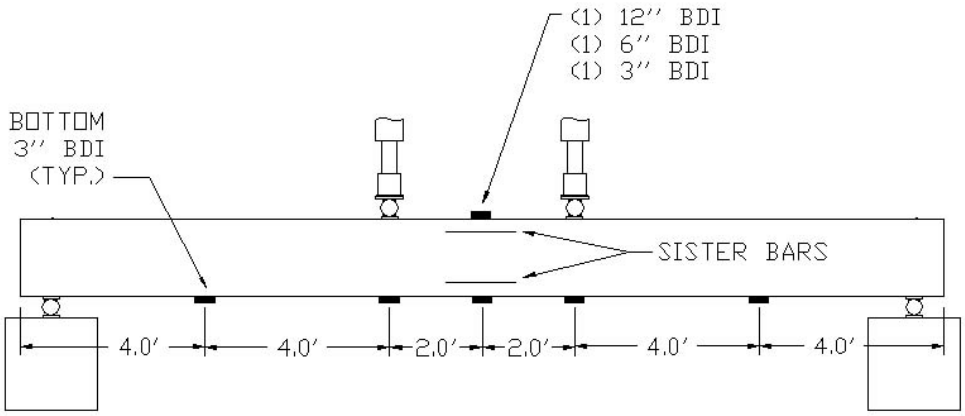

Figure 4.6 BDI and Sister Bar Locations

Linear-variable-differential-transformers (LVDT) placed beneath the beam and along its length were used to measured deflection. The locations of the LVDTs were at the center of the beam, at the two loading points and at the end supports of the beam. The LVDTs were connected to

the System 5000 data acquisition system. Figures 4.7 and 4.8 illustrate the location of the LVDTs.

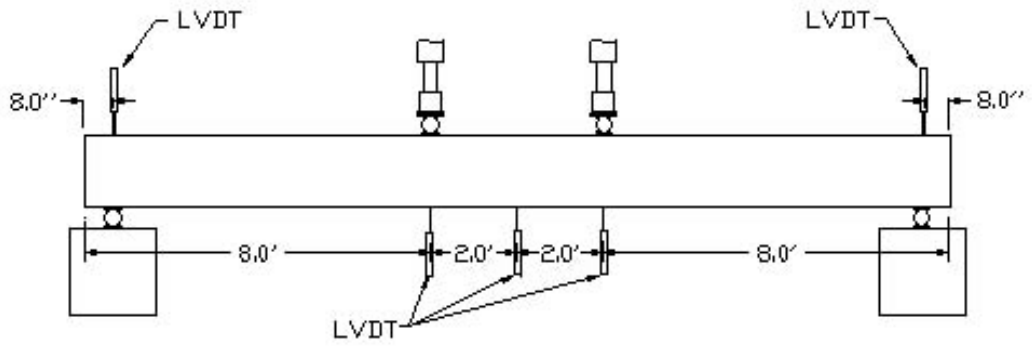

Figure 4.7 LVDT Locations

Figure 4.8 LVDT and BDI Set Up

Each beam was subjected to a total of three load cycles. The first load cycle involved loading the beam just past the point where the

tension concrete cracked. To accomplish this, the standard beam was loaded up to 12 kips per actuator and then unloaded. The two MMFX and CFRP beams were loaded up to 10 kips per actuator and then unloaded. The second load cycle was same as the first. This second load cycle was conducted to make sure that the beam, after cracking, performed in a linear fashion. The third load cycle involved loading the beam to failure. Due to the high loads of the third cycle the BDI gages were removed. The loading for this load cycle was deflection controlled. This means that the actuators loaded the beam at a constant rate of deflection per time (as opposed to the first 2 cycles which used a constant loading rate). This type of deflection control is necessary when loading to failure. However, since the beam and set-up is not a perfect system, it means that for the failure load cycle, the loads in the two actuators are not identical. Each beam was loaded until the center deflection was 7 inches. Due to the failure of the strain gages at higher strains, some data is not available at the later stages of the tests.

Figure 4.9 Typical Test Set Up

4.4 Test Results

This section describes the laboratory test results for the four test beams. For each beam a load-deflection curve and load-strain curve to failure are presented. The load-strain curves use data from the internal strain gages near both the top and bottom of the beams. The load P that is being plotted is the sum of the two loads (spaced four feet apart). Due to the set up and loading of the third load cycle, one actuator was consistently loading at a slightly higher rate than the other. This meant that the constant moment region in the center of the beam was in fact not quite constant. This can be seen by drawing a moment diagram of the beam. The higher load was then used to calculate the moment in the beam at yield. Figure 4.10 illustrates the load P that is being plotted.

Additional plots (for the other load cycles) and photographs of the failed beams are given in the Appendix.

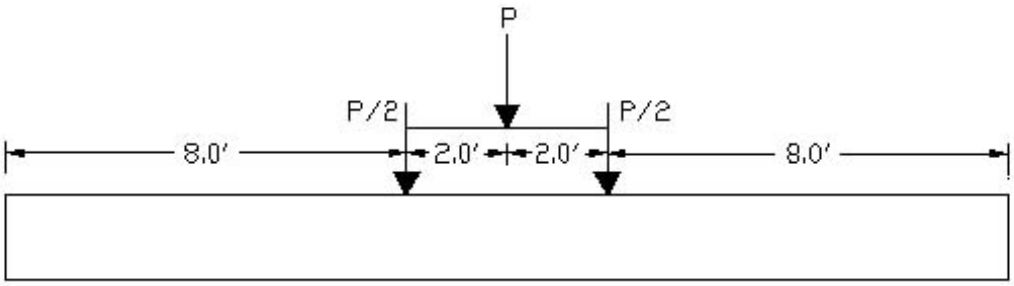

Figure 4.10 Load Set Up

4.4.1 Standard Beam

As mentioned in section 3.5, the standard beam was used as a control test for the other beams. Figures 4.11 and 4.12 illustrate the load-deflection and load-strain behavior of the standard beam.

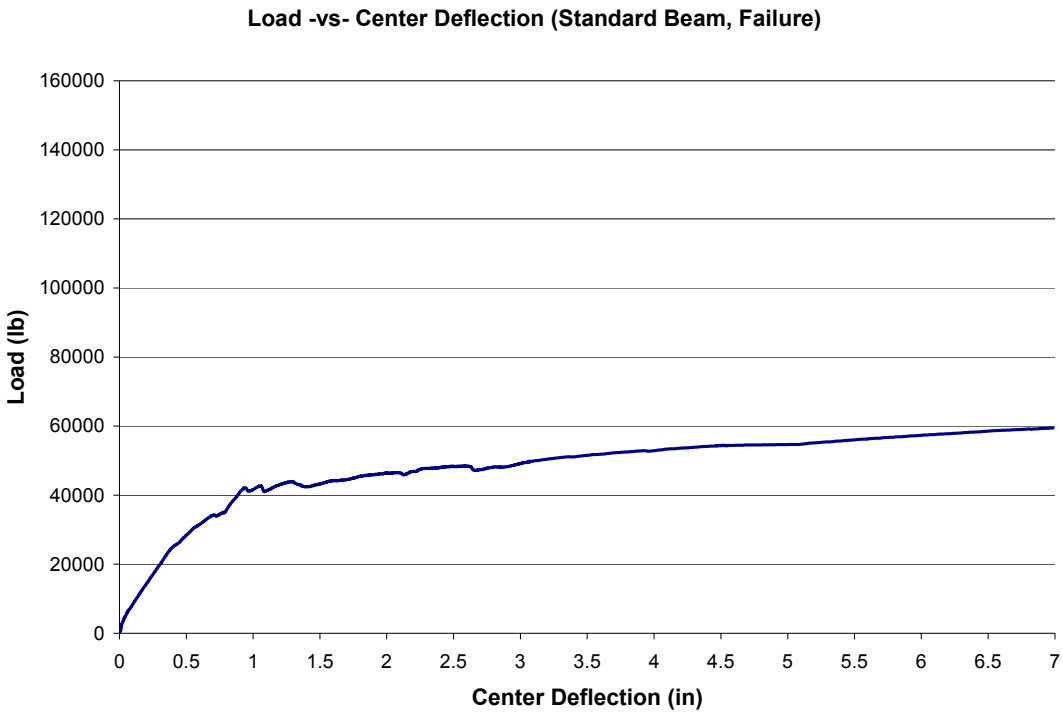

Figure 4.11 Load versus Center Deflection, Standard Beam

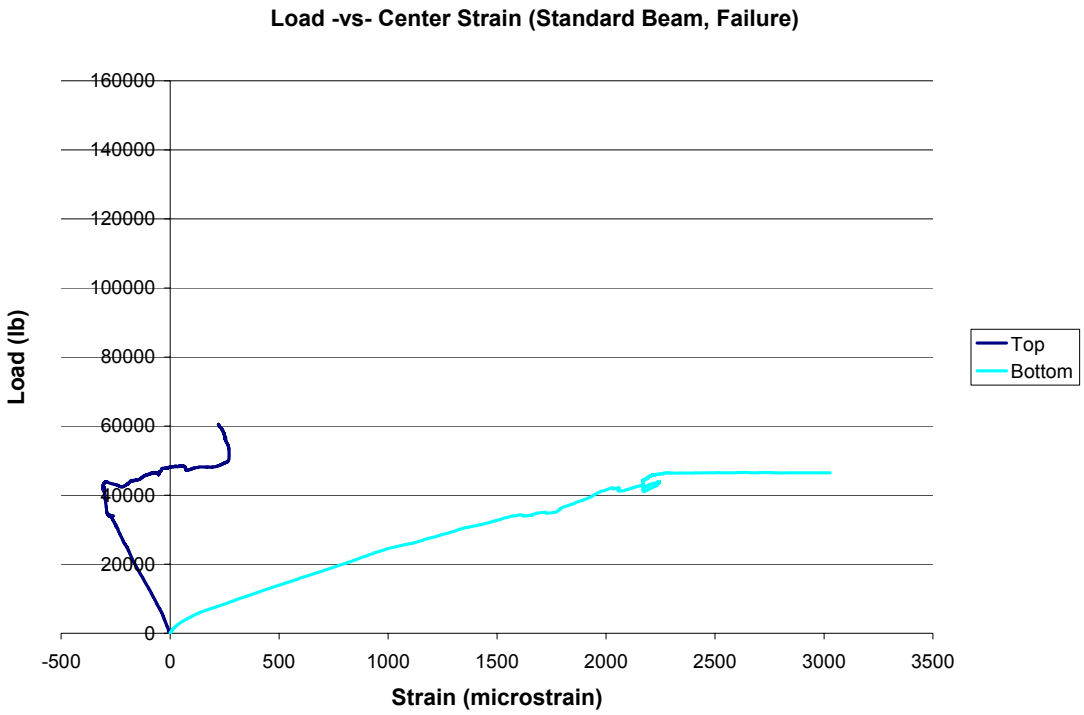

Figure 4.12 Load versus Center Strain, Standard Beam

Figure 4.11 illustrates that the standard beam started to yield at approximately 42,000 lbs. which is the total load. Using Figure 4.12 it was verified that the flexural reinforcement started to yield around 42,000 lb. The moment at yielding is estimated to be approximately 172,800 ft-lb. From Figure 4.12 the strain at yielding was approximately 0.002. A more detailed analysis of the standard beam will be presented in section 4.5.

4.4.2 MMFX4 Beam

As mentioned in section 3.5, the MMFX4 beam replicates the design used in bridge 1-712B. The yield strength of the flexural

reinforcement used in design was 60 ksi, and as such the same number of bars was used as would have been used if standard rebar was employed. Figures 4.13 and 4.14 illustrate the load-deflection and load-strain behavior of the beam.

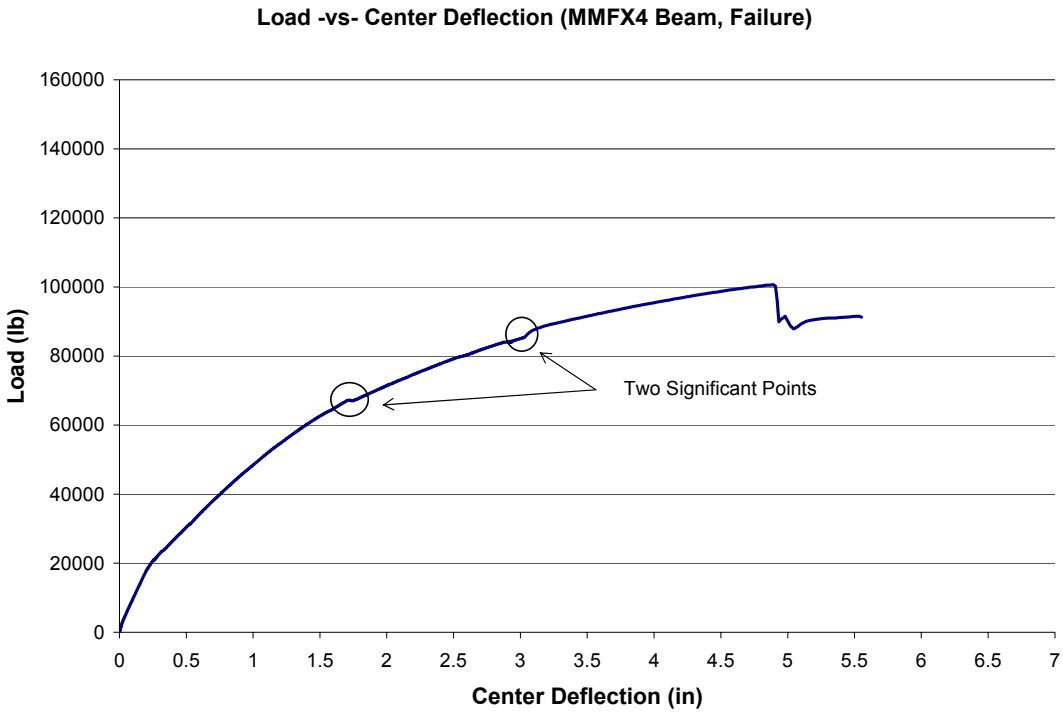

Figure 4.13 Loads versus Center Deflection, MMFX4 Beam

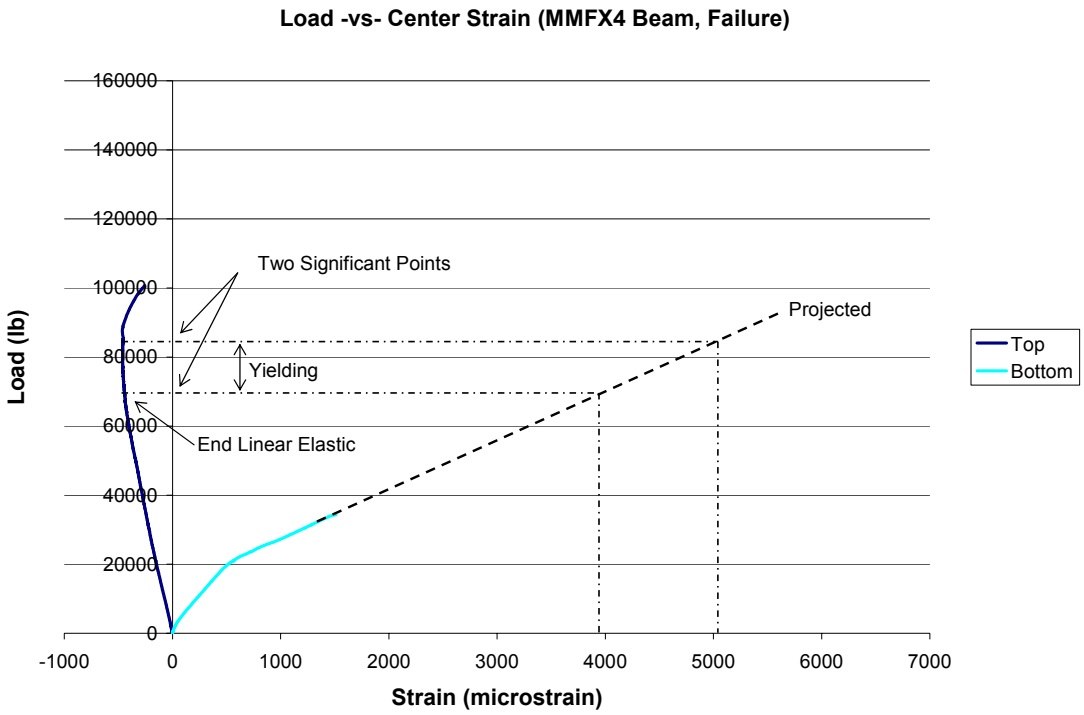

Figure 4.14 Load versus Center Strain, MMFX4 Beam

Figure 4.13 shows that the beam did not exhibit the classic linear elastic-plastic response that is common with steel flexural reinforcing. Instead, the load-displacement graph displays a smooth curve representing more gradual softening of the beam without a distinct yield point. Figure 4.13 shows that the beam, not necessarily the steel, softens as more load is applied. Based on the design calculations in chapter 3, the MMFX4 beam was expected to yield at approximately 301,490 ft-lb (which corresponds to a load of 82,000 lbs.). However, there is no clear point of yielding on the load-displacement graph. At approximately 400,000 ft-lb the concrete crushed. The moment at which the concrete crushed is much higher than

the moment necessary to yield the steel. It is not clear, however, from the load-deflection graph where the MMFX steel starts to yield, this was also the case with the tensile test results for the MMFX rebar. There are two significant points on the load-deflection graph. The two points correspond to loads of approximately 68,000 lbs. and 85,000 lbs. These points represent clear changes in the behavior of the beam and are believed to be points of yielding of the MMFX rebar. The two load points from the load-displacement graph were placed on the load axis of the load-strain plot (Figure 4.14). The two load points corresponded to two noticeable points on the top strain gage plot. The lower load point corresponds to when the beam moves into the plastic region (the plot of the top strain gage is no longer linear). Dashed-dot horizontal lines were drawn from the two load points to a projected line of the bottom (tensile bar) strain gage plot (since this gage stopped functioning). These lines intersected the projected dashed line of the bottom strain gage plot. Two dashed-dot vertical lines were drawn from the points of intersection to the x-axis (strain). The tensile strain corresponding to these two points are approximately 0.0039 and 0.0051. These strains fall within the range of when the MMFX rebar is expected to yield. Using 123 ksi as the yield strength of the MMFX rebar (tested value), the corresponding strain at yield is approximately 0.0042. The moments, corresponding to the two load points, ranged between 254,700 and 314,230 ft-lb which also fall into the range of the design yielding moment of 301,490 ft-lb. Due to the difference of the two actuator loads, the beam likely started yielding under

the higher actuator load and the yielding progressed along the beam to the location of the second actuator. It is also useful to compare the response of the MMFX4 beam to the standard beam. Figure 4.5 illustrates the load-deflection graph for both the standard and MMFX4 beams.

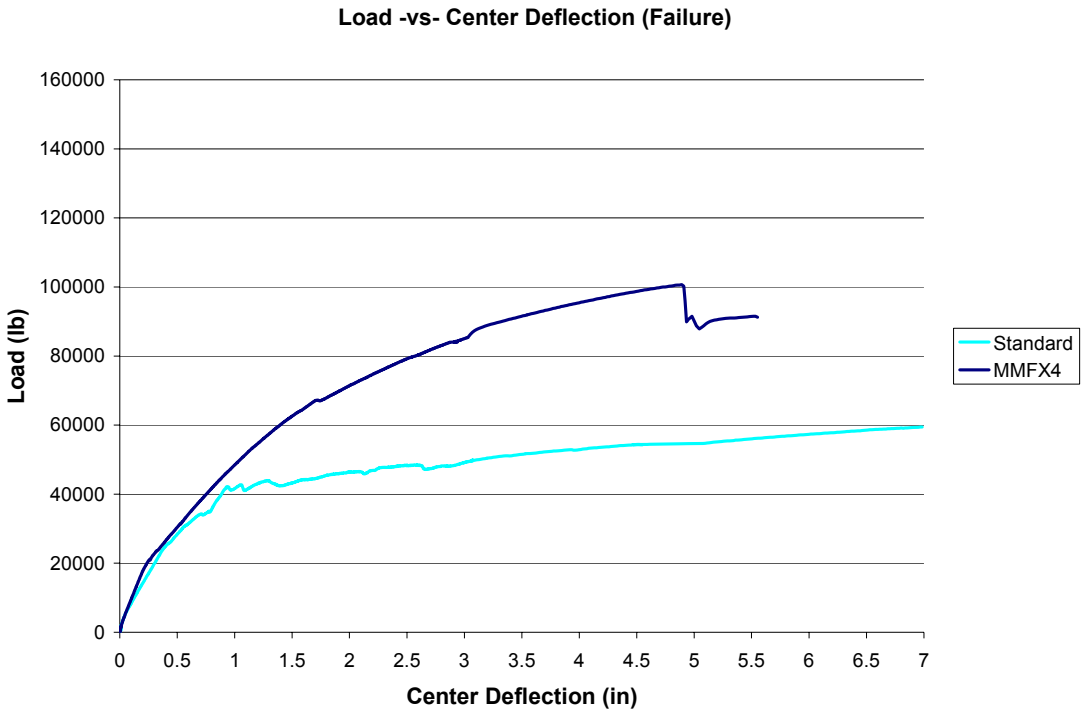

Figure 4.15 Comparison of Standard Beam to MMFX4 Beam

From the above graph it can be seen that the MMFX4 beam has a higher load capacity but does not exhibit as clear a plastic region. The ultimate deflection of the MMFX4 beam is on the order of 4 inches (corresponding to L/56). The standard beam had not yet completely failed as a deflection of 7 inches. In terms of ductility, while the standard beam clearly has more

ductility, the MMFX4 beam also exhibits ductility. The strain diagram in Figure 4.14 does not help illustrate the yielding of the MMFX bars. The bottom strain gage stopped reading strain at approximately 34,500 lbs. and 1,500 microstrain (well short of the yield strain of 4,200 microstrain). A more detailed analysis of the MMFX4 beam is presented in section 4.5.

4.4.3 MMFX2 Beam

The MMFX2 beam was designed assuming the actual yield strength of MMFX steel. By using the actual yield strength less steel was used in the beam, and by design it is expected to have had a moment capacity that is similar to the standard beam. Figures 4.16 and 4.17 illustrate the load-deflection and load-strain behavior of the MMFX2 beam.

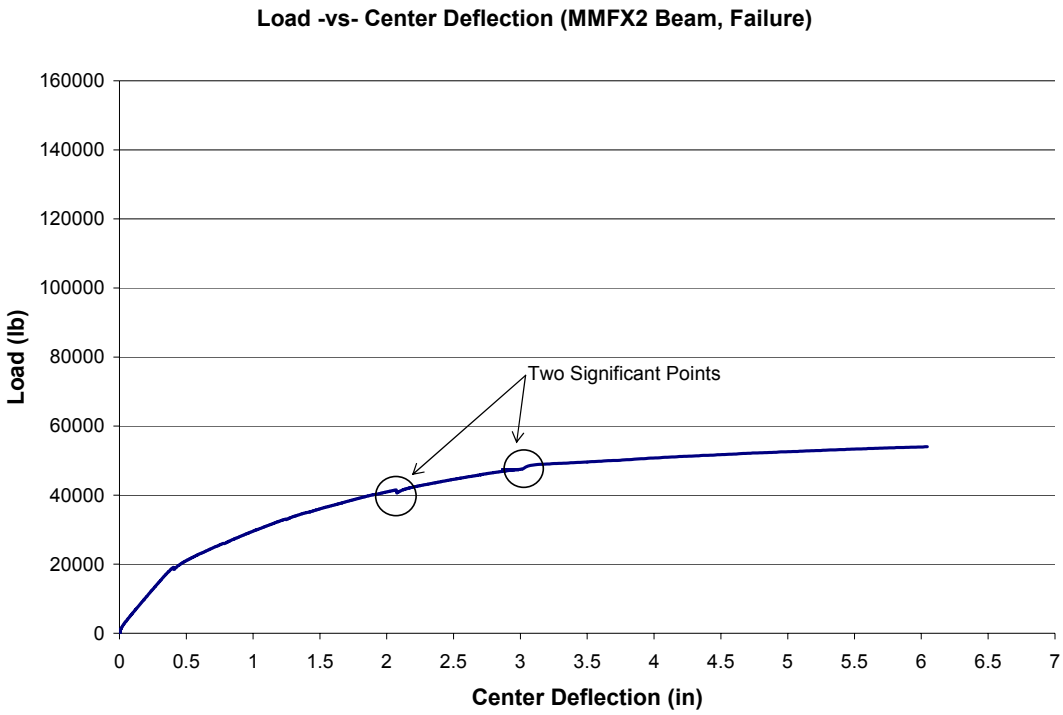

Figure 4.16 Load versus Center Deflection, MMFX2 Beam

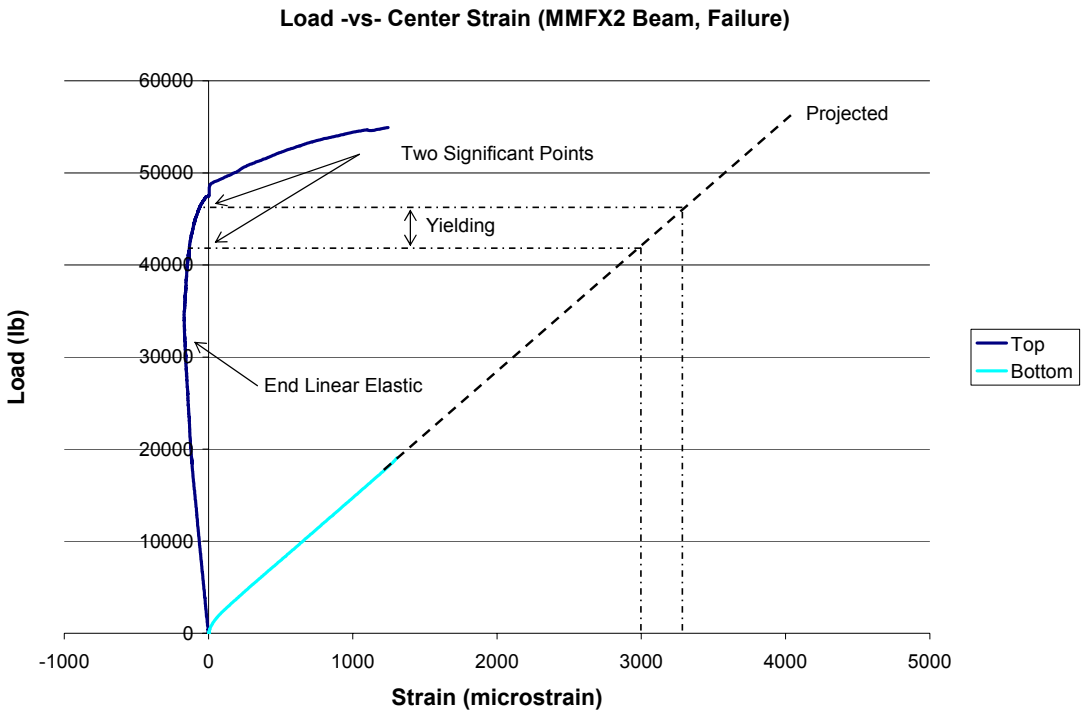

Figure 4.17 Load versus Center Strain, MMFX2 Beam

The load-deflection curve in Figure 4.16 demonstrates the same behavior as the MMFX4 beam. Again, since the bottom strain gage stopped reading data early on in the test, it is not useful for finding the yielding point of the flexural reinforcement. Based on the design calculations in chapter 3, the MMFX2 beam was expected to yield at approximately 154,300 ft-lb (which corresponds to a load of 42 kips). However, there is no clear point of yielding on the load-displacement graph. There are two significant points on the load-deflection graph. The two points correspond to the loads of approximately 41,000 lbs. and 47,500 lbs. These points represent clear changes in the behavior of the beam and are believed to be points of

yielding of the MMFX rebar. Using the same method as the MMFX4 beam (see Figure 4.17) the two significant points correspond to moments of 154,750 and 177,980 ft-lb which are just outside the design yielding moment, calculated in chapter 3, of 154,300 ft-lb. Additionally, the strains in the bottom gage, using a projection of the bottom strain data, read 0.003 and 0.0032 which are low slightly lower than the yield strain of the MMFX rebar of 0.0042. It should be noted that the projection of the bottom strain data may not be as accurate for the MMFX2 beam. This is due to the failure of the bottom strain gage at approximately 18,000 lbs. From Figure 4.16 it can be seen that the plot changes slope at approximately 19,000 lbs. just after the strain gage for the MMFX2 beam failed. Looking back at Figures 4.13 and 4.14 for the MMFX4 beam, it can be seen that once the load-deflection plot changed slopes (approximately at 20,000 lbs.) the bottom strain gage plot also changed slopes. The MMFX2 beam's bottom strain gage failed before the load-deflection graph changed slopes. This may account for the corresponding strains, using the projection of the bottom strain gage plot, being lower than expected. However, the load points of 41,000 and 47,500 lbs. do correlate to a change in the compression strain plot in Figure 4.17. It is also useful to compare the response of the MMFX4 beam to the standard beam. Figure 4.18 illustrates the load-deflection graph for both the standard and MMFX2 beams.

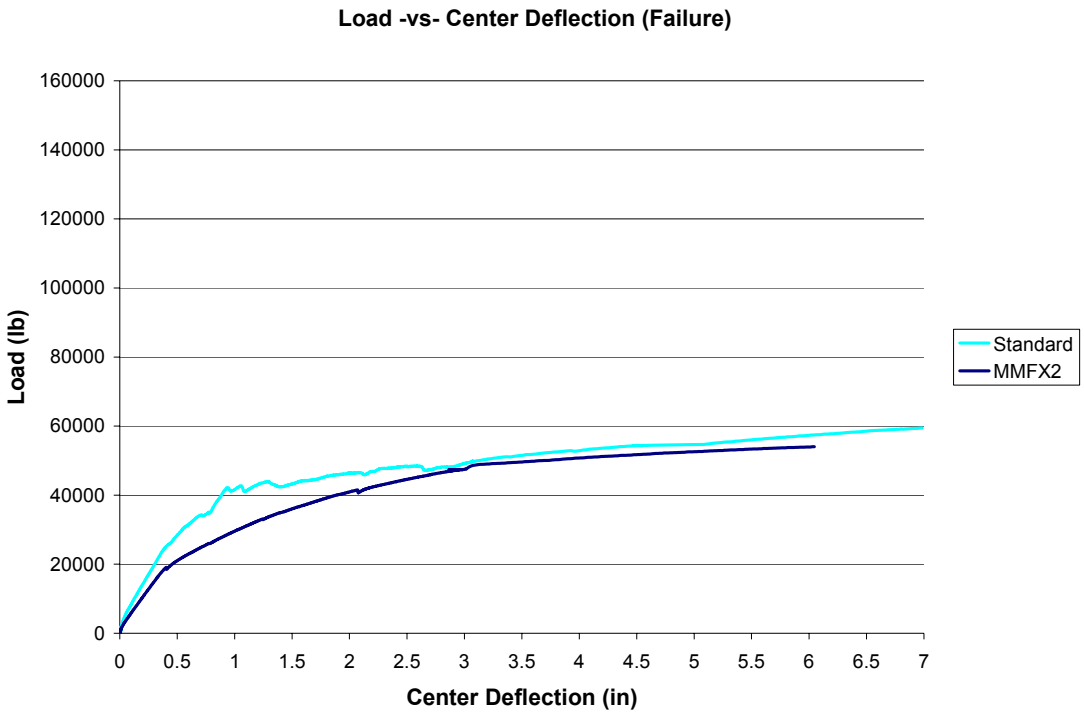

Figure 4.18 Comparison of Standard Beam to MMFX2 Beam

Figure 4.18 illustrates that the MMFX2 beam had very similar strength to that of the standard beam (distinct bar sizes make it impossible to select a specific area of steel and so the two designs were made to be as close as possible). Again it is not clear exactly where the MMFX steel yields. Also, the MMFX2 beam softens more gradually as the load increases and does not have a pronounced linear elastic-plastic behavior. The comparison of the two beams shows that by using the higher yield strength in design for the MMFX beam less flexural reinforcement was used and the strength of the beam is very similar to the standard beam which had four bars of flexural reinforcement. The ultimate deflection of the MMFX2 beam is on

the order of 6 inches (corresponding to L/37). Ductility, which can be defined by the area under the curve, is similar but somewhat less for the MMFX2 beam. A more detailed analysis of the MMFX2 beam is presented in section 4.5.

4.4.4 CFRP Beam

The CFRP, unlike the steel reinforced beam, behaves linear until either the concrete crushed or the CFRP rebar fractures. Figures 4.19 and 4.20 illustrate the load-deflection and load-strain behavior of the CFRP beam.

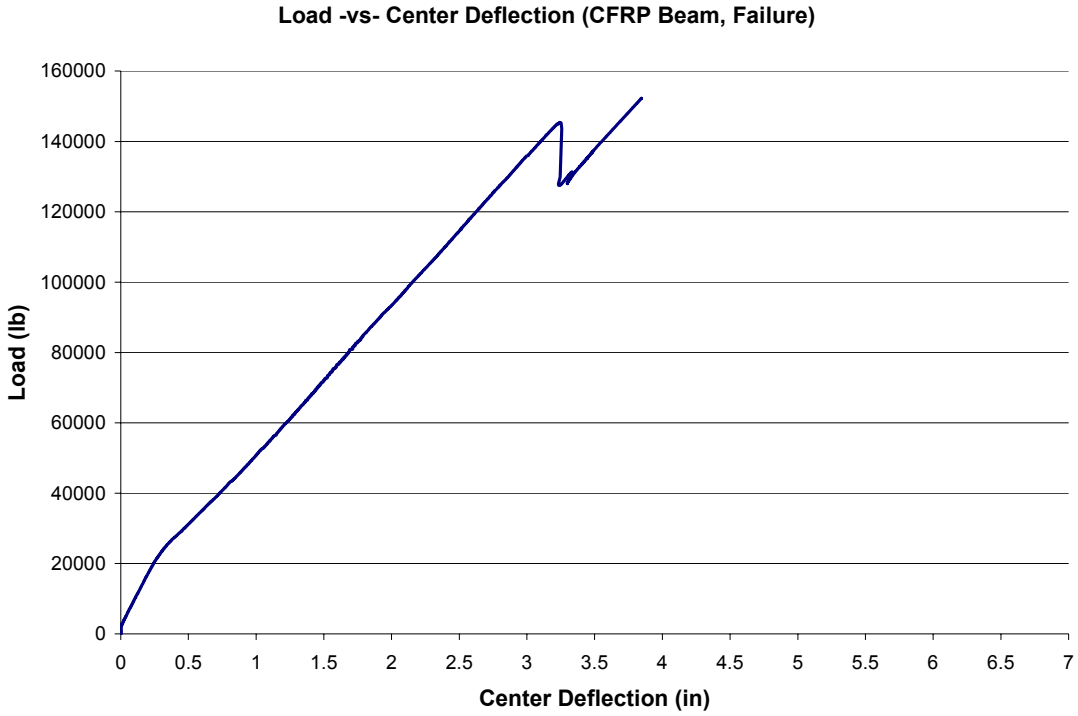

Figure 4.19 Load versus Center Deflection, CFRP Beam

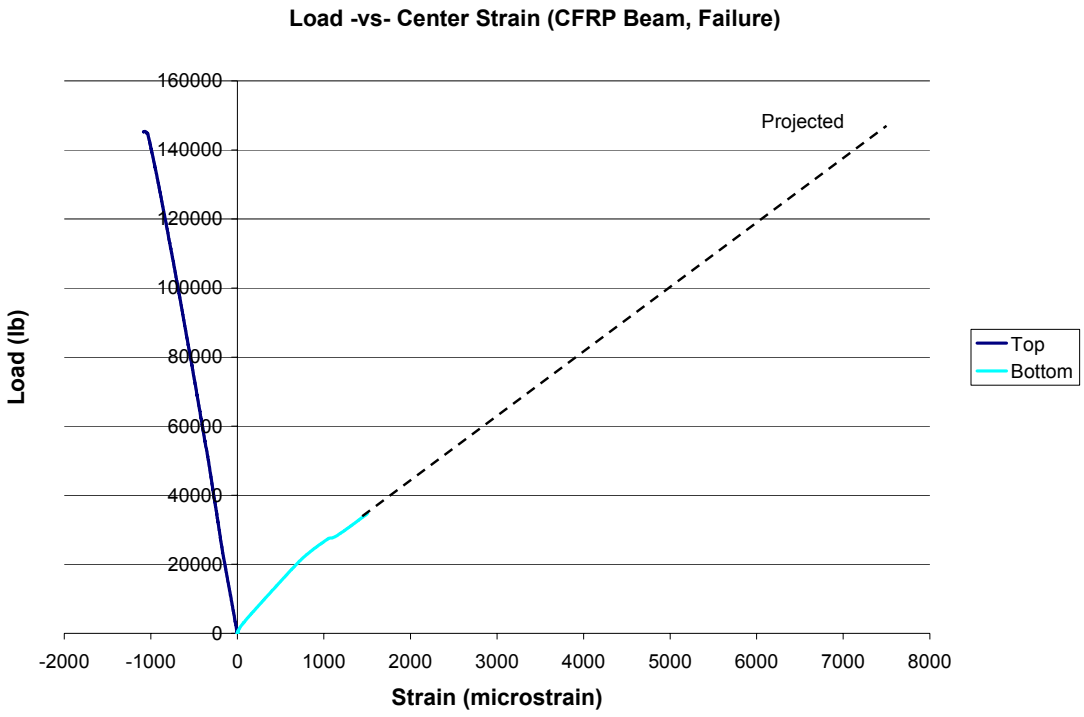

Figure 4.20 Load versus Center Strain, CFRP Beam

Figure 4.19 illustrates that the CFRP beam behaves linearly until the point where the compression concrete crushes. Figure 4.19 also shows that the CFRP rebar has not fractured but carries load after the concrete crushes. The concrete crushed at a total load of approximately 145,000 lbs. The moment at crushing was calculated to be approximately 553,890 ft-lb.

The bottom strain gage stopped reading strain at approximately 34,700 lbs. and 1,500 microstrain. A more detailed analysis of the CFRP beam is presented in section 4.5.

Figure 4.21 compares the load-deflection plots of the CFRP beam to the standard beam.

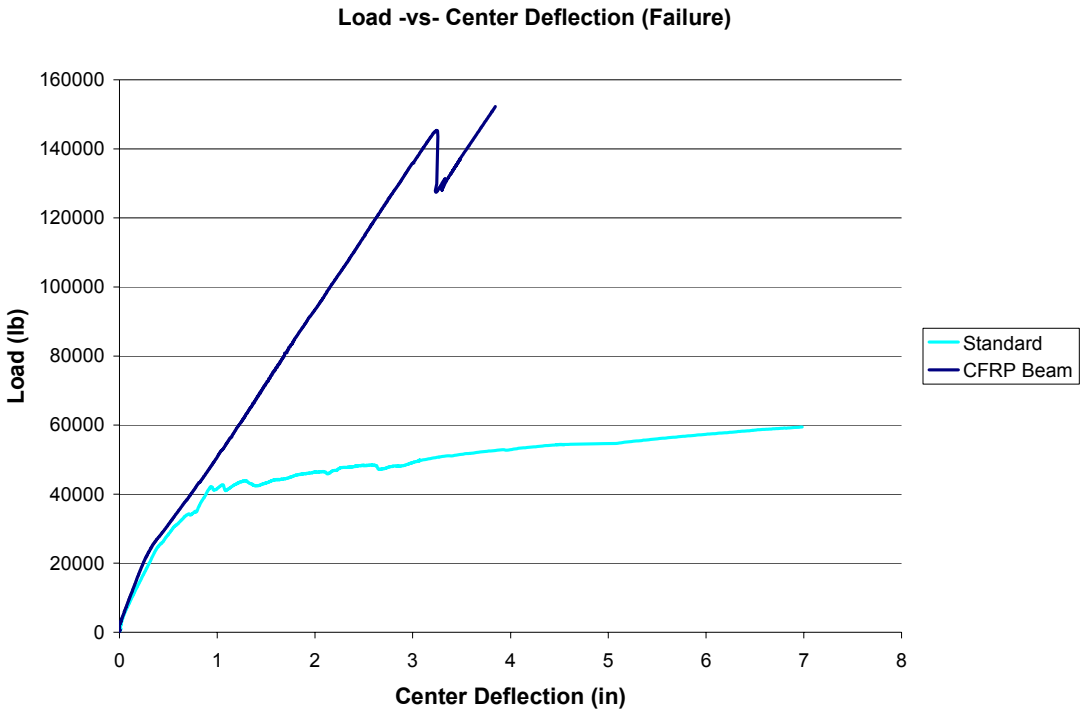

Figure 4.21 Comparison of Standard Beam to CFRP Beam

Since deflection controlled the design of the CFRP test beam the deflections in the service load region of the load-deflection graph are very similar to that of the standard beam. Had the amount of CFRP reinforcing in the beam needed for strength been placed in the beam, deflections

would have been greater in the service load region. The ultimate deflection of the CFRP is on the order of 3.8 inches (corresponding to L/59). The CFRP beam lacks a yield plateau and has much less ductility than the standard beam. The CFRP beam also has a much higher capacity than the standard beam.

4.5 Comparison of Laboratory Results to Theoretical Design

Section 4.4 presented the basic results of the four point bending tests and made comparisons of some of the tests to others. This section will compare the test results to the theoretical/design calculations through tables for each beam. The tables report the failure moment (yield or compression failure), deflection at yield, cracking moment, and load carried at L/800. The theoretical/design calculations use the actual material property values discussed section 4.2. The actual calculated yield moments (standard, MMFX4, and MMFX2 beams) and compression failure moment (CFRP beam), as discussed in section 4.4, used the higher actuator load from the third load cycle and a total span length of the beam of 18.67 feet. This length takes into account the 8 inch overhang at the end supports of the beam. The actual yield moments and compression failure moment were calculated by taking the actuator loads corresponding to the failure of the beam (either yield or compression failure) from the laboratory test data and drawing a moment diagram for each beam. The theoretical/ design moments were calculated by dividing the design moment capacities of the beams in chapter 3 by 7.33 feet (the distance of the actuators from the supports). The 18.76 feet is also used in the new

calculation of the L/800 value. The L/800 value corresponding to a span of 18.67 feet is 0.28 inches. The actual failure deflection (yield or compression failure) of the beams was found by using the load-deflection graphs for each beam. Using Excel spreadsheets set-up to calculate the theoretical deflections of the beams the theoretical/design deflections at yield were found. Using the load necessary to reach the design moment capacity of the beam the corresponding deflection was calculated. The identification of cracking moments for the tested beams were found using load values from the load-deflection and load-strain data from the first load cycle where the two actuator loads where consistent with each other. The actual cracking moments of the test beams were found using the load-deflection and load-strain plots for the first and second load cycles. The theoretical/design cracking moments of the test beams were calculated using traditional methods and the ACI 440 guide. The actual load at L/800 was obtained from the load-deflection data for each of the beams. The theoretical/design load at L/800 was calculated using the deflection Excel spreadsheets by calculating the load necessary to reach a deflection of L/800. Note that the yield deflection and load at L/800 were calculated for the mid-span of the test beams. As mentioned earlier, the load-deflection and load-strain plots for the first and second load cycle are found in the Appendix.

4.5.1 Standard Beam

The following table compares the theoretical/design calculations to the actual values from the laboratory tests.

Table 4.3 Standard Beam Comparison

Test Results

Yield Moment	Yield Deflection	Cracking Moment	Load at L/800
159,237 ft-lb	0.94 inches	48,385 ft-lb	20,153 lbs

Theoretical/Design Calculations

Yield Moment	Yield Deflection	Cracking Moment	Load at L/800
160,790 ft-lb	0.71 inches	63,520 ft-lb	26,000 lbs

The test results are approximate values since the yielding point from the load-deflection and load-strain plots is not very precise. However, the identified yielding moment of the test beam is very close to the theoretical/design calculation. The somewhat lower cracking moment, load at L/800 and the higher yield deflection of the test beam as compared to the theoretical calculations may be due to the concrete cover of the shear stirrups. The stirrups had a concrete cover of 1.5 inches on the bottom of the beam and 1.0 inch on the sides of the beam; this is how all the beams were fabricated. The one inch cover on the sides may have caused the beam to crack somewhat early. As a result of the beam cracking earlier than the design cracking moment, deflections and the load at L/800 would be directly effected. Furthermore, prediction of concrete cracking is based on empirical modulus of rupture of the concrete of $7.5\sqrt{f'_c}$. As predicted, the failure mode of the beam was the yielding of the flexural reinforcement. This was clearly reached in the test. Due to high ductility of this beam, and due to the limitations of the laboratory testing machine, the test was not taken out to the point where the compression concrete crushed.

4.5.2 MMFX4 Beam

The MMFX4 beam did not behave the same way as the standard beam. None of the plots of the beams load-deflection and load-strain behavior, as well as the stress-strain behavior of the MMFX, illustrated a clear point of yield. As a result, in Table 4.4 a range of values are given for the yield moment as well as the deflection of the beam at yield. The table compares the theoretical/design calculations to the actual values from the laboratory tests.

Table 4.4 MMFX4 Beam Comparison

Test Results

Yield Moment	Yield Deflection	Cracking Moment	Load at L/800
254,700 - 314,230 ft-lb	1.8 - 3.0 inches	44,230 ft-lb	21,916 lbs

Theoretical/Design Calculations

Yield Moment	Yield Deflection	Cracking Moment	Load at L/800
301,490 ft-lb	1.51 inches	67,010 ft-lb	27,320 lbs

From Table 4.4 it can be seen that the range of moments calculated in section 4.4.2 are accurate and fall within the design yield moment region. Again, the range of moments were calculated by projecting the bottom strain gage plot from the load-strain graph to load points found on the load-deflection graph and correlating them to where the compression

strain gage data started to change slope. Through this method of projections the reported range of yielding moments are not exact. In comparison to the standard beam, the MMFX4 beam exhibited a higher moment capacity due to the higher yield strength of the MMFX rebar. Again, early cracking of the beam directly effected the yield deflection and the load carried at L/800 causing the respective values to be higher and lower than predicted.

4.5.3 MMFX2 Beam

The MMFX2 beam displayed the same characteristics as the MMFX 4 bar beam. Table 4.5 compares the theoretical/design calculations to the actual values from the laboratory tests.

Table 4.5 MMFX2 Beam Comparison

Test Results

Yield Moment	Yield Deflection	Cracking Moment	Load at L/800
154,750 - 177,980 ft-lb	2.0 - 3.0 inches	42,818 ft-lb	16,275 lbs

Theoretical/Design Calculations

Yield Moment	Yield Deflection	Cracking Moment	Load at L/800
154,300 ft-lb	0.905 inches	67,010 ft-lb	25,260 lbs

The range of yielding moments was calculated using the same method as was used for the MMFX4 beam. The range of yielding moments calculated for the MMFX2 beam is slightly above the theoretical/design moment (but

still, the predicted capacity is relatively accurate). In comparison to the standard beam the MMFX2 beam had approximately the same moment capacity but with half of the flexural reinforcement. The beam cracking early may have caused the high yield deflection and low load at L/800.

4.5.4 CFRP Beam

Table 4.6 compares the theoretical/design calculations to the actual values from the laboratory tests.

Table 4.6 CFRP Beam Comparison

Test Results

Crushing Moment	Crushing Deflection	Cracking Moment	Load at L/800
555,537 ft-lb	3.24 inches	41,196 ft-lb	22,273 lbs

Theoretical/Design Calculations

Crushing Moment	Crushing Deflection	Cracking Moment	Load at L/800
546,050 ft-lb	2.64 inches	62,410 ft-lb	25,400 lbs

As predicted the design failure mode of the CFRP reinforced beam was the of the compression concrete crushing. The moment equation used for the design of the CFRP beam was very accurate in predicting the beams ultimate capacity. Because the equation uses the stress in the flexural reinforcement at the time of failure of the compression concrete, the moment equation is based on the modulus of the CFRP bars and not the ultimate stress. Even though the ultimate stress of the bars should be known through testing procedures it is not necessary for the calculation of the moment capacity of the beam. The

ACI 440 R-01 guide, as mentioned previously, provides several equations for the calculation of the moment capacity of a beam reinforced with FRP. Again, the early cracking moment may have been due to the one inch cover of the shear reinforcement.

Figure 4.22 illustrates the failure of the CFRP reinforced beam.

Figure 4.22 Failure of the CFRP Reinforced Beam

Chapter 5

DIAGNOSTIC LOAD TEST OF BRIDGE 1-712B

5.1 Instrumentation

When the seven concrete beams for bridge 1-712B were fabricated, they were all instrumented with strain gages. The strain gages used to instrument the bridge beams consisted of two sister bars in a set up identical to that used for the test beams as explained in section 3.5. One of the two gages was located in the bottom of the beam and the other was located in the top of the beam. Both gages were placed at the mid-span of the beams. The bottom gage was placed in the center of the beams cross section and 2.25 inches up from the bottom of the beam. The top gage was also placed in the center of the beams cross section and 3.25 inches down from the top of the beam. It should be noted that the beams were 15 inches deep with 5 inches of composite concrete deck being added in the field. As such, the top strain gage ends up being 8.25 inches down from the top of the final 20 inch deep beam. The lead wires from the gages were run out of the ends of the beams. Once the beams were placed on the bridge the lead wires were run out of the south edge of the bridge and connected to a permanent junction box that was located on the abutment wall. Figures 5.1 and 5.2 illustrate the location and set up of the junction box.

Figure 5.1 Location of the Junction Box

Figure 5.2 Set Up of the Junction Box

5.2 Diagnostic Load Test Procedure

A diagnostic load test of bridge 1-712B was conducted on March 18, 2003. During the test, the bridge was loaded with a single three axle dump truck filled with sand and weighing 58,060 lbs. The truck's front axle weighed 15,670 lbs. and the two back axles weighed 21,370 and 21,020 lbs. each. Only one truck was used for the diagnostic load test because bridge 1-712B was designed for a single lane load. Figures 5.3 and 5.4 illustrate the truck used for the test and the spacing and weights of the trucks axles.

Figure 5.3 Load Test Truck

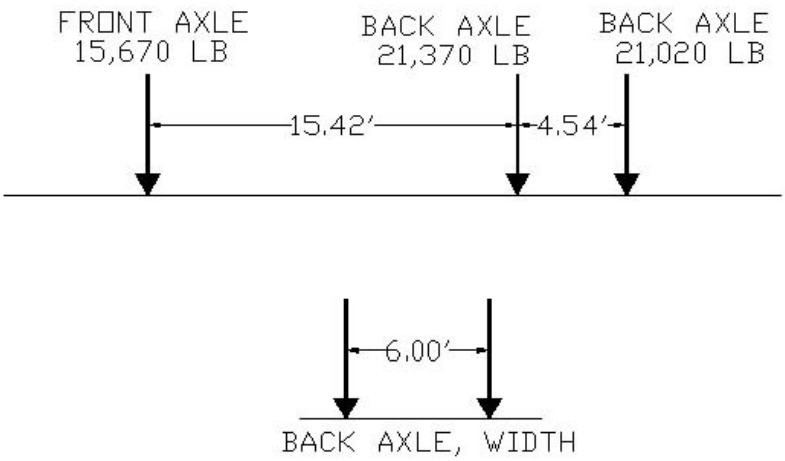

Figure 5.4 Axle Weights and Spacing

Five static tests were run on the bridge. The first static test involved placing the front axles of the truck at the quarter point of the bridge. For this test the truck was centered width wise on the bridge. The second static test involved placing the front axles of the truck at midspan of the bridge, again with the truck centered width wise. The third static test involved centering the rear axle tandem at midspan and again centered width wise. The fourth and fifth tests involved placing the rear axle tandem at midspan of the bridge but with the truck located one foot off of the concrete parapets on either edge of the bridge. Each of the five tests were run twice to check for consistency of the response. It should be noted that the test procedure, as mentioned, was run in two cycles (test one through five were run and then repeated). Figure 5.5 illustrates the location of the centroid of the loading axle(s) for each of the five tests. It

also should be noted that because of the 15.42 foot spacing between the front axle and the forward rear axle, each test consisted of only the front axle or rear axle tandem being on the bridge at a time (i.e. only a single axle load). The dots in Figure 5.5 represent the location of the center of the axle(s) of the test truck on the bridge. The center of the tires were located a distance of 3 feet on either side of the dots.

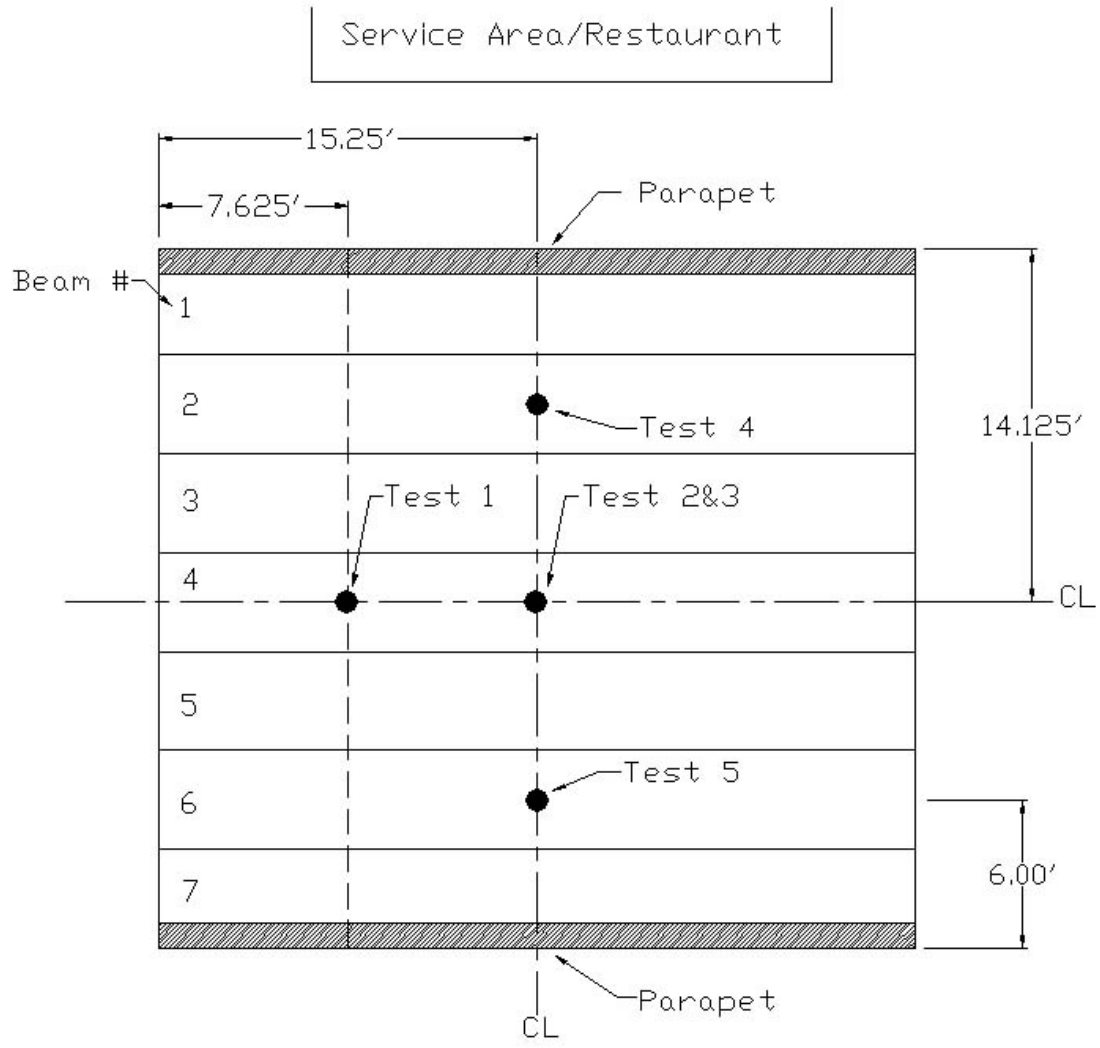

Figure 5.5 Load Test Set Up

5.3 Diagnostic Load Test Results

Figures 5.8 through 5.12 illustrate the strain distribution across the width of the bridge 1-712B beams. The strain readings were zeroed out based on initial strain readings taken before the load test. After the

final test was finished the strains were read again. It was noticed that there was some drift between the first and second load cycle strain readings. The magnitude in some cases was on the order of 10 microstrain. The drift in strains may be due to the way the test was conducted. Since the load test truck represents a fairly heavy load for the bridge, permanent strains may have been induced into the beams on the initial load cycle. For this reason only the strain data recorded during the first load cycle will be used in all calculations found in this section and section 5.4.

Using the data acquired by MMFX mill reports and concrete cylinder tests, material properties fro the steel and concrete were found to be f_y = 114 ksi, f'_c of the slab = 6.645 ksi, and f'_c of the beams = 10.102 ksi. Based on these values the theoretical cracking moment of the beams was calculated to be approximately 201 ft-kip which corresponds to 124 microstrain in the bottom face of the beams. Through strain analysis of the dead load and recorded live load strains, along with visual inspection of the bridge, the bridge beams were found to have cracked (either prior to or during the load test). Figures 5.6 and 5.7 illustrate cracks that were observed at the midspan of the bottom face of the bridge beams.

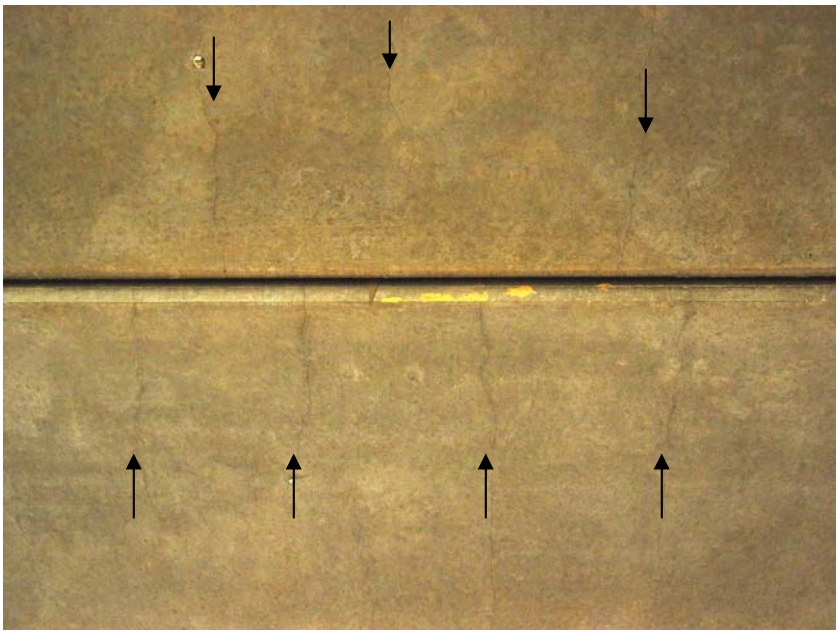

Figure 5.6 Cracked Bridge 1-712B Beam (Bottom Face)

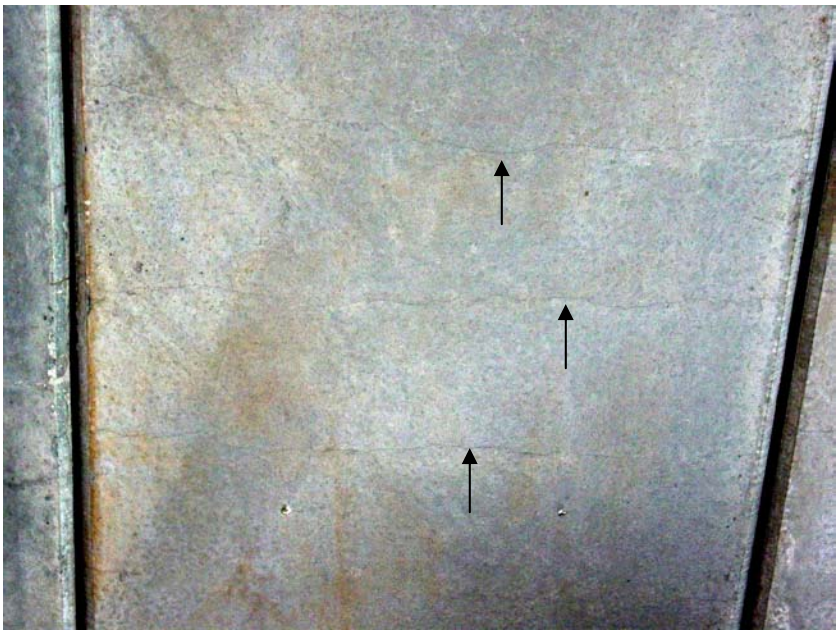

Figure 5.7 Cracked Bridge 1-712B Beam (Bottom Face)

The strain induced in the bottom face of the beams due to dead load was calculated to be approximately 76 microstrain. The remaining strain necessary to theoretically crack the beams, if the dead load induced strain is subtracted out from the calculated cracking strain of 124 microstrain, is 48 microstrain. Figures 5.10 through 5.12 (representing rear axle loadings) illustrate that the live load strains recorded during the diagnostic load test surpass the 48 microstrain needed to theoretically crack the beams.

In section 5.4 an analysis of the behavior of the bridge beams will be compared to the MMFX4 laboratory test beam.

Figures 5.8 through 5.12 illustrate the strains that were recorded in all seven beams during the five load tests. Each graph presents the first and second load cycles as described in section 5.2 and illustrated in Figure 5.5.

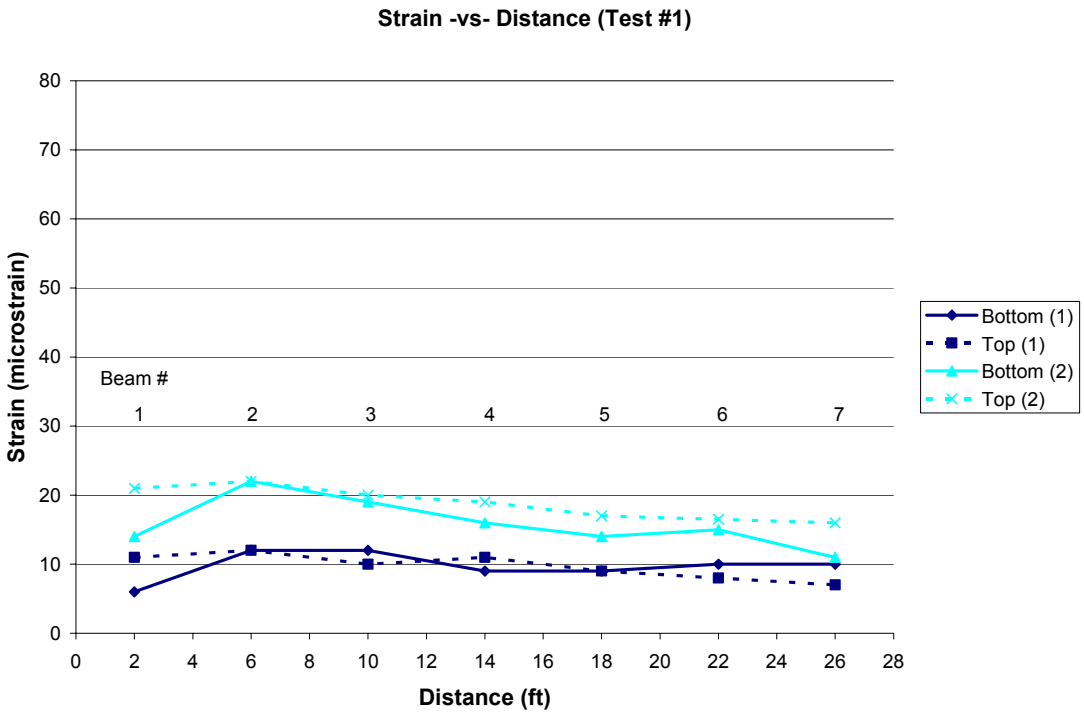

Figure 5.8 Strain Distribution for Test #1

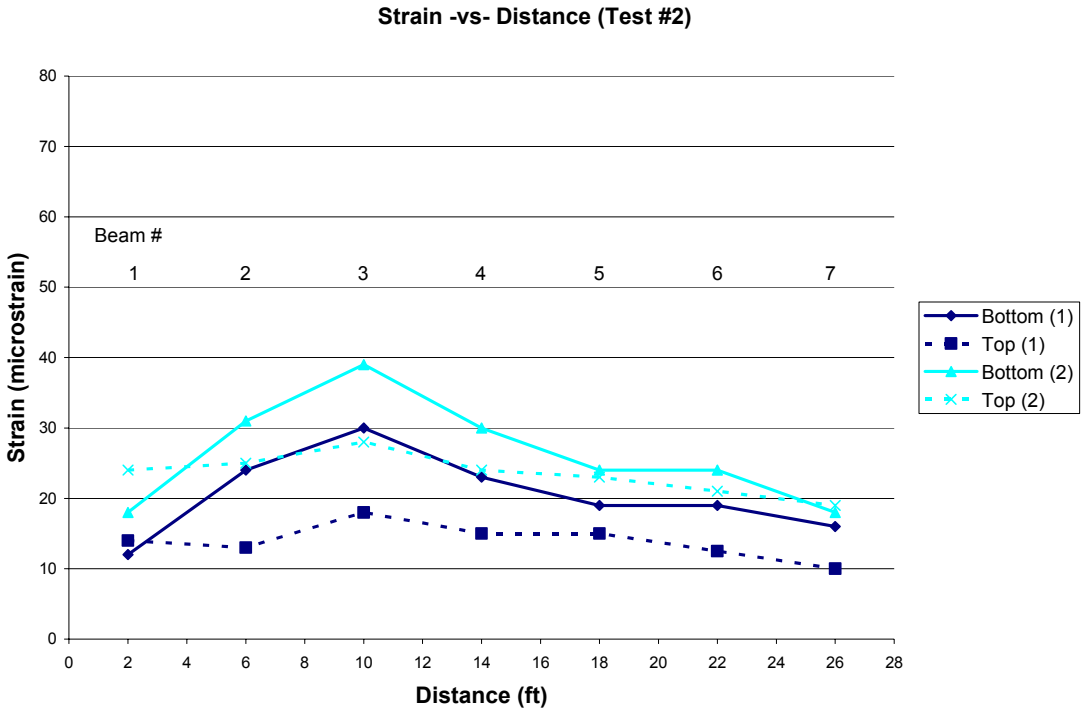

Figure 5.9 Strain Distribution for Test #2

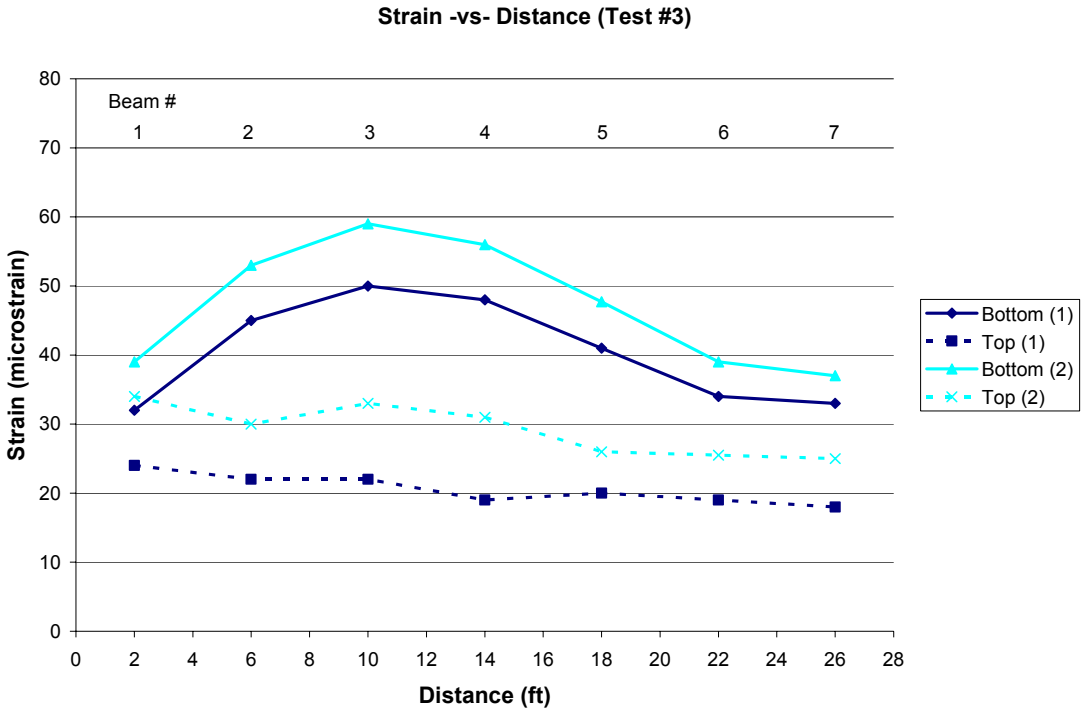

Figure 5.10 Strain Distribution for Test #3

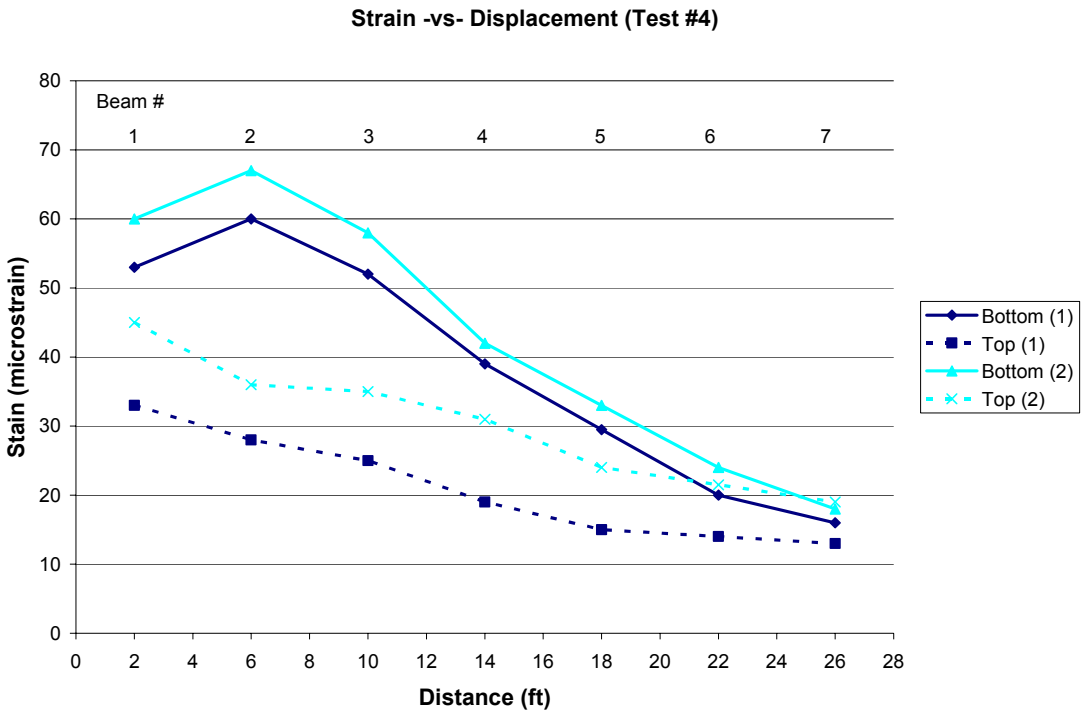

Figure 5.11 Strain Distribution for Test #4

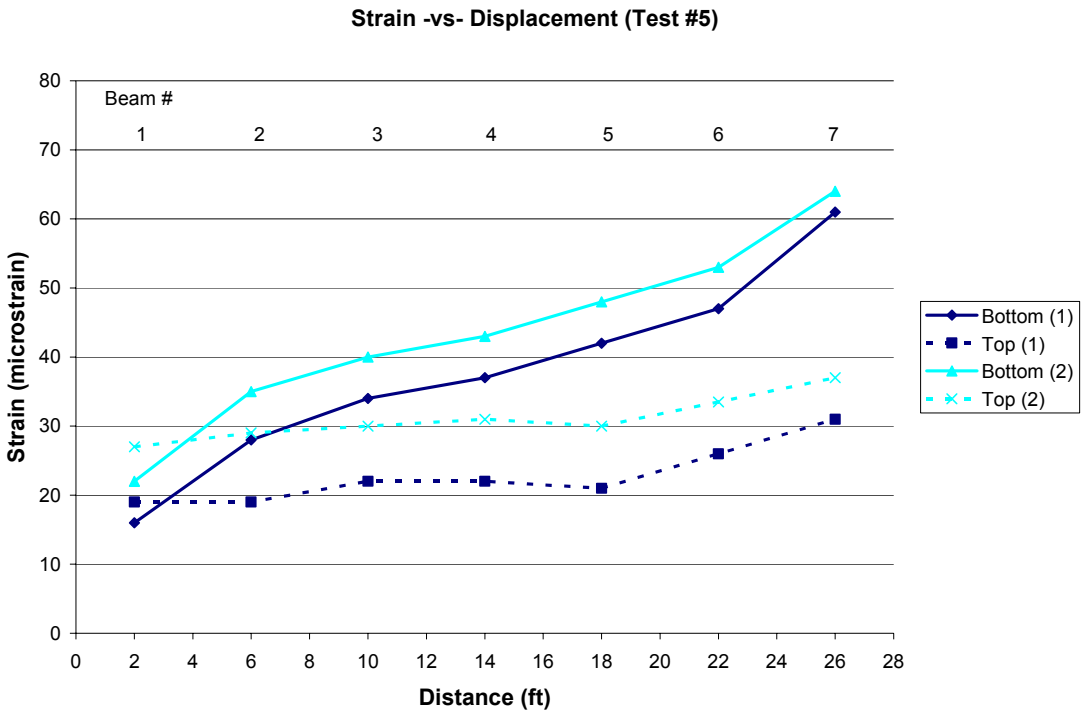

Figure 5.12 Strain Distribution for Test #5

The previous graphs illustrate how the load was distributed transversely through the bridge beams. The data points on the graphs represent the strain in each of the seven beams. The points are plotted at the center of the beam, 4 feet from the center of the adjacent beam. Recall that the bridge is approximately 28 feet wide, with seven 4 foot wide beams. In the graphs, straight lines are used to connect the data points. The graphs show that the strain does distribute to all of the beams in all of the tests. The data point which goes from 0 to 4 feet (data point at 2 feet) in the graphs corresponds to beam #1 in Figure 5.5 while the beam which goes from 24 to 28 feet (data point at 26 feet) corresponds to

beam #7 in Figure 5.5. Please note that the bottom strain gage of the beam #5 (which goes from 16 to 20 feet corresponding to the data point at 18 feet) was estimated because all the data recorded by that strain gage was found to be suspect. The data associated with that beam was estimated by averaging the strains for beams #4 and #6. Also, note that the top strain gage in beam #6 (which goes from 20 to 24 feet corresponding to the data point at 22 feet) was not working during the test and the strains shown on the plots have been again estimated by averaging strains of adjacent beams.

Figures 5.8 to 5.10, which involve loadings centered width wise on the bridge, indicate that one side of the bridge appears to have more stiffness than the other. This may be due to the added stiffness and orientation of the parapets and may also be due to the support conditions (acting somewhere between simply supported and fixed-fixed) of each beam. It can also be seen from the graphs that the strains recorded during the load test were relatively low. The highest strain recorded was just under 70 microstrain. This corresponds to approximately 2 ksi for the steel rebar. An interesting observation can be made by looking at the top strain readings. All of the readings are positive which would indicate that the top strain gages, located 8.25 inches down from the top of the beam, were in tension. The positive strain readings in the top strain gages suggest that the neutral axis of the beams is above the gages as would be expected for a beam that has cracked.

Distribution Factor

Using the test results from the bottom gages of the first load cycle, a distribution factor (DF) for the beams of the bridge can be found. The distribution factor was found by dividing the maximum strain recorded in a given beam by the sum of the strain readings from all seven beams. Using this procedure, Test #5 produced the highest distribution factor. Using the bottom strain gage data from the first test of Test #5 the distribution factor calculated was 0.230. The distribution factor used in the design of the bridge was 0.283. Comparing the distribution factor calculated from the load test to the design distribution factor shows that the design value was conservative (experimental DF is 18.7% lower than the design DF). When the truck was positioned in the center of the bridge the load was distributed more uniformly over all of the beams than when the truck was located on either side of the bridge. The distribution factors calculated using the first load cycle ranged from 0.176 to 0.230. The worst loading case for the bridge was found to be when the truck was located next to either of the parapets.

Support Fixity

Tests were used to verify the end conditions of the bridge. Bridge 1-712B was designed as simply supported. The theoretical strains that the front axle of the load truck would produce at midspan of the bridge with the truck located at both the quarter point and midspan of the bridge (Test #1 and #2) were normalized so they could be compared to

the corresponding normalized strains for each beam found during the test. Table 5.1 gives both the theoretical and measured normalized strains produced by the load truck for the two end conditions. The first end condition analyzed was simply supported (SS) and the second was fixed-fixed (FF).

Table 5.1 Normalized Strains

Theoretical			Measured (First Cycle)						
	SS	**FF**	***1***	***2***	***3***	***4***	***5***	***6***	***7***
Test #1	**0.502**	**0.251**	0.500	0.500	**0.400**	**0.391**	**0.474**	0.526	0.625
Test #2	**1**	**1**	1	1	**1**	**1**	**1**	1	1
				% Fixity	40	44	11		

The headings in Table 5.1 (1 through 7) represent the bridge beams; Figure 5.5 shows the bridge beam numbering. The bolded values under the Measured (First Cycle) headings represent the normalized strains for beams directly beneath the test truck. These beams were the best candidates for comparison since the load truck was directly loading them. If the bridge beams were actually acting as simply supported the corresponding normalized strains would match the normalized strain values that appear under the SS heading in Table 5.1. If the bridge beams were acting as fixed-fixed the corresponding normalized strains would match the values that appear under the FF heading in Table 5.1. From Table 5.1 it can be seen that the beams that are carrying the truck, beams

#3, #4 and #5, fall in-between the simply supported and fixed-fixed end conditions (100% fixity means a FF boundary condition while 0% fixity means a SS boundary condition). Beam #3 had a calculated ratio of 60% simply supported and 40% fixed-fixed (i.e. 40% fixity). Beam #4 had a calculated ratio of 56% simply supported and 44% fixed-fixed (i.e. 44% fixity). Beam #5 had a calculated ratio of 89% simply supported and 11% fixed-fixed (i.e. 11% fixity). Using the average of these values the bridge beams behave as having 32% fixity. It is very possible that the degree of fixity will decrease over the life of the bridge.

5.4 Correlation to Design and Laboratory Tests

The data that was recorded during the diagnostic bridge load test was also compared to the laboratory tests that were performed on the MMFX4 beam. As mentioned in section 3.5, the MMFX4 beam is reinforced with the same percentage of MMFX rebar as the bridge beams and has the same depth. One difference between them is that the MMFX4 beam is one-third the width of the bridge beams and has one-third the number of reinforcing bars (but same percentage of steel).

All five bridge tests were compared to the MMFX4 laboratory beam test. For each test, the moment that caused the recorded strain in each beam during the load test truck is compared to the moment that caused the same strain in the laboratory test. It should be noted that only the bottom strains were used since the locations of the top strains were not at the same depth. At a given strain the moment in each bridge beam

produced by the test truck was calculated based on the total moment and the distribution of strains across the bridge width. Essentially, individual DFs were calculated for each beam and the total moment was distributed accordingly. The total moment was calculated using either the front and rear tandem axle(s). Using simply supported conditions, total moments were calculated for a single beam using the respective load truck axle(s) locations on the bridge. The moment produced at midspan of the beam due to the front axle being at the quarter point of the beam was 60 ft-kip. The moment produced at midspan of the beam due to the front axle being at the midspan of the beam was 119.5 ft-kip. The moment produced at midspan of the beam due to the rear tandem axles being at midspan of the beam was 274 ft-kip. Once the total moment (for each respective test) was calculated and distributed to each of the seven bridge beams, it was divided by 3 (recall the lab beam is one-third width) so it could be compared to the laboratory beam moments at a given strain. The comparison of the bridge beam moments to the laboratory beam is not expected to yield an exact relationship. The cross sections of the bridge beams are slightly different from that of the laboratory beam. The bridge beams have a 5 inch concrete overlay with strength of 6.6 ksi where the laboratory beam has a concrete strength of 10.1 ksi throughout the entire beam. This difference in concrete strength is a relatively significant difference as one can see by using a transformed section analysis. Also the concrete overlay on the bridge has an MMFX grid that reinforces the slab. This extra reinforcing is not found in the laboratory beam. This is

not expected to cause significant differences in response. Finally, assumptions in calculating moments versus measuring response directly are also present.

Tables 5.2 to 5.6 compare the corresponding moments in the bridge and laboratory beams at various levels of strain recorded in the bottom of the beams. In other words, when the bridge and laboratory beam have the same strain in the bottom sister bar, what is the comparison of applied moment? It should be noted that Tables 5.2 to 5.6 uses the data from the first load cycle that was run on the bridge and data from the post-cracked load cycle run on the MMFX4 beam.

Table 5.2 Comparison of Moments for Test #1

Test #1 (First Load Cycle)							
Beam #	***1***	***2***	***3***	***4***	***5***	***6***	***7***
Strain (microstrain)	6.00	12.00	12.00	9.00	9.00	10.00	10.00
DF	0.088	0.176	0.176	0.132	0.132	0.147	0.147
Moment*DF (ft-kip)	7.91	15.81	15.81	11.86	11.86	13.18	13.18
Moment/3 (ft-kip)	**2.64**	**5.27**	**5.27**	**3.95**	**3.95**	**4.39**	**4.39**
MMFX4 Beam Moment at Strain Value (ft-kip)	**2.91**	**5.22**	**5.22**	**4.27**	**4.27**	**4.58**	**4.58**
Difference %	9.43	0.98	0.98	7.41	7.41	4.09	4.09

Table 5.3 Comparison of Moments for Test #2

Test #2 (First Load Cycle)							
Beam #	***1***	***2***	***3***	***4***	***5***	***6***	***7***
Strain (microstrain)	12.00	24.00	30.00	23.00	19.00	19.00	16.00
DF	0.084	0.168	0.210	0.161	0.133	0.133	0.112
Moment*DF (ft-kip)	10.03	20.05	25.07	19.22	15.88	15.88	13.37
Moment/3 (ft-kip)	**3.34**	**6.68**	**8.36**	**6.41**	**5.29**	**5.29**	**4.46**

MMFX4 Beam Moment at Strain Value (ft-kip)	**5.22**	**8.29**	**9.79**	**8.02**	**7.14**	**7.14**	**6.57**
Difference %	35.97	19.37	14.65	20.13	25.88	25.88	32.17

Table 5.4 Comparison of Moments for Test #3

Test #3 (First Load Cycle)							
Beam #	***1***	***2***	***3***	***4***	***5***	***6***	***7***
Strain (microstrain)	32.00	45.00	50.00	48.00	41.00	34.00	33.00
DF	0.113	0.159	0.177	0.170	0.145	0.120	0.117
Moment*DF (ft-kip)	31.08	43.70	48.56	46.61	39.82	33.02	32.05
Moment/3 (ft-kip)	**10.36**	**14.57**	**16.19**	**15.54**	**13.27**	**11.01**	**10.68**
MMFX4 Beam Moment at Strain Value (ft-kip)	**10.01**	**13.02**	**13.76**	**13.42**	**11.93**	**10.60**	**10.30**
Difference %	3.48	11.88	17.63	15.78	11.25	3.83	3.71

Table 5.5 Comparison of Moments for Test #4

Test #4 (First Load Cycle)							
Beam #	***1***	***2***	***3***	***4***	***5***	***6***	***7***
Strain (microstrain)	53.00	60.00	52.00	39.00	29.50	20.00	16.00
DF	0.197	0.223	0.193	0.145	0.109	0.074	0.059
Moment*DF (ft-kip)	54.05	61.19	53.03	39.77	30.08	20.40	16.32
Moment/3 (ft-kip)	**18.02**	**20.40**	**17.68**	**13.26**	**10.03**	**6.80**	**5.44**

MMFX4 Beam Moment at Strain Value (ft-kip)	14.40	15.54	14.17	11.74	9.74	7.52	6.57
Difference %	25.11	31.25	24.74	12.92	2.96	9.59	17.22

Table 5.6 Comparison of Moments for Test #5

Test #5 (First Load Cycle)							
Beam #	*1*	*2*	*3*	*4*	*5*	*6*	*7*
Strain (microstrain)	16.00	28.00	34.00	37.00	42.00	47.00	61.00
DF	0.060	0.106	0.128	0.140	0.158	0.177	0.230
Moment*DF (ft-kip)	16.59	29.04	35.26	38.37	43.56	48.74	63.26
Moment/3 (ft-kip)	**5.53**	**9.68**	**11.75**	**12.79**	**14.52**	**16.25**	**21.09**
MMFX4 Beam Moment at Strain Value (ft-kip)	**6.57**	**9.44**	**10.60**	**11.18**	**12.11**	**13.29**	**15.68**
Difference %	15.81	2.54	10.89	14.41	19.90	22.26	34.49

The percent difference values in the last row of the tables correspond to the difference between the moments in the laboratory beam to the field beams at the same strain level. Tables 5.2 to 5.6 illustrate that the difference between the laboratory and the field beams results range from 0.98% to 35.97%. This means that the beams in the field compare relatively well to the laboratory beam, however there is still some difference between moments corresponding to similar strains in the bridge beams and the laboratory beam. This most likely difference come from differences in support conditions and the fact that the bridge beams and laboratory beam have different strength concrete (6.645 ksi and 10.102 ksi respectively) in the top 5 inches of the beams. Considering a bridge beam with one third width (same width as the laboratory beam), the

bridge beams top 5 inches of concrete can be transformed into a new section if the concrete strength is changed from 6.645 ksi to 10.102 ksi (the concrete strength used throughout the MMFX4 beam). Changing the concrete strength from 6.645 to 10.102 ksi yields a new width (with equivalent strength) of 10.52 inches. Now both the transformed bridge beams and laboratory beam have a concrete strength of 10.102 ksi but have different cross sections and thus different moments of inertia. By comparing the theoretical stress in both beams given by $\sigma = My/I$ for the same applied moment, a ratio between the bridge beams and laboratory beam can be calculated. Using the above mentioned stress equation, the moment of inertia of the transformed cross section of the bridge beam, and the moment of inertia of the laboratory beam, the stress in the bridge beams was calculated to be approximately 16.3% smaller than the stress in the laboratory beam. The above stress calculation can easily be transformed into strain using the modulus of concrete to yield the same 16.3% difference between the strain in the bridge beams and the laboratory beam. This theoretical comparison gives some insight into the differences in moment at the same strain between the bridge beams and laboratory beam. Also, the moment calculations in Tables 5.2 to 5.6 assumed that the bridge beams acted as simply supported so that they could be compared to the MMFX4 beam (which was simply supported in the laboratory test). Section 5.3 showed that the actual bridge beams behave with 32% fixity. If the moments produced by the test truck were recalculated taking in to account the 32% fixity, the total moment that was

calculated assuming simply supported would decrease in magnitude and may have somewhat more compatibility with the MMFX4 laboratory beam. Both of these factors could make the compared moments and strains even more consistent.

Chapter 6

CONCLUSIONS

Corrosion of steel rebar in concrete beams and decks reduces the design life of many concrete structures. New types of rebar such as epoxy coated, stainless clad, FRP, and MMFX rebar have been introduced to reduce or prevent corrosion. DelDOT chose to utilize MMFX and CFRP rebar in their design and alternative design for the reconstruction of bridge 1-712B. To validate the design methods and the performance of MMFX and CFRP rebar a laboratory and field study was conducted.

6.1 Summary of Laboratory Results

The following is a summary of results from the four point bending tests of the standard beam, MMFX4 beam, MMFX2 beam, and the CFRP beam.

- Both ultimate loads and mode of failure were predicted with good accuracy using traditional equations for the MMFX reinforced beams and the new ACI 440 R-01 guidelines for the CFRP beam.
- Yield deflection calculations were smaller and load at L/800 calculations were greater than the actual measured yield deflection and load at L/800 values for all beams. This may have been due to early cracking. All beams cracked at a similar load level. However, crack width sizes were not recorded during the tests.

- The MMFX4 beam did not display a distinct yield point. By projecting the data on the load-strain plots, the predicted yield moment was found to lie within the observed range.

- The MMFX4 beam, which had approximately twice the amount of tensile reinforcement ($A_s f_y$) of the standard beam, displayed a higher strength than the standard beam.

- The MMFX2 beam also did not display a distinct yield point. By projecting the data on the load-strain plots, the predicted yield moment was found to lie just outside of the observed range.

- The MMFX2 beam, which had a comparable amount of tensile reinforcement ($A_s f_y$) of the standard beam, had a comparable strength to the standard beam.

- Both MMFX beams failed in the desired mode. For both beams, the MMFX rebar yielded prior to failure.

- While both MMFX beams reached relatively high deformation states before failing, neither displayed as much ductility as the standard beam. The MMFX2 beam did display more ductility than the MMFX4 beam which was closer to being over-reinforced.

- The CFRP beam failed as desired, with the compression concrete crushing before the CFRP rebar fractured. The ultimate moment was predicted well by the ACI 440 R-01 design guidelines.

- Due to the low modulus of the CFRP rebar, the design of this beam was controlled by deflection. The high CFRP reinforcement ratio enabled this beam to deform similarly to the standard beam.

- Due to the high percentage of CFRP reinforcement, the CFRP beam's strength was much higher than the other beams.

- Tensile tests performed on the CFRP rebar identified the elastic modulus of the bars but were unable to reach the rupture stress of the bars. Most of the

moment capacity equations in the ACI 440 R-01 do not use the ultimate strength of the bars, but rather use the modulus of the bars to calculate the stress in the bars at the time of failure of the compression concrete.

6.2 Diagnostic Load Test Summary

The following is a summary of the results of the diagnostic load test that was performed on bridge 1-712B using a 29 ton three axle dump truck.

- The maximum live load strain at the level of the tensile reinforcement was approximately 70 microstrain. This corresponds to a steel rebar stress of 2 ksi.
- The distribution factor of the bridge calculated by using the results of the load test was 0.230 as compared to the design value of 0.283. This means that the actual bridge is distributing load better than assumed in the design (18.7% improvement).
- The bridge was designed to act as a simply supported span. The results of the load test indicate that the bridge has approximately 32% fixity at its supports.
- Both the measured strains during the test, as well as visual inspection, confirm that the bridge beams have cracked.
- Both AASHTO and ACI have placed limits on the yield strength (75 ksi and 80 ksi respectively) that can be used for the flexural reinforcement in concrete beams. These limits are to limit the yield strain of higher strength steel to be about equal to the maximum usable concrete strain in compression. Having a yield strength of approximately of 100 ksi, MMFX rebar falls outside of these limits. As such, its use as the primary reinforcement in the concrete beams is questionable. MMFX may, however, be used in concrete decks.

6.3 General Observations and Comments

Through observations in the laboratory and field, the following recommendations are made:

- Since MMFX has a yield strength close to twice that of regular steel, designers must be careful to not design beams that are over-reinforced when using MMFX as a direct replacement for standard steel reinforcement.
- Designers must also be aware that MMFX does not exhibit a clear yield point and its ductility is clearly less than that of regular steel rebar.
- MMFX reinforced beams may exhibit larger cracks than standard reinforced beams, especially if fewer higher strength bars are used for the tensile reinforcement.
- When designing with CFRP it was found that deflection controlled the design. As such, CFRP beams will have somewhat excessive strength.

6.4 Recommendations for Future Work

Based on the work done here, the following are needed areas of future study:

- Since tensile testing of the CFRP rebar to failure was difficult due to slipping of the rebar prior to failure, better ways of gripping the CFRP rebar are needed.
- Since MMFX has a distinctly different stress-strain behavior from normal rebar (no distinct yield point), analytical methods are needed to allow better prediction of MMFX reinforced beam load-deformation behavior up to failure.
- Current AASHTO and ACI Codes limit the use of high strength steel for conventional reinforced concrete beams. Additional testing should be conducted to evaluate the given limits

- Continued monitoring of the MMFX corrosion resistance properties are needed. As part of a corollary study, researchers at the University of Delaware are studying corrosion of MMFX rebar in bridge 1-712B and bridge 1-119.

Appendix

LOAD-DEFLECTION AND LOAD-STRAIN GRAPHS

On the following pages one will find photographs of the four laboratory test beams as well as graphs from the first, second and third load cycles. The graphs will be presented by illustrating first, the load-deflection behavior followed by a corresponding load-strain graph. The graphs will be in the order of successive load cycles; pre-cracked cycle, post-cracked cycle, and failure cycle, for each of the four beams. The graphs will be in the following order:

The following pictures were taken during the laboratory testing of the standard beam.

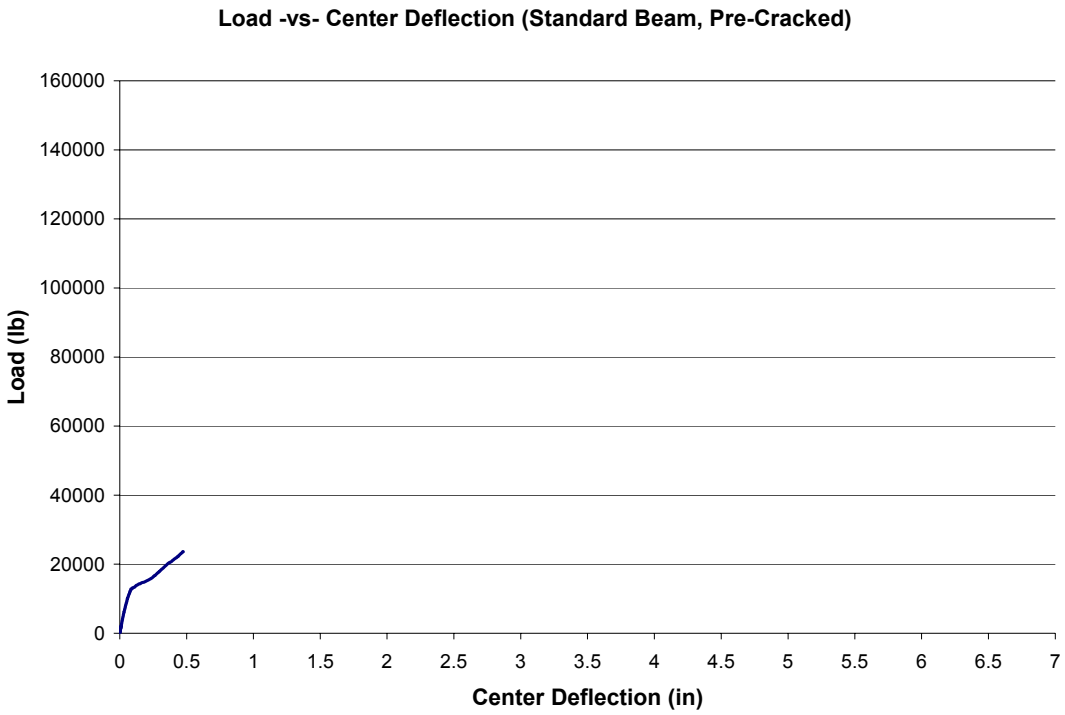
Load -vs- Center Deflection (Standard Beam, Pre-Cracked)
160000
140000
120000
100000
80000
60000
40000
20000
0
Load (lb)
0
0.5
1
1.5
2
2.5
3
3.5
4
4.5
5
5.5
6
6.5
7
Center Deflection (in)

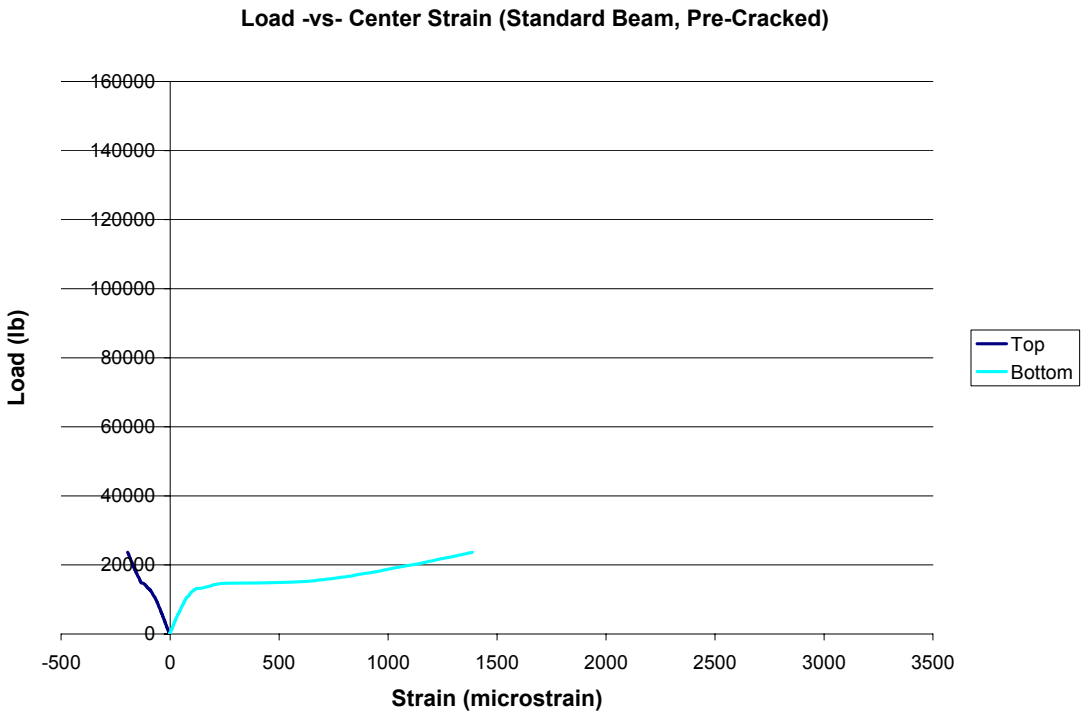
Load -vs- Center Strain (Standard Beam, Pre-Cracked)
160000
140000
120000
100000
80000
60000
40000
20000
0
Load (lb)
-500
0
500
1000
1500
2000
2500
3000
3500
Strain (microstrain)
Top
Bottom

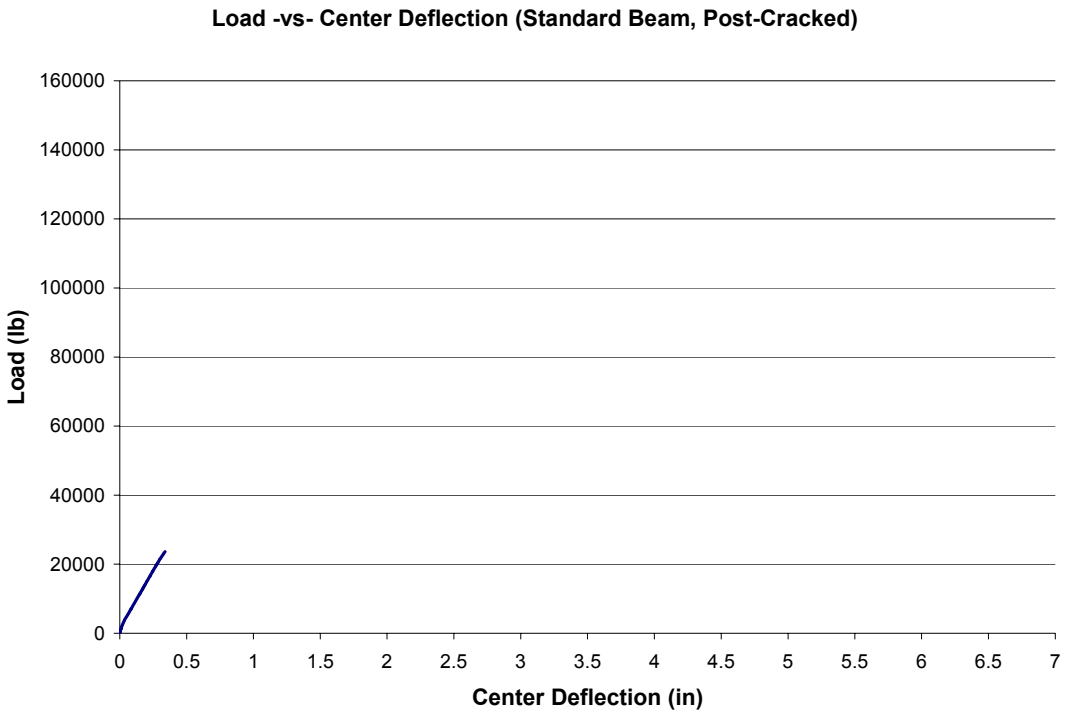
Load -vs- Center Deflection (Standard Beam, Post-Cracked)
160000
140000
120000
100000
80000
60000
40000
20000
0
Load (lb)
0
0.5
1
1.5
2
2.5
3
3.5
4
4.5
5
5.5
6
6.5
7
Center Deflection (in)

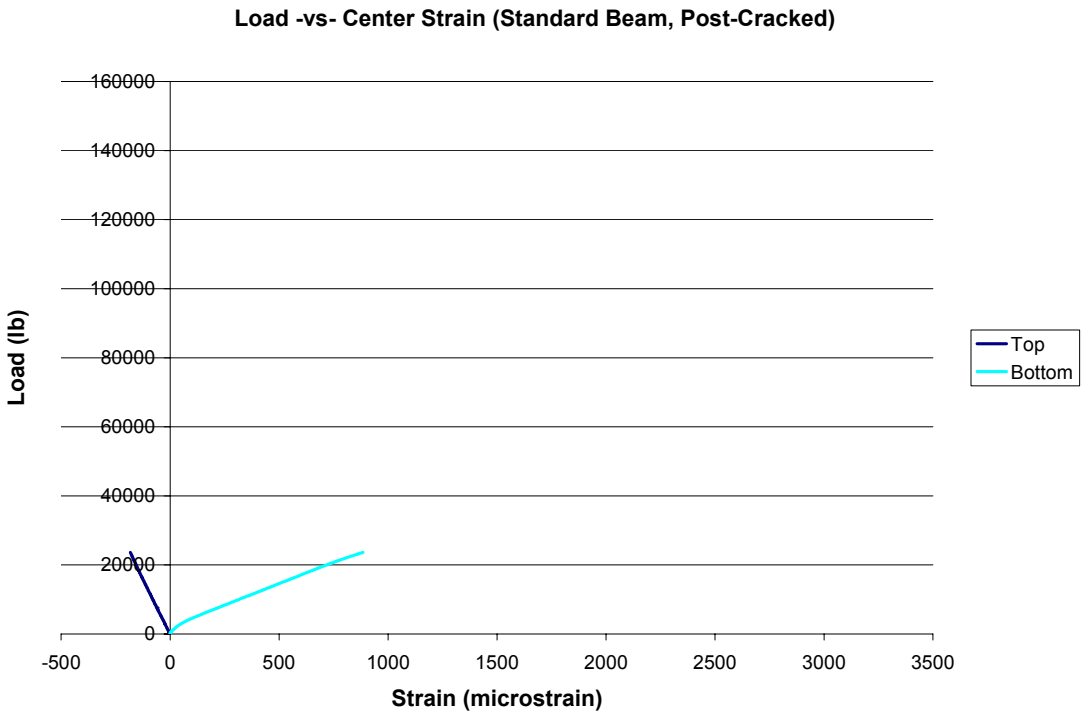
Load -vs- Center Strain (Standard Beam, Post-Cracked)
160000
140000
120000
100000
80000
60000
40000
20000
0
Load (lb)
-500
0
500
1000
1500
2000
2500
3000
3500
Strain (microstrain)
Top
Bottom

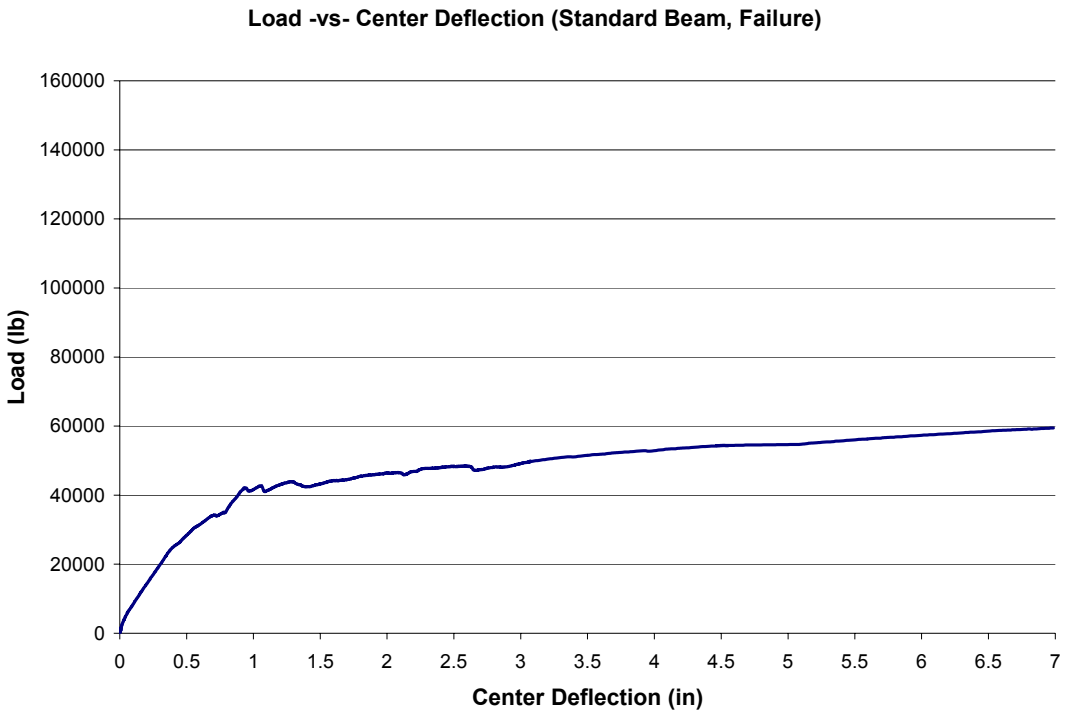
Load -vs- Center Deflection (Standard Beam, Failure)
160000
140000
120000
100000
80000
60000
40000
20000
0
Load (lb)
0
0.5
1
1.5
2
2.5
3
3.5
4
4.5
5
5.5
6
6.5
7
Center Deflection (in)

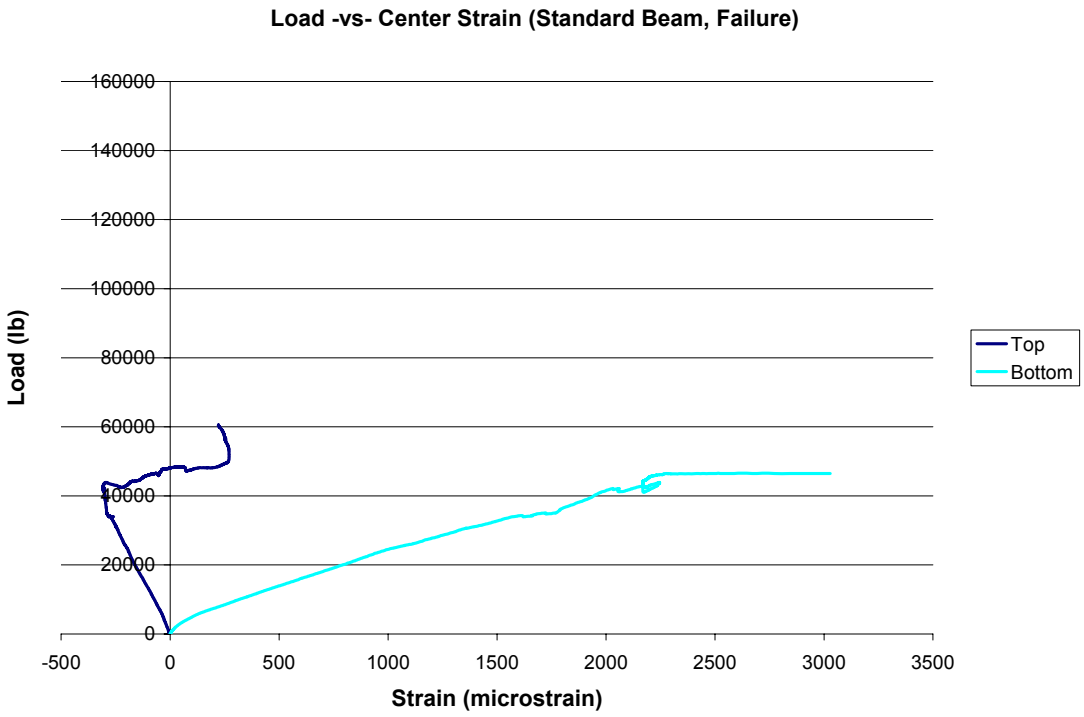
Load -vs- Center Strain (Standard Beam, Failure)
160000
140000
120000
100000
80000
60000
40000
20000
0
Load (lb)
-500
0
500
1000
1500
2000
2500
3000
3500
Strain (microstrain)
Top
Bottom

The following pictures were taken during the laboratory testing of the CFRP beam.

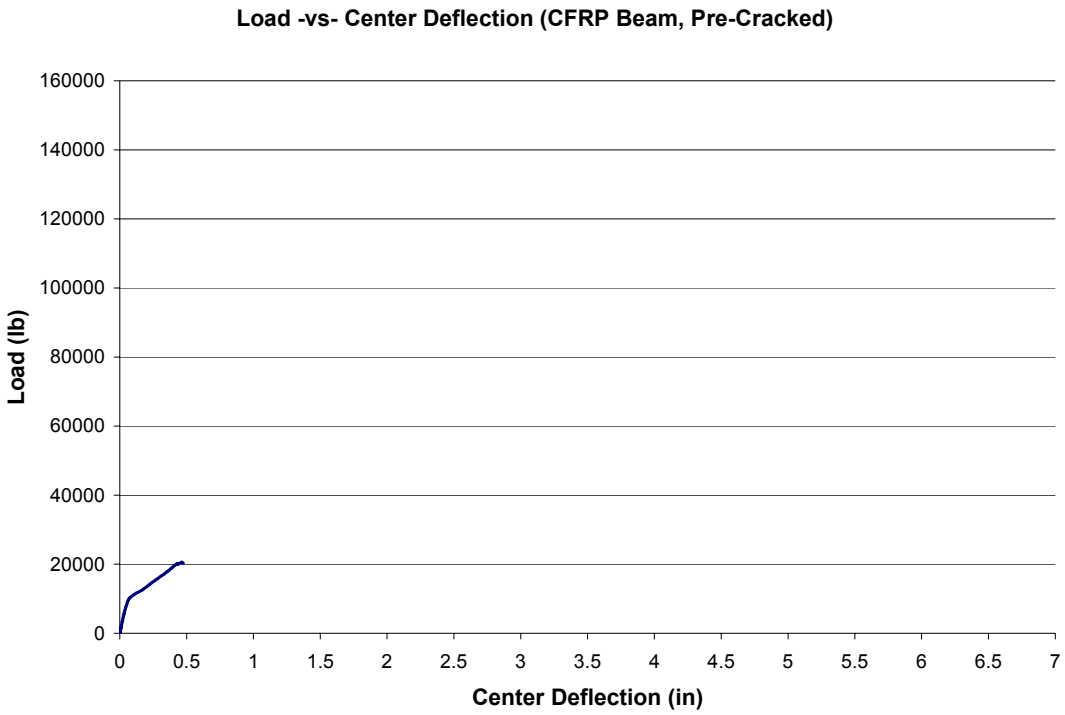
Load -vs- Center Deflection (CFRP Beam, Pre-Cracked)
160000
140000
120000
100000
80000
60000
40000
20000
0
Load (lb)
0
0.5
1
1.5
2
2.5
3
3.5
4
4.5
5
5.5
6
6.5
7
Center Deflection (in)

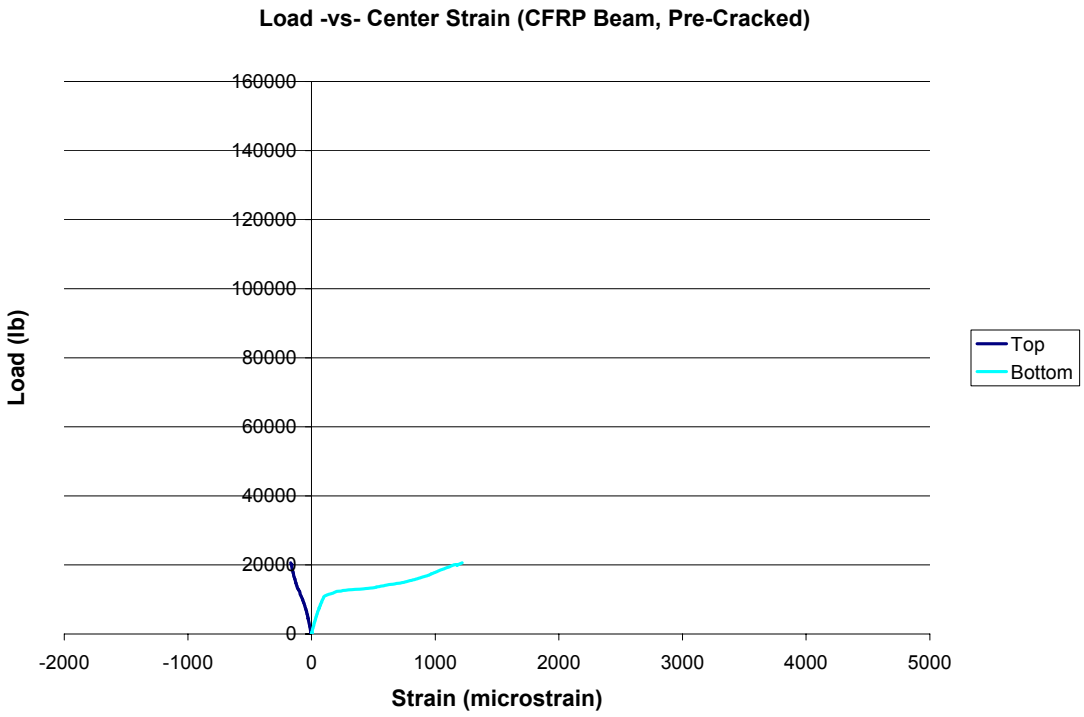
Load -vs- Center Strain (CFRP Beam, Pre-Cracked)
160000
140000
120000
100000
80000
60000
40000
20000
0
Load (lb)
-2000
-1000
0
1000
2000
3000
4000
5000
Strain (microstrain)
Top
Bottom

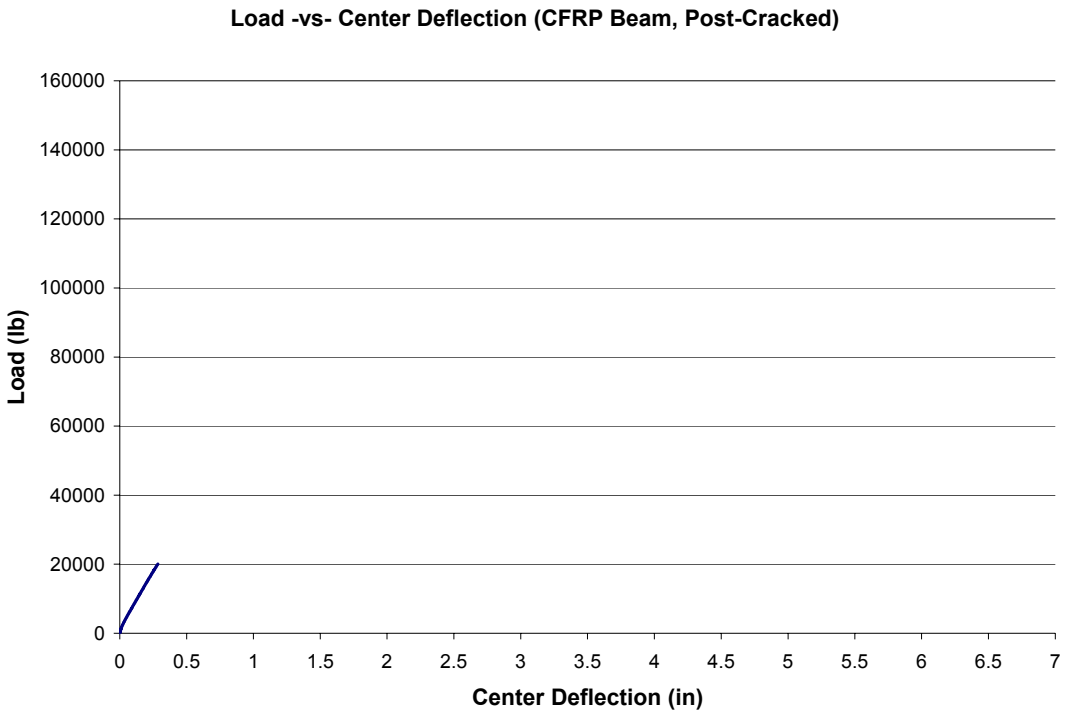
Load -vs- Center Deflection (CFRP Beam, Post-Cracked)
160000
140000
120000
100000
80000
60000
40000
20000
0
Load (lb)
0
0.5
1
1.5
2
2.5
3
3.5
4
4.5
5
5.5
6
6.5
7
Center Deflection (in)

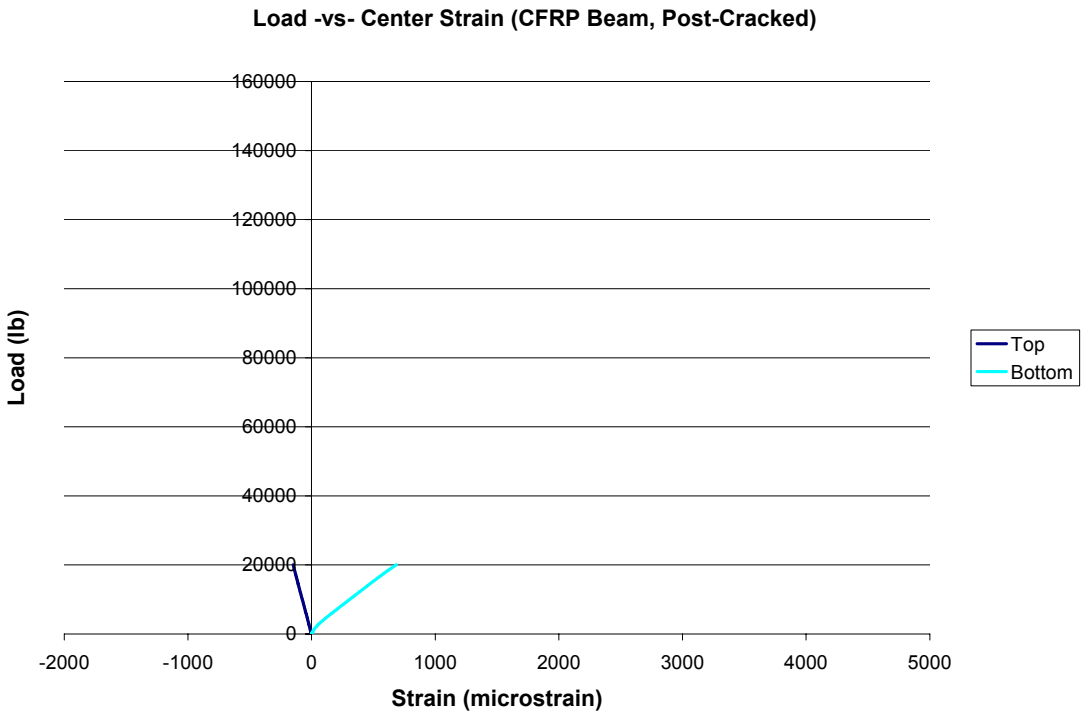
Load -vs- Center Strain (CFRP Beam, Post-Cracked)
160000
140000
120000
100000
80000
60000
40000
20000
0
Load (lb)
-2000
-1000
0
1000
2000
3000
4000
5000
Strain (microstrain)
Top
Bottom

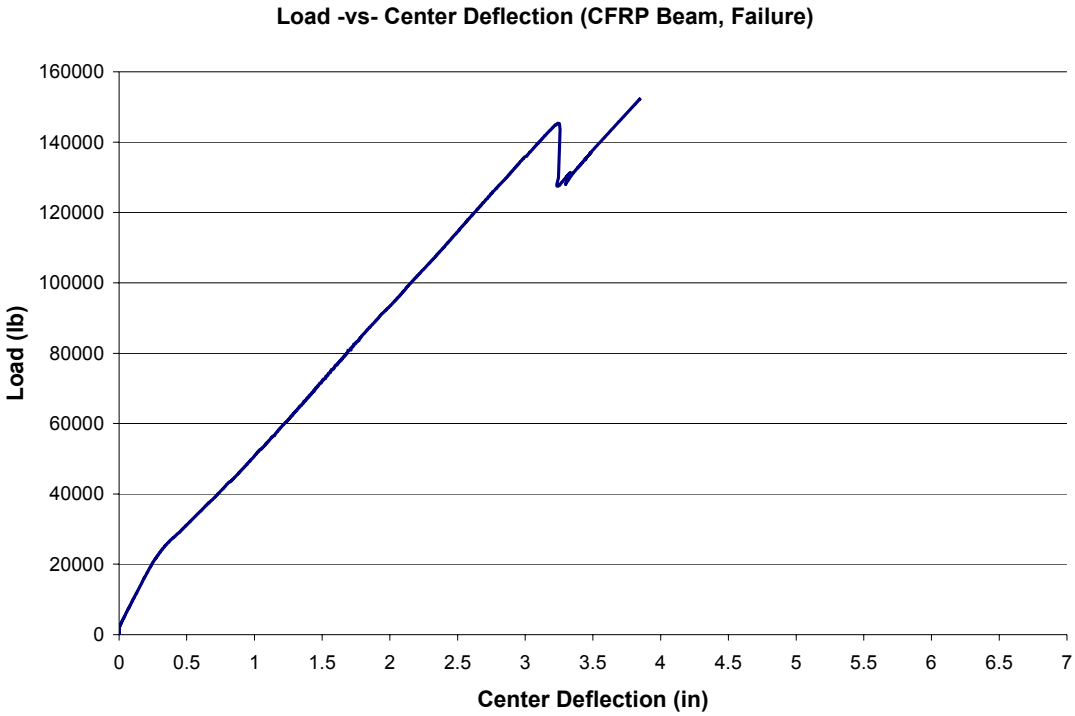
Load -vs- Center Deflection (CFRP Beam, Failure)
Load (lb)
160000
140000
120000
100000
80000
60000
40000
20000
0
0
0.5
1
1.5
2
2.5
3
3.5
4
4.5
5
5.5
6
6.5
7
Center Deflection (in)

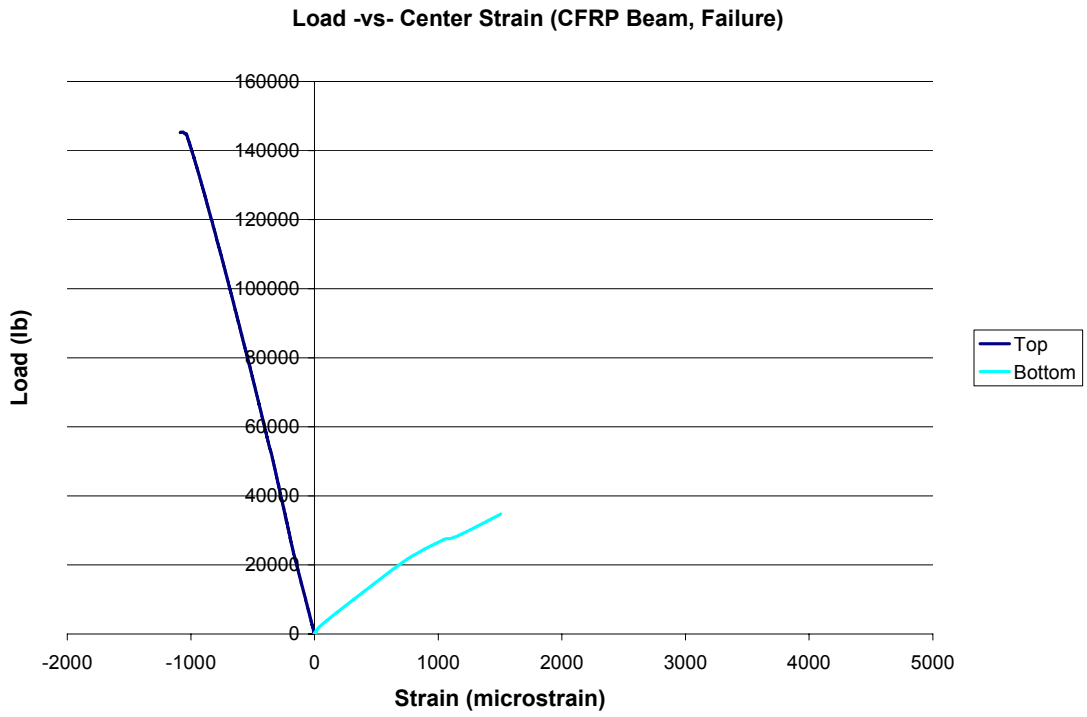
Load -vs- Center Strain (CFRP Beam, Failure)
Load (lb)
160000
140000
120000
100000
80000
60000
40000
20000
0
-2000
-1000
0
1000
2000
3000
4000
5000
Strain (microstrain)
Top
Bottom

The following pictures were taken during the laboratory testing of the MMFX4 beam.

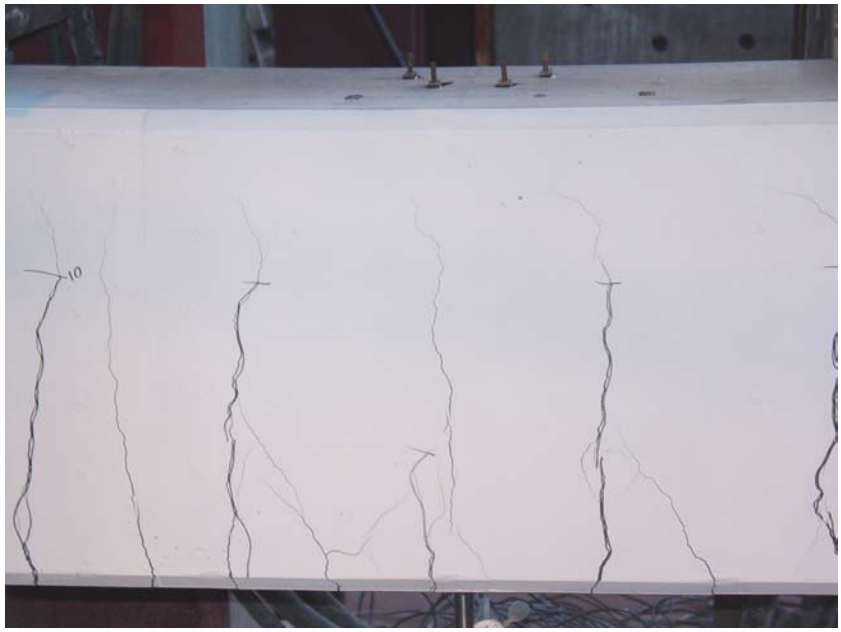

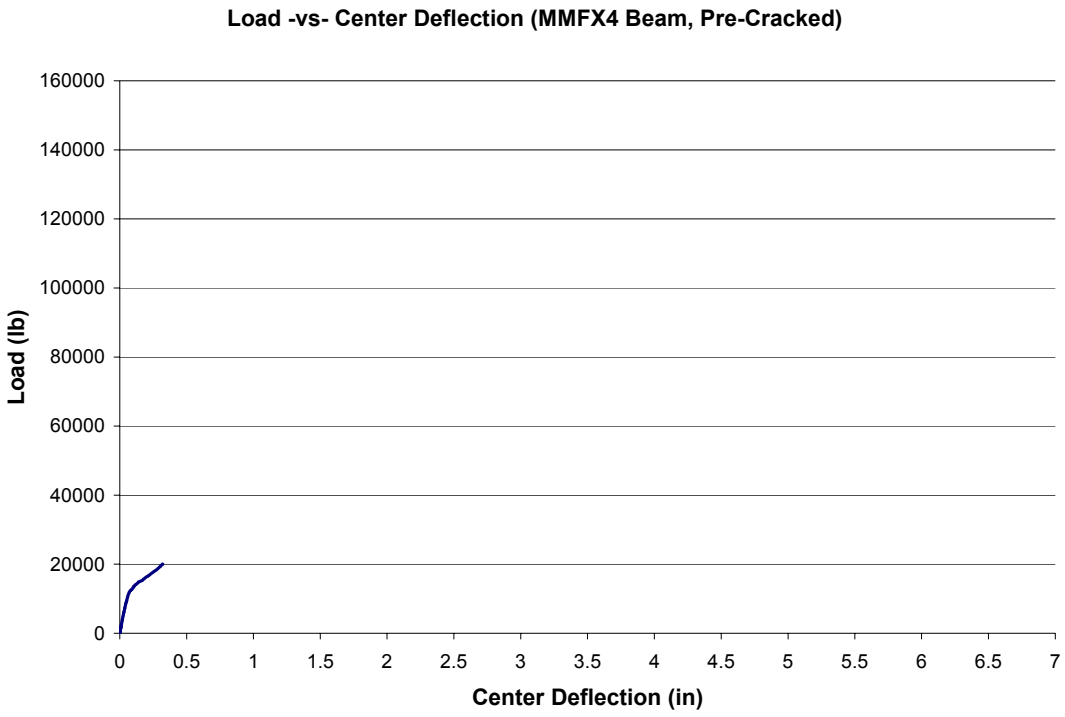
Load -vs- Center Deflection (MMFX4 Beam, Pre-Cracked)
160000
140000
120000
100000
80000
60000
40000
20000
0
Load (lb)
0
0.5
1
1.5
2
2.5
3
3.5
4
4.5
5
5.5
6
6.5
7
Center Deflection (in)

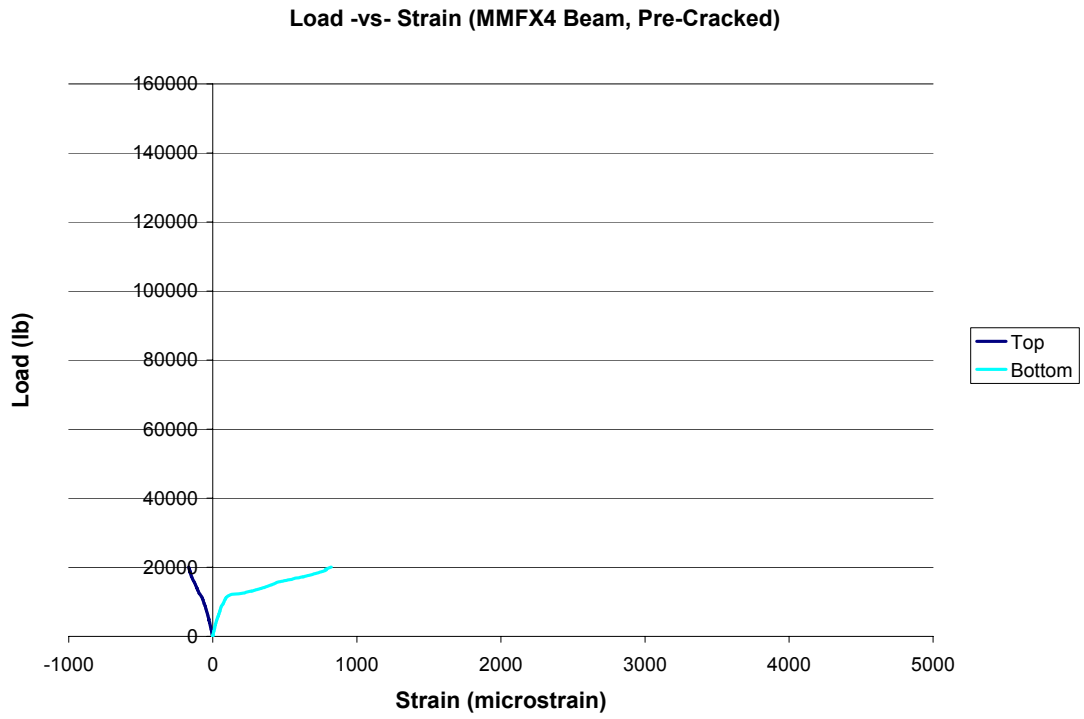
Load -vs- Strain (MMFX4 Beam, Pre-Cracked)
160000
140000
120000
100000
80000
60000
40000
20000
0
Load (lb)
-1000
0
1000
2000
3000
4000
5000
Strain (microstrain)
Top
Bottom

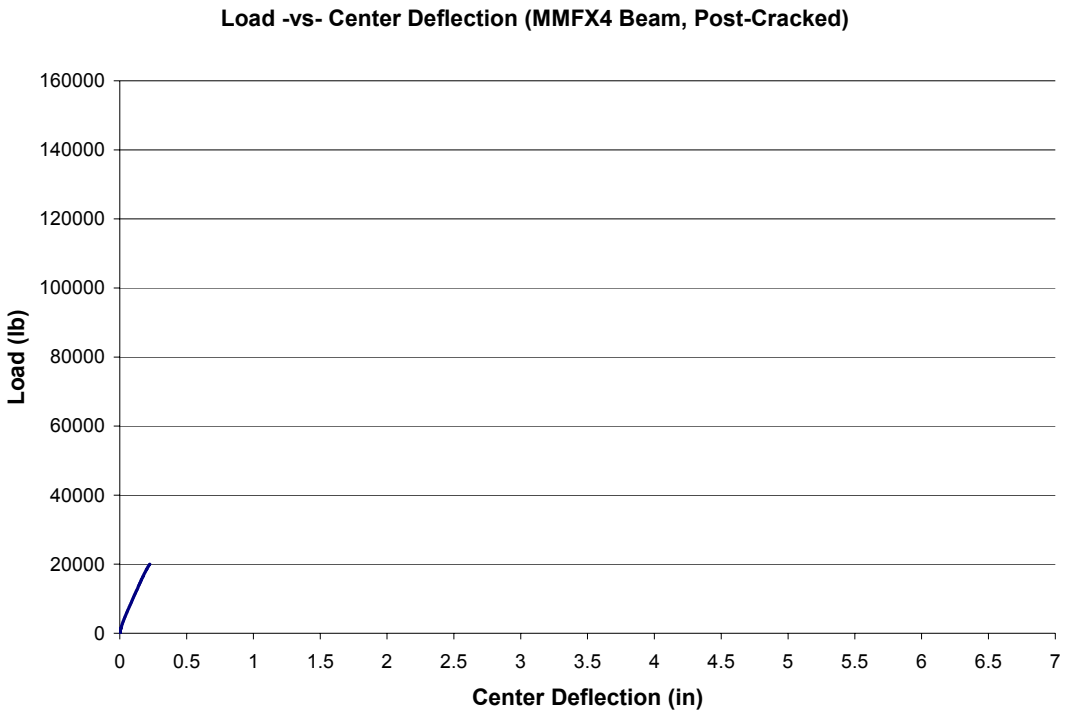
Load -vs- Center Deflection (MMFX4 Beam, Post-Cracked)
160000
140000
120000
100000
80000
60000
40000
20000
0
Load (lb)
0
0.5
1
1.5
2
2.5
3
3.5
4
4.5
5
5.5
6
6.5
7
Center Deflection (in)

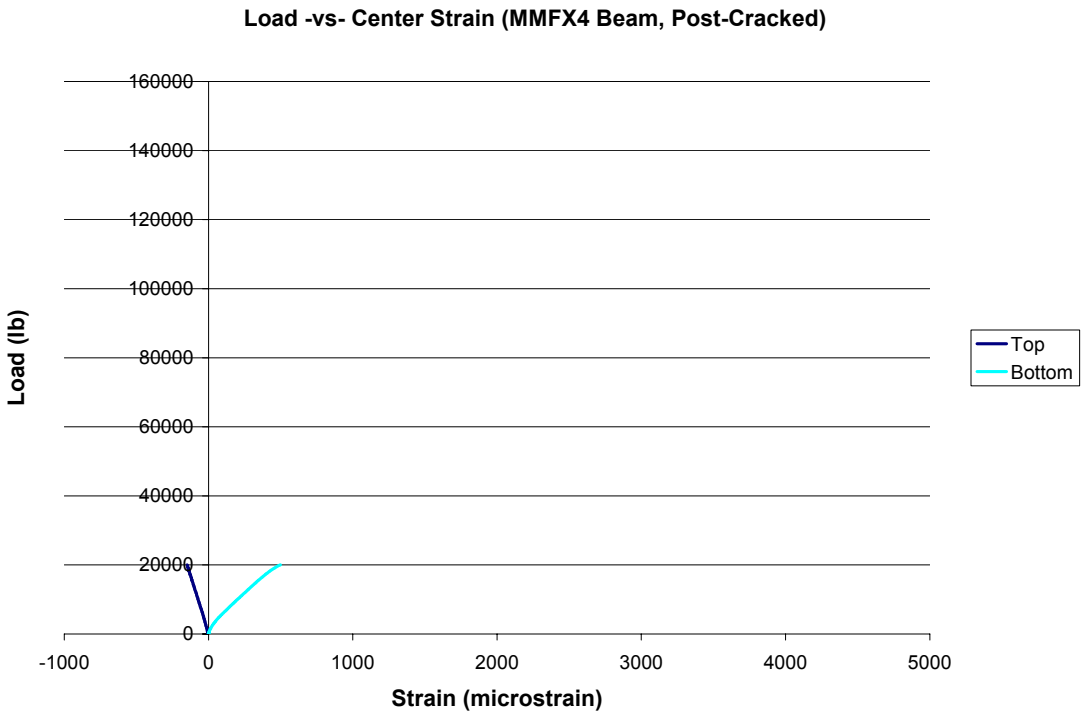
Load -vs- Center Strain (MMFX4 Beam, Post-Cracked)
160000
140000
120000
100000
80000
60000
40000
20000
0
Load (lb)
-1000
0
1000
2000
3000
4000
5000
Strain (microstrain)
Top
Bottom

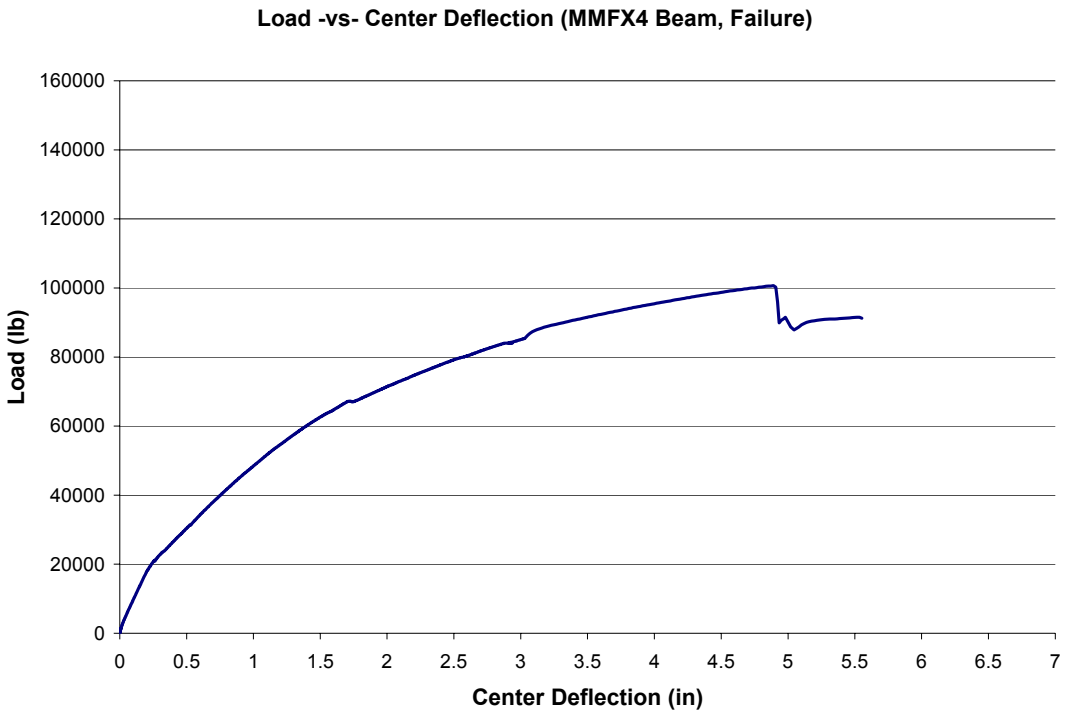
Load -vs- Center Deflection (MMFX4 Beam, Failure)
160000
140000
120000
100000
80000
60000
40000
20000
0
Load (lb)
0
0.5
1
1.5
2
2.5
3
3.5
4
4.5
5
5.5
6
6.5
7
Center Deflection (in)

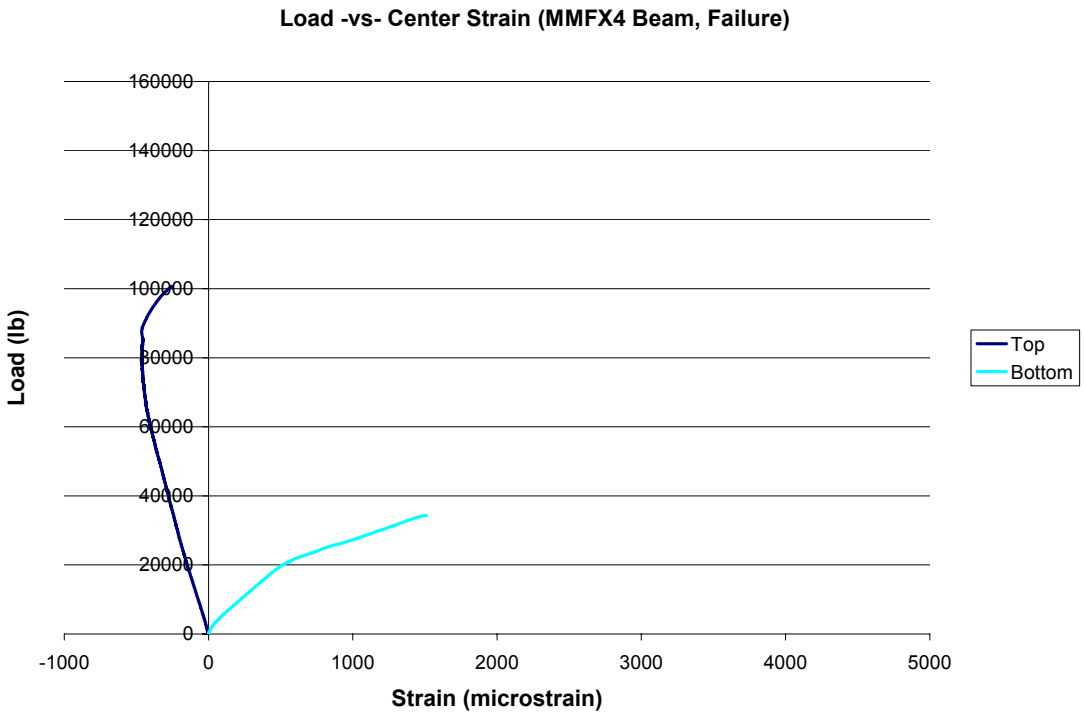
Load -vs- Center Strain (MMFX4 Beam, Failure)
160000
140000
120000
100000
80000
60000
40000
20000
0
Load (lb)
-1000
0
1000
2000
3000
4000
5000
Strain (microstrain)
Top
Bottom

The following pictures were taken during the laboratory testing of the MMFX2 beam.

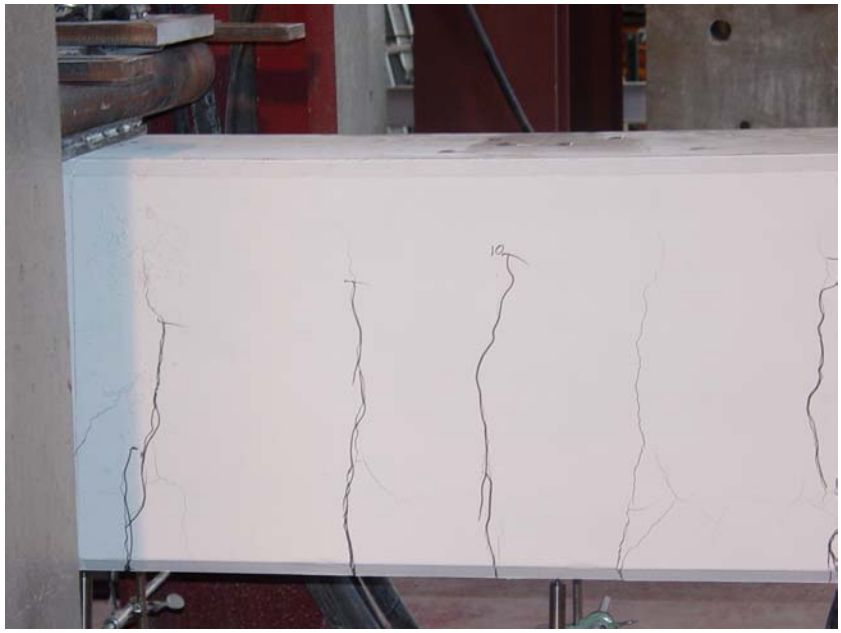

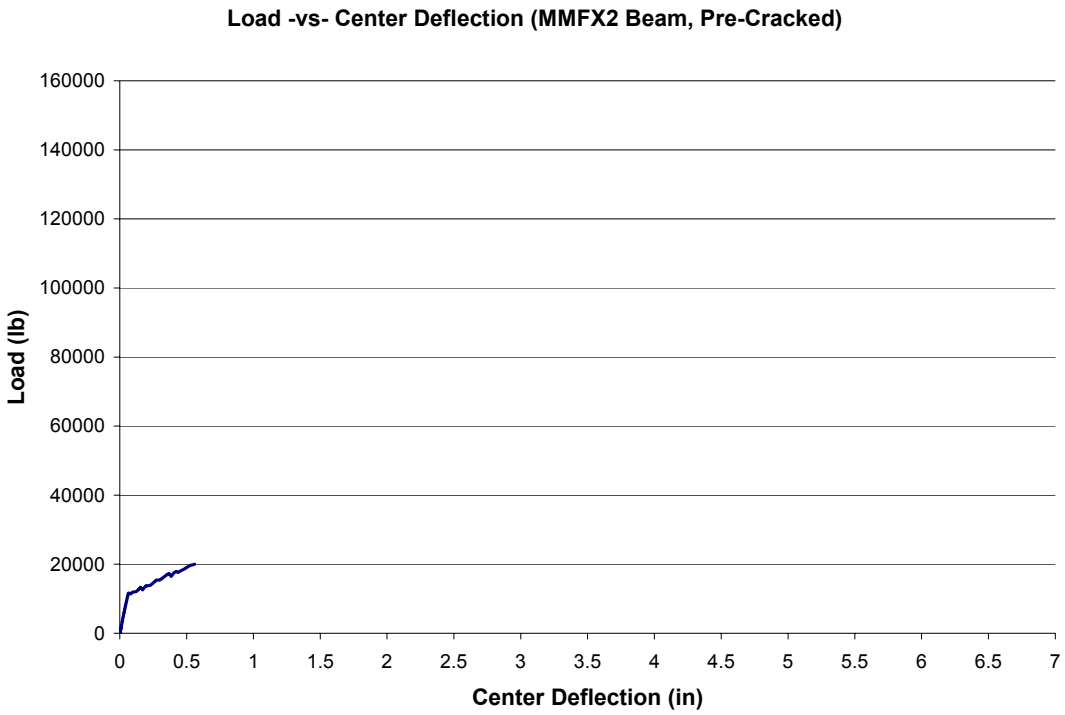
Load -vs- Center Deflection (MMFX2 Beam, Pre-Cracked)
160000
140000
120000
100000
80000
60000
40000
20000
0
Load (lb)
0
0.5
1
1.5
2
2.5
3
3.5
4
4.5
5
5.5
6
6.5
7
Center Deflection (in)

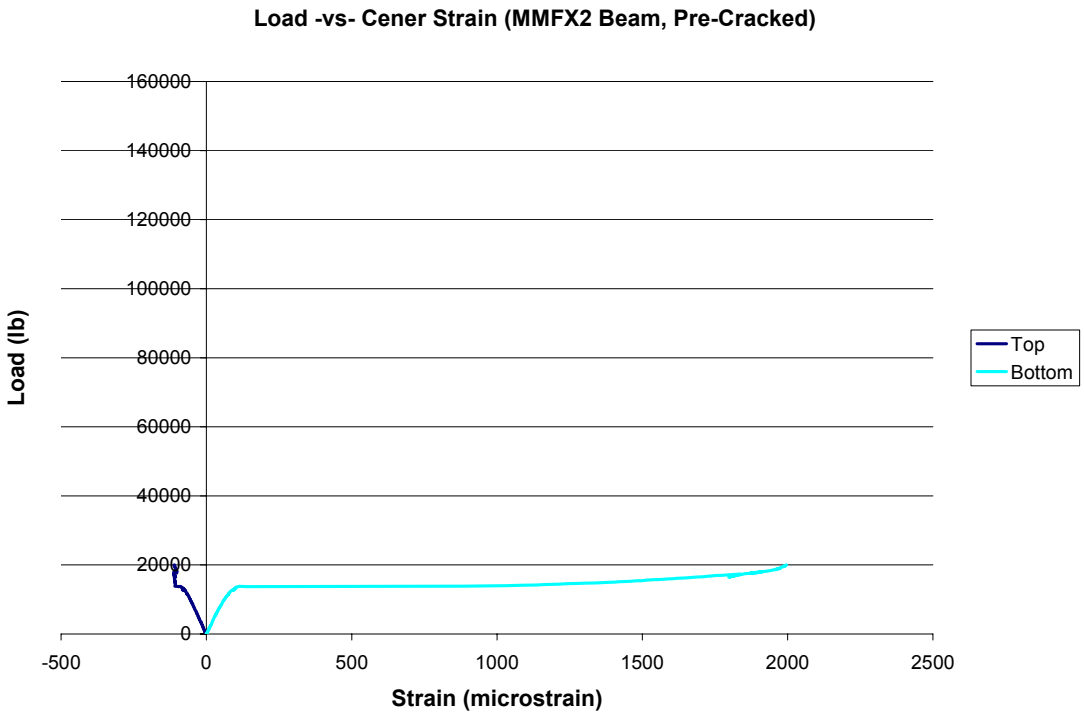
Load -vs- Cener Strain (MMFX2 Beam, Pre-Cracked)
160000
140000
120000
100000
80000
60000
40000
20000
0
Load (lb)
-500
0
500
1000
1500
2000
2500
Strain (microstrain)
Top
Bottom

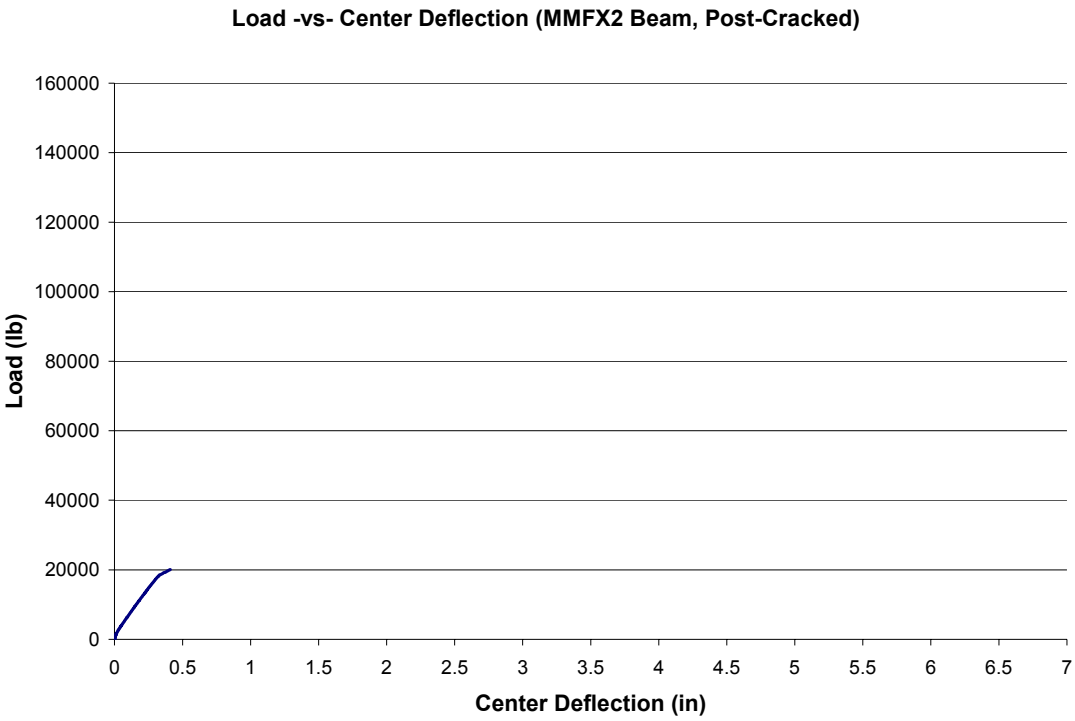
Load -vs- Center Deflection (MMFX2 Beam, Post-Cracked)
160000
140000
120000
100000
80000
60000
40000
20000
0
Load (lb)
0
0.5
1
1.5
2
2.5
3
3.5
4
4.5
5
5.5
6
6.5
7
Center Deflection (in)

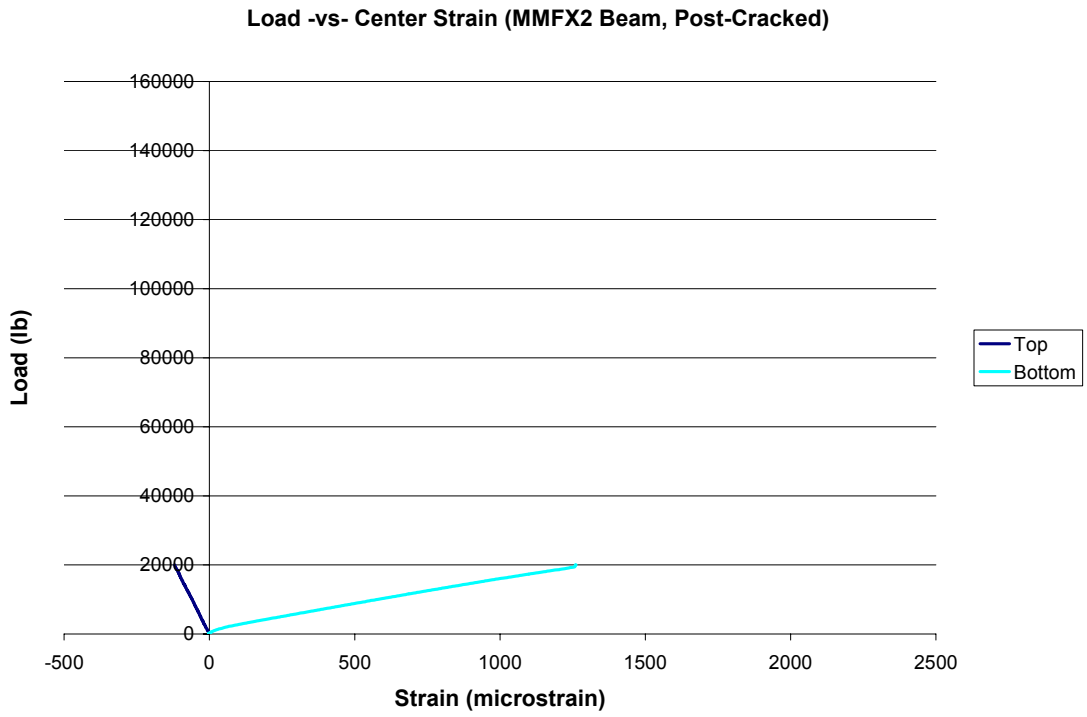
Load -vs- Center Strain (MMFX2 Beam, Post-Cracked)
160000
140000
120000
100000
80000
60000
40000
20000
0
Load (lb)
-500
0
500
1000
1500
2000
2500
Strain (microstrain)
Top
Bottom

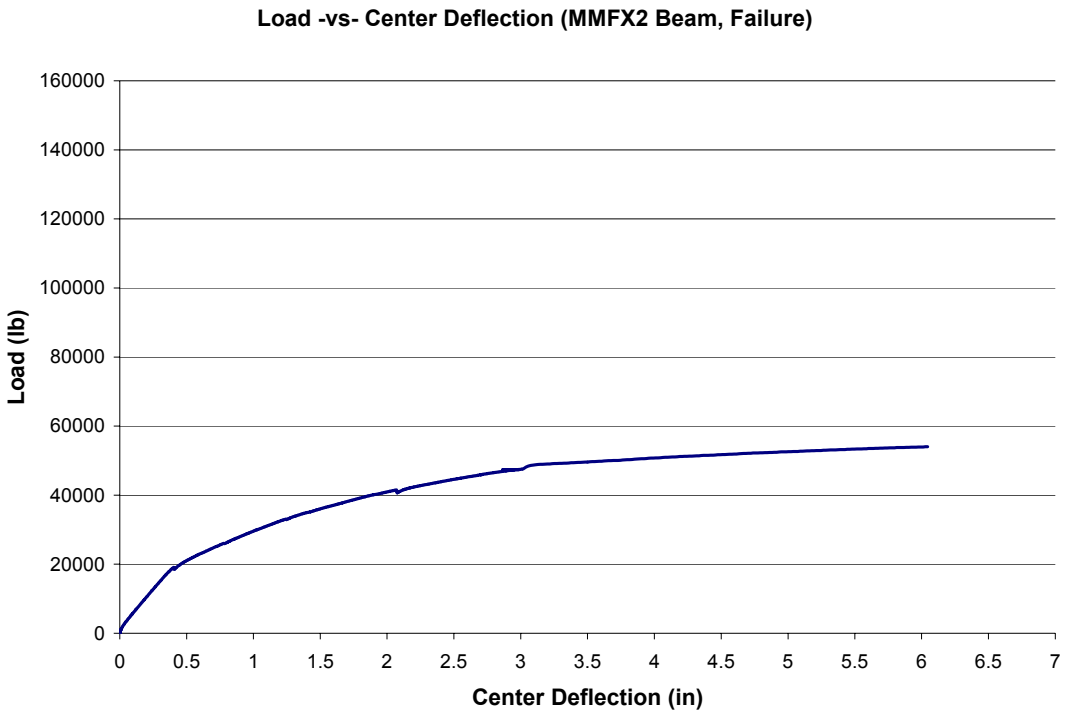
Load -vs- Center Deflection (MMFX2 Beam, Failure)
160000
140000
120000
100000
80000
60000
40000
20000
0
Load (lb)
0
0.5
1
1.5
2
2.5
3
3.5
4
4.5
5
5.5
6
6.5
7
Center Deflection (in)

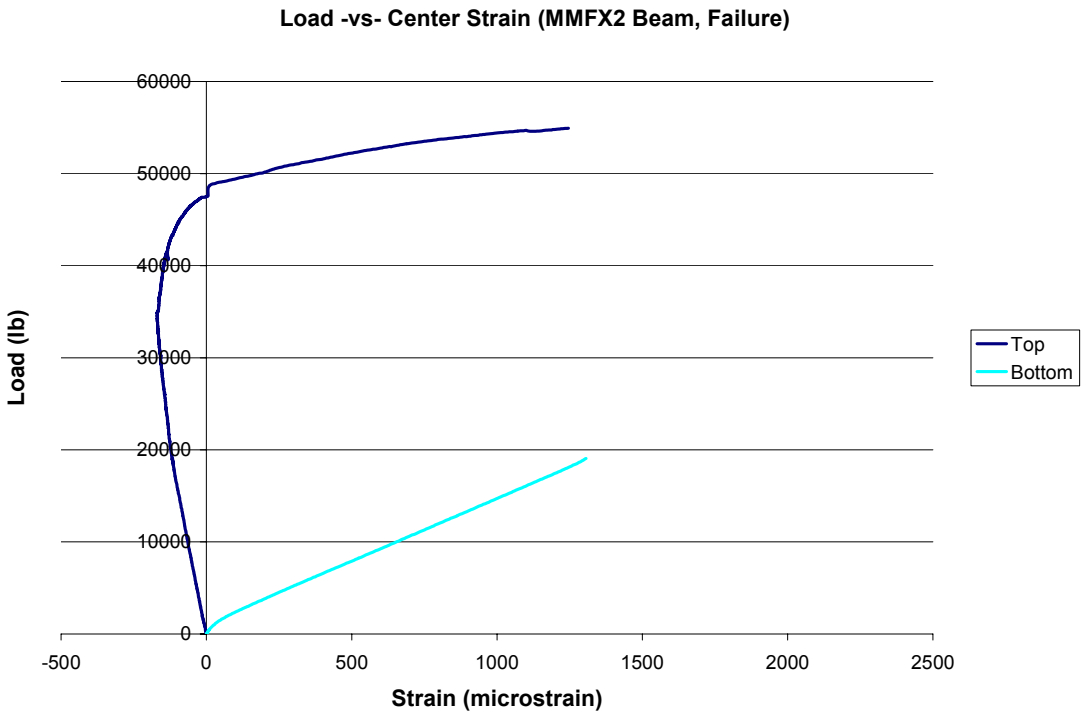
Load -vs- Center Strain (MMFX2 Beam, Failure)
60000
50000
40000
30000
20000
10000
0
Load (lb)
-500
0
500
1000
1500
2000
2500
Strain (microstrain)
Top
Bottom

Corrosion Monitoring of Bridge 1-712B with V2000 Sensors

by Michael J. Chajes and Wei Liu

The V2000 corrosion sensor consists of an electrode of silver wire which is inside a plastic braid. It is embedded in the grout surrounding the steel rebar. The braid prevents the wire from coming into contact with the steel rebar. The pore water of the grout performs the function of an electrolyte between the steel rebar and the V2000 sensor. Therefore, the condition of the steel with respect to corrosion can be monitored by measuring the electrical potential between the steel rebar and the V2000 sensor. If corrosion is present, the electrochemical activity will register on the electrode as increased voltage and current. For normal steel, there is no corrosion activity when the voltage is below 300mV. Active corrosion will increase the voltage to a level higher than 400mV.

An array of nine sensors was embedded in the bridge deck. Figure 1 shows the locations of sensors measuring from the northeast corner of the deck.

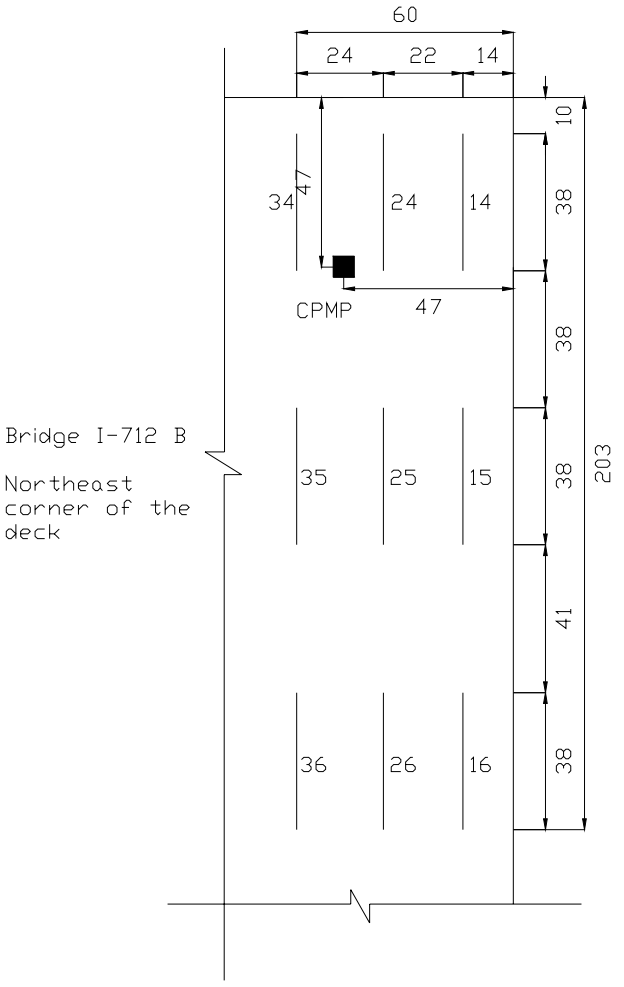

Figure 1 Location of V2000 sensors and CPMP unit.

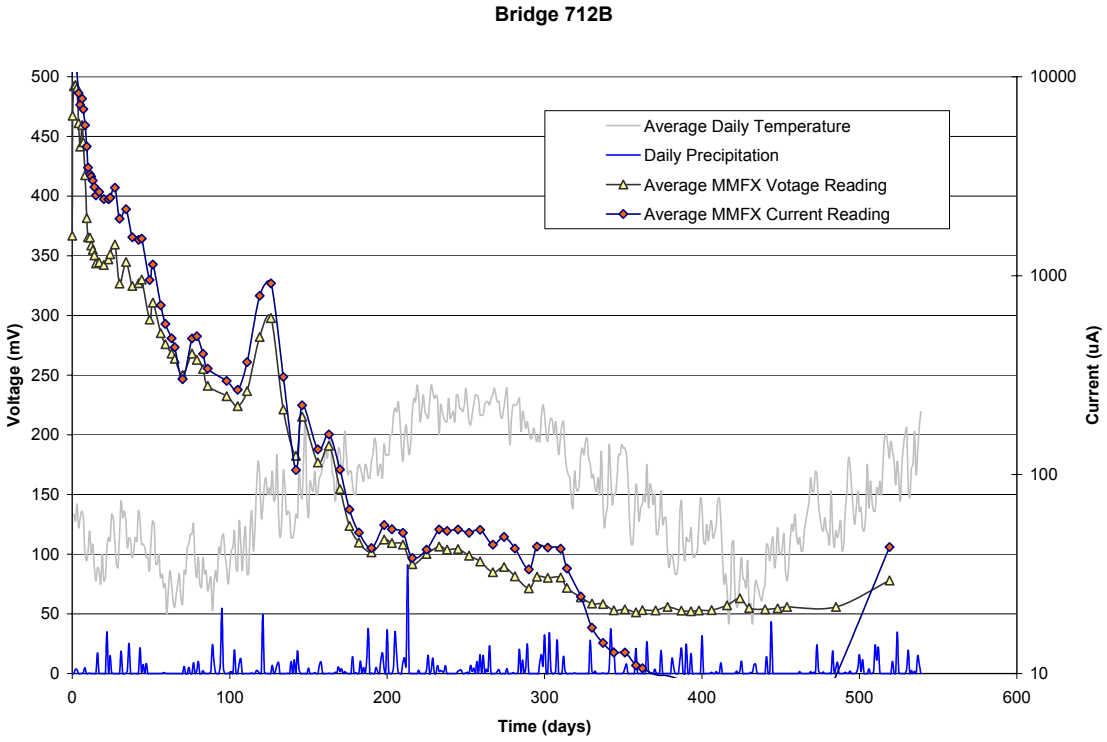

Figure 2 Average voltage and current readings as functions of time. Also shown in the figure are the daily average temperature and precipitation.

The voltage and current from each sensor have been monitored. The average voltage and current from the nine sensors are plotted in Figure 2 as functions of time. The average daily temperature and daily precipitation in Figure 2 are the data recorded at New Castle County Airport by National Weather Services. The ambient temperature and humidity at the time of each measurement were also recorded. However, temperature inside the concrete can be very different from ambient temperature. Therefore, average daily temperature in the region serves as a better reference here.

Both voltage and current were high initially and then declined along with time. Measured data showed some temperature dependence. However, moisture or precipitation has basically no effect on the data.

Note that voltage is plotted on linear scale while current is on logarithm scale in Figure 2. The relationship between current and voltage is exponential since they were tracking each other closely in the figure. Figure 3 is a direct plot of current as a function of voltage. During the first 250 days, voltage decreased from 500mV to 100mV, while current decreased from 10mA to about 50μA, following an exponential dependence. The current reduced to a very small value when voltage became less than 100mA, indicating the cease of electrochemical activity.

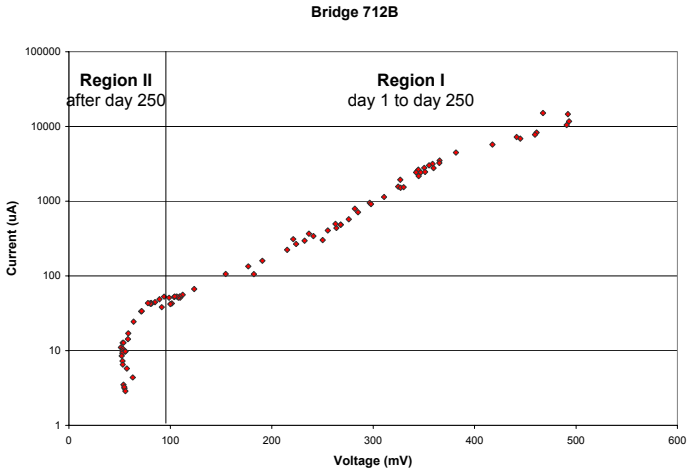

Figure 3 Current as a function of voltage.

Three V2000 sensors were embedded in Beams B1, B3, and D1 during fabrication. Sensors covered the entire length of the beams. Data obtained from the beams are similar to the corrosion data from the deck.

Because the chemical battery formed by the sensor and the MMFX rebar is very weak, the current reading is usually unstable. It increases rapidly to a maximum value within about 2 seconds and then decreases exponentially with time. Figure 4 shows the current as a function of time during a single measurement of the V2000 sensor in Beam B3. All the current readings in this project were taken at or near the maximum. The monitoring data is meaningful only if consistent measurement method is used throughout the entire process.

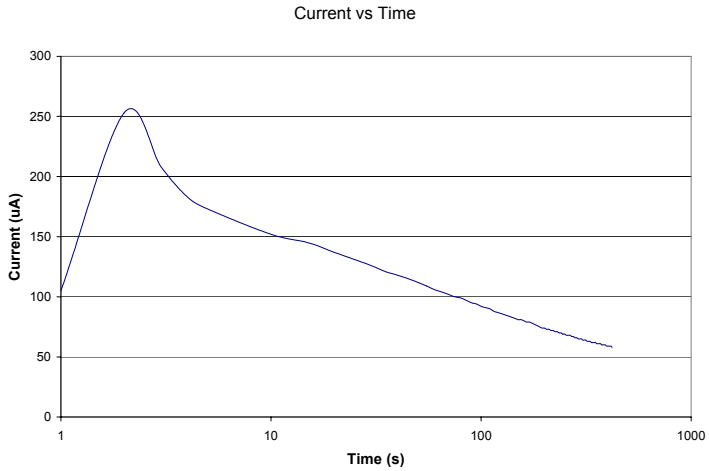

Figure 4 Current decreases as an exponential function of time.

Figure 5 Corrosion penetration monitoring with CPMP

A CPMP unit was also embedded in the deck, as shown in Figure 5. The CPMP was designed to monitor the rate of penetration of moisture from the surface into the structure. The unit consists of 6 small sections of standard rebar located at 6 depths in 1cm increments. Each bar is monitored for the onset of corrosion with a V2000 sensor. Ideally, an early warning can be obtained from the CPMP unit when moisture penetrates into the structure and reaches the depths of each small rebar.

Moisture penetrates into the deck from its top surface. The monitoring data has confirmed that higher bars in the CPMP unit usually have higher voltage.

Figure 6 Four types of short rebars. From upper left corner clockwise: stainless clad, MMFX, epoxy-coated, and normal rebar.

A comparative study of MMFX, stainless clad, epoxy-coated, and normal steel rebar was conducted. Six-inch sections of different types of bars were tied to the MMFX grid in the deck and monitored with V2000 sensors as shown in Figure 6. Although no conclusive results have been obtained to date, the following facts were observed:

- MMFX and normal steel rebar behave similarly.
- Stainless clad bars yielded unstable corrosion readings which are strongly dependent upon ambient temperature.

- Epoxy-coated bars have relatively high voltage readings but very low current readings through the entire monitoring process.

- For epoxy-coated bar, the integrity of the coating is very important—the rebar is vulnerable to corrosion when the coating is damaged but not if the coating is intact. Some specimens were purposely damaged in the study.

TDR Monitoring for Selected Beams

Time Domain Reflectometry (TDR) is an effective method of detecting corrosion and voids. When using TDR as a corrosion monitoring method, a sensor is embedded in concrete with the steel rebar during construction. Corrosion damage can be detected in a way similar to radar. An electromagnetic pulse is sent down the transmission line formed by the sensor and the rebar. Reflections caused by corrosion and voids can be observed.

Three TDR sensors were installed in Beams B1, D1, and B3. A new geometry was used in which the steel rebar was connected to ground, i.e. the outer conductor of the leading coaxial cable, while the sensor was connected to the center conductor of the coaxial cable. Before this project, the steel rebar was usually connected to the center conductor and the sensor was acting as ground. The old geometry suffered several drawbacks including large initial reflection and high attenuation. Compared to a previous TDR field testing on Bridge 8F, signal attenuation was greatly reduced and measurement sensitivity was improved in the new geometry. The connection to the leading coaxial cable was also improved. The initial reflection has been reduced to an acceptable level as shown in Figure 7 and Figure 8.

The sensors were installed one day before the pour while workers were still working on the beams. No protection procedure was used. As a result, the sensor in Beam D1 was damaged. It was broken in the middle of the beam. It was unknown whether the damage happened before or during the pour. However, due the nature of the TDR sensor, it can still provide useful information for the first half of the beam. The TDR data from this beam is shown in Figure 8. The incident electromagnetic pulse encountered the open end caused by the broken wire at around 150ns. Hugh reflection was generated there. The exact location can be easily calculated from the travel time.

All three sensors have been giving highly repeatable results for the past two years. Differential TDR has been used in the monitoring. By differentially comparing two TDR readings taken over time, corrosion damage occurring within the time period will be revealed as localized waveform change. Figure 7 and Figure 8 show TDR readings taken on Beams B3 and D1 eight months apart. The repeatability of the signals verifies the integrity of the bridge. It also demonstrates that the TDR method is viable for field application.

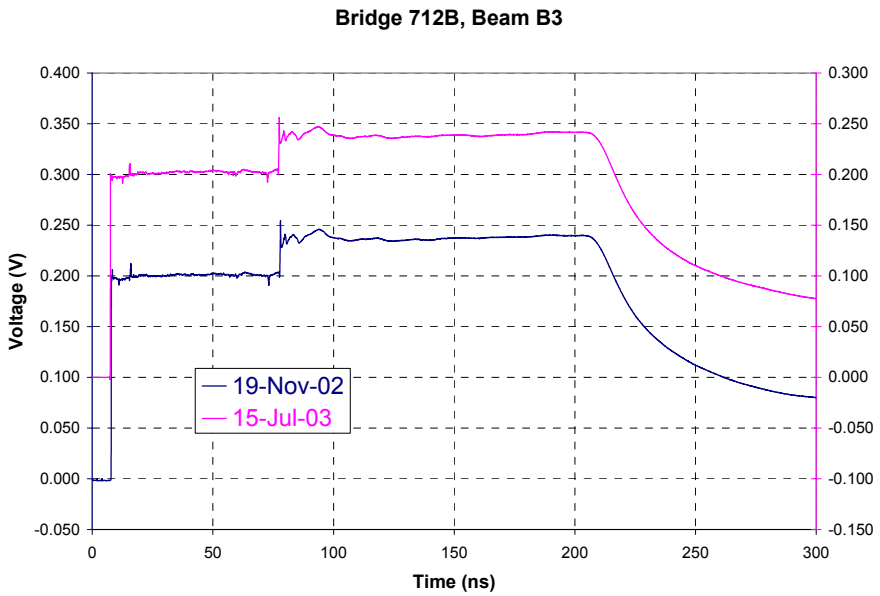

Figure 7 TDR returns from Beam B3.

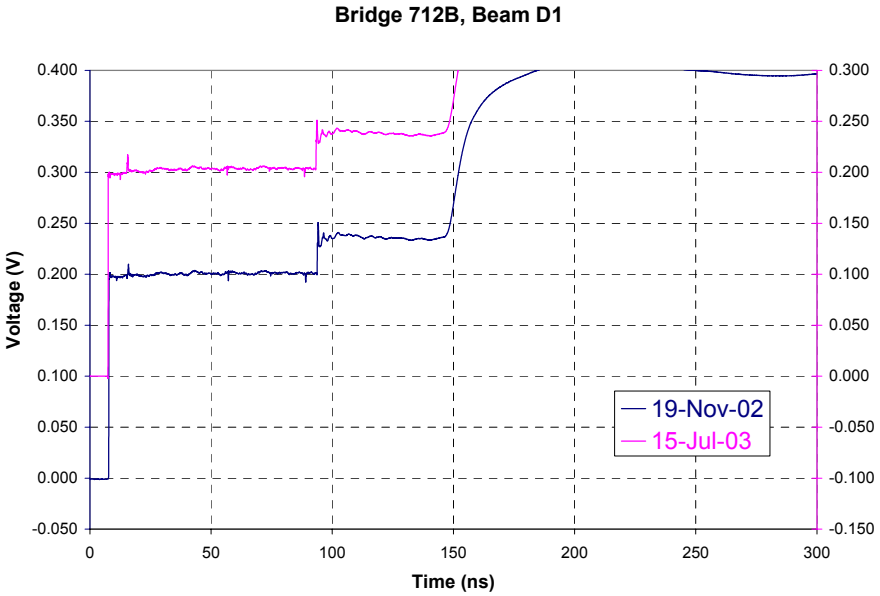

Figure 8 TDR returns from Beam D1 with damaged sensor.